DEPARTMENT OF COMMERCE
FREDERICK H. MUELLER, Acting Secretary

WEATHER BUREAU
F. W. REICHELDERFER, Chief

MONTHLY WEATHER REVIEW

JAMES E. CASKEY, JR., Editor

Volume 87
Number 5

MAY 1959

Closed July 15, 1959
Issued August 15, 1959

SOME STATISTICS ON THE MAGNITUDE OF THE AGEOSTROPHIC WIND OBTAINED FROM CONSTANT LEVEL BALLOON DATA*

J. K. ANGELL
U.S. Weather Bureau, Washington, D.C.

[Manuscript received February 11, 1959; revised March 11, 1959]

ABSTRACT

On the basis of wind speeds and accelerations derived from U.S. Navy sponsored 300-mb. constant level balloon or transosonde flights made during 1953, 1955, and 1956, statistics are presented on the magnitude of the ageostrophic wind and its variation with latitude and wind speed. These statistics indicate that at 300 mb. the average angle between wind and geostrophic wind is 11 degrees and the mean magnitude of the vector deviation between wind and geostrophic wind is 12 m. sec.$^{-1}$. The data also show that, through the use of the geostrophic and gradient wind approximations, half the time errors greater than 29 percent and 11 percent, respectively, are introduced into the derived results.

1. INTRODUCTION

Previous evaluations of the magnitude of the ageostrophic wind have in large part been based on comparisons of wind data with geostrophic wind data obtained from synoptic weather maps, as illustrated by the works of Neiburger et al. [1] and Machta [2]. A few evaluations of the ageostrophic wind have been based on estimations of the partial wind derivatives in the equations of motion, as illustrated by the work of Godson [3]. Durst and Gilbert [4] and Neiburger and Angell [5] evaluated the ageostrophic wind by determining the value of the individual wind derivatives from constant level balloon flights and introducing this value into the equation of motion. Since limited constant level balloon data were available for analysis in the latter two papers, it seemed desirable to carry through further analysis upon the receipt of more constant level balloon or transosonde data. This paper presents statistics on the magnitude of the ageostrophic wind, the variation of this magnitude with latitude and speed, and indicates the errors made in assuming the wind to be geostrophic or gradient, all based on 635 evaluations of the ageostrophic wind from 28 transosonde flights made at 300 mb. Of these 28 transosonde flights, 8 were launched from Minneapolis, Minn. in 1953, 4 were launched from Vernalis, Calif. in 1955, and 16 were launched from Oppama, Japan in 1956. The average duration of these flights was 65 hours and the average trajectory length was 4,700 nautical miles. The flights were positioned at 1-hourly or 2-hourly intervals by means of the excellent Federal Communications Commission (FCC) radio-direction-finding network. Anderson [6] found, by comparison of FCC positions with transosonde positions determined by photographs of the underlying terrain, that within the United States two-thirds of the time the FCC positions are in error by less than 20 nautical miles. Over the Atlantic and Pacific Oceans one would expect this error to be larger owing to the greater distances between tracking stations and balloons.

*This work was performed under Office of Naval Research Contract Nonr-333(21) for the Naval Research Laboratory in connection with BuAer Problem No. TED-NRL-MA505.

511937—59——1

2. DETERMINATION OF THE WIND AND AGEOSTROPHIC WIND

With minor approximations, the vector equation of motion may be written:

$$\frac{d\mathbf{V}}{dt}=f(\mathbf{V}-\mathbf{V}_g)\times\mathbf{k}+\mathbf{F} \tag{1}$$

where $\mathbf{V}$ is the horizontal component of the velocity, $\mathbf{V}_g$ is the geostrophic velocity, f is the Coriolis parameter, $\mathbf{F}$ is the frictional force per unit mass, and $\mathbf{k}$ is the unit vertical vector. The term on the left hand side of (1) represents the change of horizontal velocity following the three-dimensional path of an air parcel and may be expanded into three terms involving partial derivatives,

$$\frac{d\mathbf{V}}{dt}=\frac{\partial\mathbf{V}}{\partial t}+\mathbf{V}\cdot\nabla\mathbf{V}+w\frac{\partial\mathbf{V}}{\partial z} \tag{2}$$

where w is the vertical velocity and ∇ is the horizontal differential operator. The constant level balloon data determine the sum-value of the first two terms on the right hand side of (2). The sum of these two terms (local change of velocity plus horizontal advection of velocity) is hereafter called the partial acceleration. The value of the third term on the right hand side of (2), the vertical advection of velocity, may be approximated along a constant level balloon trajectory by determining the vertical motion by the adiabatic technique (vertical motion proportional to the change of temperature following the balloon and inversely proportional to the deviation of the lapse rate from the process lapse rate along the trajectory), and by determining the vertical wind shear from rawin data. Based on a limited number of computations from the 1953 flights and reported in reference [5], the magnitude of the vertical advection of velocity averages about 25 percent of the magnitude of the partial acceleration, and thus is certainly not negligible. Nevertheless, in this paper it is assumed that the partial acceleration data derived from the transosondes represents a reasonable approximation to the total acceleration since the bulk of the transosonde positions are over oceans where it is impractical to estimate the vertical advection of velocity by the techniques described above.

In order to pass from the value of the acceleration to the value of the geostrophic deviation it is necessary, as seen from (1), to neglect friction. While attempts have been made to estimate the magnitude of the frictional force from a combination of radiosonde and transosonde data, the evaluations, particularly over the oceans, are far too crude for inclusion here. Hence, an additional degree of uncertainty (in addition to the neglect of the vertical advection of velocity) enters into the values of the geostrophic deviations presented below.

With the neglect of friction and the vertical advection of velocity we find, after taking the dot product of (1) with the unit vector along and normal to the wind, that, respectively,

$$dV/dt=fV_g\sin i \tag{3}$$

and

$$Vd\theta/dt=-f(V-V_g\cos i) \tag{4}$$

where $d\theta/dt$ is the angular velocity of an air parcel and i is the angle of indraft (the angle between wind and geostrophic wind). Taking into account the findings of Neiburger and Angell with respect to the time intervals for which the velocity and acceleration should be computed in order to avoid large errors in these parameters due to radio-direction-finding errors in the positioning of the transosondes, the speed was determined from a 4-hour transosonde displacement; the tangential acceleration (dV/dt) was determined from the change in 4-hour average transosonde speed in 8 hours; and the normal acceleration ($Vd\theta/dt$) was determined as the product of the mean transosonde speed during an 8-hour time interval and the change of 4-hour average transosonde direction in 8 hours.

Upon eliminating the geostrophic wind speed between (3) and (4), the angle of indraft can be expressed in terms of three known variables; namely, the tangential acceleration, the normal acceleration, and the Coriolis acceleration (fV). From knowledge of the angle of indraft, the geostrophic wind can be evaluated from either (3) or (4). The cross-contour component of the ageostrophic wind ($V\sin i$) can then be determined as well as the along-contour component of the ageostrophic wind ($V\cos i-V_g$). In the diagrams in this paper $V-V_g$ is substituted for $V\cos i-V_g$ since, for the magnitudes of the angles of indraft obtained at 300 mb., the two quantities are practically identical.

3. VELOCITY AND AGEOSTROPHIC VELOCITY STATISTICS

In this section and in sections 4 and 5 we show by means of histograms and cumulative frequency curves the magnitudes of various velocity and ageostorophic velocity parameters obtained from the transosonde flights. Where comparison of two parameters is desirable, histograms and cumulative frequency curves are superimposed on the same diagram.

The magnitude of the 4-hour average wind speed at 300 mb. for this series of transosonde flights is indicated in the upper diagram of figure 1. Based upon 755 calculations, the mean wind speed is 38 m. sec.$^{-1}$ while the mode is 20–30 m. sec.$^{-1}$. Ten percent of the winds exceed 67 m. sec.$^{-1}$. The maximum wind speed determined from a 4-hour transosonde displacement is 150 m. sec.$^{-1}$. This value occurred on Flight 23 approximately 1,000 miles east-southeast of Tokyo in January 1956, and is undoubtedly one of the largest, reasonably reliable, values of wind speed ever recorded.

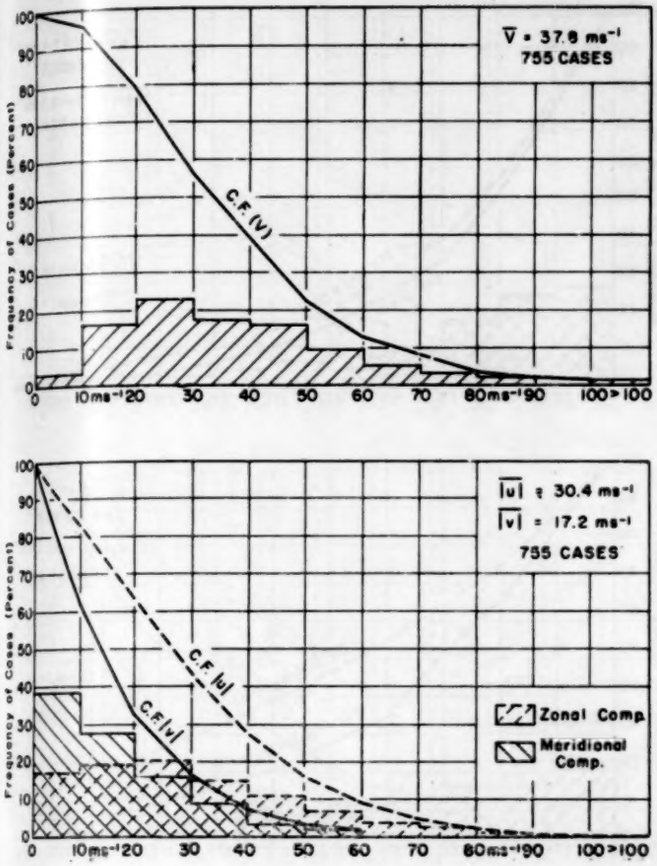

FIGURE 1.—Magnitude of the 300-mb. wind speed, V, (top) and its zonal, $|u|$, and meridional, $|v|$, components (bottom).

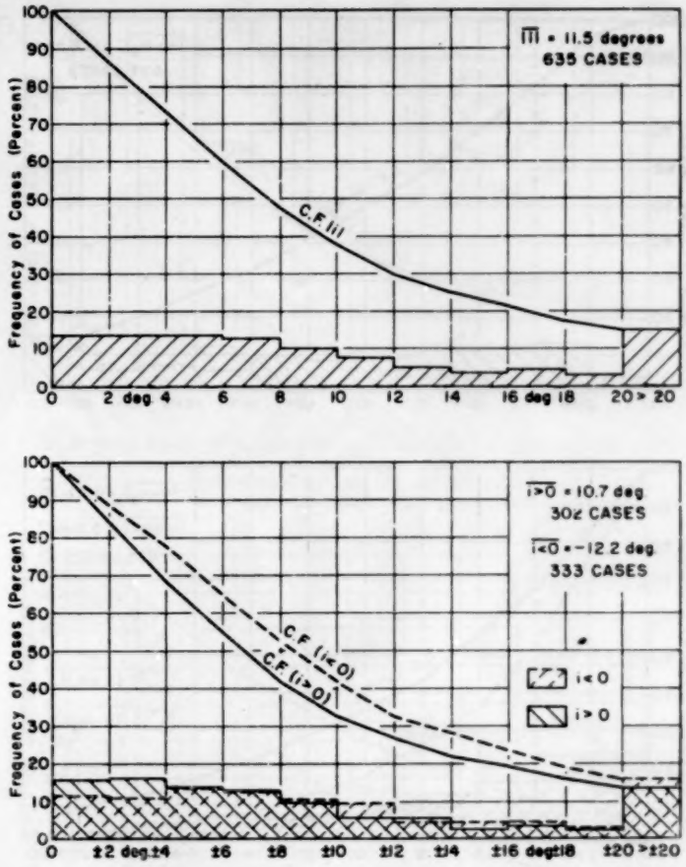
$\overline{|i|}$ = 11.5 degrees
635 CASES
C.F.|i|
Frequency of Cases (Percent)
2 deg 4 6 8 10 12 14 16 deg 18 20> 20
$\overline{i>0}$ = 10.7 deg
302 CASES
$\overline{i<0}$ = −12.2 deg
333 CASES
C.F.(i<0)
C.F.(i>0)
i<0
i>0
±2 deg ±4 ±6 ±8 ±10 ±12 ±14 ±16 deg ±18 ±20 >±20

FIGURE 2.—Absolute magnitude (top) and algebraic magnitude (bottom) of angle of indraft, i, at 300 mb.

The magnitudes of the zonal and meridional wind components are indicated in the lower diagram of figure 1. These data demonstrate the well known fact that the mean value of the zonal wind component (here 30 m. sec.$^{-1}$) is considerably larger than the mean value of the meridional wind component (17 m. sec.$^{-1}$).

The absolute magnitude of the angle of indraft, indicated in the top diagram of figure 2, is based on 635 calculations. The mode is indistinct and lies in the range 0–6 degrees, while the median is 8 degrees and the mean is 11 degrees. In 15 percent of the cases the angle exceeds 20 degrees. The considerable difference between median and mean is attributable to a relatively few large values of the angle of indraft of doubtful validity. For comparison, Godson found by substituting synoptic wind data at 700 mb. in the equation of motion a mean value of 14 degrees for the angle of indraft. The larger mean mean value for his data would be expected since the magnitude of the angle of indraft is inversely proportional to the wind speed, as shown in section 6 of this paper.

In the lower diagram of figure 2 is shown the algebraic magnitude of the angle of indraft, considered positive when the flow is toward low pressure and negative when the flow is toward high pressure. It is evident from the cumulative frequency curves in this diagram that in the mean the angle of indraft is of greater magnitude when the flow is toward high pressure than when the flow is toward low pressure. It is believed that this tendency is at least partially connected with the occasional loss of geostrophic control in regions of inertial instability in the deceleration region downstream from sharply curved ridges.

The magnitude of the vector geostrophic deviation $|\mathbf{V}-\mathbf{V}_g|$ is indicated in the upper diagram of figure 3. The mode is 2–4 m. sec.$^{-1}$, the median is 10 m. sec.$^{-1}$ and the mean is 12 m. sec.$^{-1}$. In 15 percent of the cases the deviation is greater than 20 m. sec.$^{-1}$. For comparison, Machta found an average value of 13 m. sec.$^{-1}$ for the vector geostrophic deviation at 300 mb. during the winter months. His data were obtained by comparing the wind and pressure gradient (geostrophic wind) on analyzed synoptic maps.

The absolute magnitudes of the cross-contour ($V \sin i$) and along-contour ($V-V_g$) components of the vector geostrophic deviation are given in the lower diagram of figure 3. In the case of the cross-contour component, the

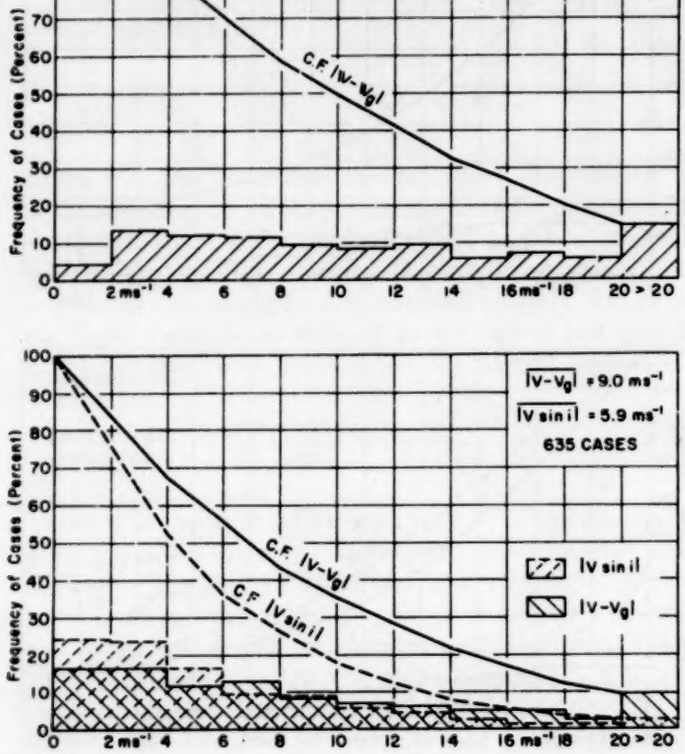

FIGURE 3.—Magnitude of the 300-mb. vector geostrophic deviation, $|\mathbf{V}-\mathbf{V}_g|$, (top) and its cross-contour, $|V \sin i|$, and along-contour, $|V-V_g|$, components (bottom).

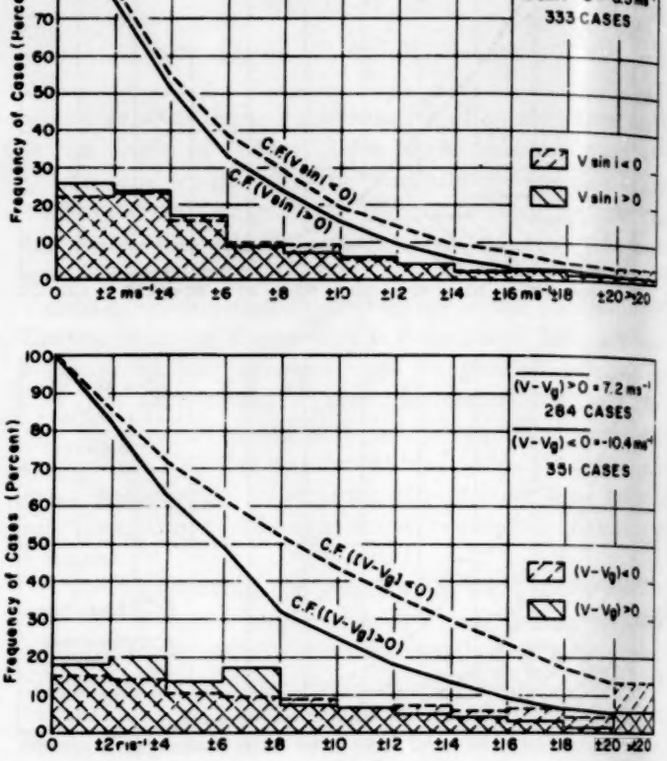

FIGURE 4.—Algebraic magnitude of the 300-mb. cross-contour flow, $V \sin i$, (top) and along-contour component of the vector geostrophic deviation, $V-V_g$, (bottom).

mode, the median, and the mean are respectively 0–4 m. sec.$^{-1}$, 4 m. sec.$^{-1}$, and 6 m. sec.$^{-1}$ whereas for the along-contour component they are, respectively, 0–4, m. sec.$^{-1}$, 7 m. sec.$^{-1}$, and 9 m. sec.$^{-1}$. In the case of the cross-contour component, 10 percent of the values exceed 13 m. sec.$^{-1}$ whereas in the case of the along-contour component, 10 percent of the values exceed 19 m. sec.$^{-1}$. For comparison, Neiburger et al. found at 700 mb. a mean value of 3 m. sec.$^{-1}$ for the along-contour component of the vector geostrophic deviation. This smaller value would be expected since the magnitude of this component is a function of the wind speed, as will be shown below.

The algebraic magnitude of the cross-contour flow is shown in the upper diagram of figure 4. In agreement with the findings for the angle of indraft, the cumulative frequency curves indicate that the magnitude of the cross-contour flow is greater when the flow is toward high pressure than when the flow is toward low pressure.

The algebraic magnitude of the along-contour component of the vector geostrophic deviation is given in the lower diagram of figure 4. In this diagram the difference between the cumulative frequency curves is striking indeed, with the difference between the wind speed and geostrophic wind speed being much larger, in the mean, when the flow is cyclonic than when the flow is anticyclonic. The respective median values are -8 m. sec.$^{-1}$ and 6 m. sec.$^{-1}$. It may be that this asymmetry is due to the existence of a type of upper bound on the degree to which the wind may be supergeostrophic on ridges (twice the geostrophic value), whereas there is no such bound in troughs.

4. ERRORS RESULTING FROM THE USE OF GEOSTROPHIC AND GRADIENT WIND EQUATIONS

The magnitude of the partial acceleration ($\partial\mathbf{V}/\partial t+\mathbf{V}\cdot\nabla\mathbf{V}$) in comparison with the Coriolis acceleration (fV) is of interest since the geostrophic assumption states that the partial acceleration is negligible in comparison with the Coriolis acceleration. The magnitude of the ratio of partial acceleration and Coriolis acceleration is given in the upper diagram of figure 5. The mode of the ratio is roughly 0.10–0.20 while the median is 0.29 and in 10 percent of the cases the ratio exceeds 0.83. In other words these data suggest that,

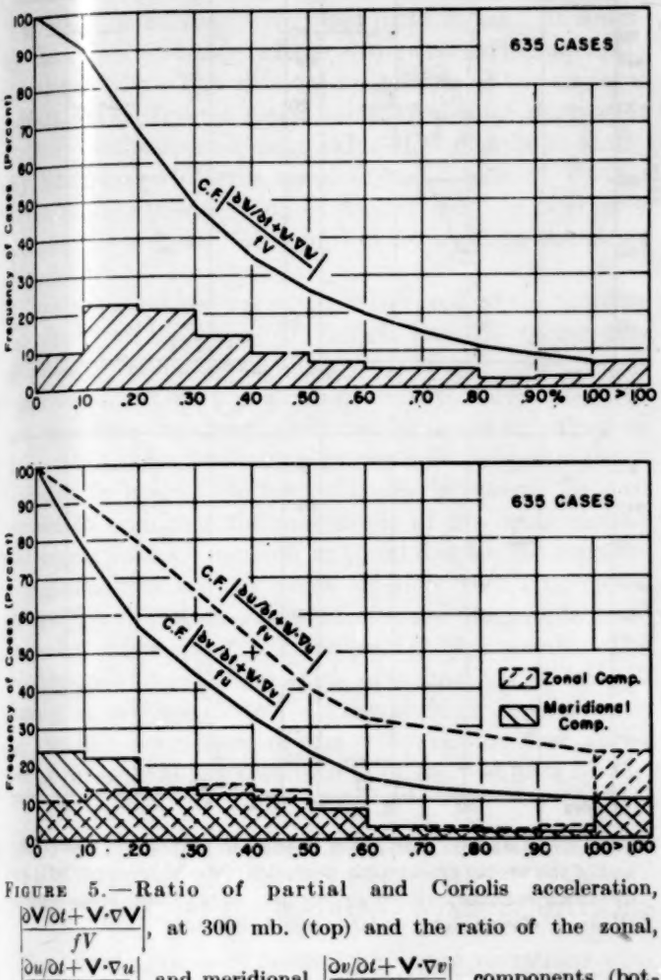
635 CASES
Frequency of Cases (Percent)
C.F. |∂V/∂t+V·∇V / fV|
0 .10 .20 .30 .40 .50 .60 .70 .80 .90% 1.00 > 1.00
635 CASES
Frequency of Cases (Percent)
C.F. |∂u/∂t+V·∇u / fu|
C.F. |∂v/∂t+V·∇v / fu|
Zonal Comp.
Meridional Comp.
0 .10 .20 .30 .40 .50 .60 .70 .80 .90 1.00 > 1.00

FIGURE 5.—Ratio of partial and Coriolis acceleration, $\left|\frac{\partial V/\partial t+\mathbf{V}\cdot\nabla\mathbf{V}}{fV}\right|$, at 300 mb. (top) and the ratio of the zonal, $\left|\frac{\partial u/\partial t+\mathbf{V}\cdot\nabla u}{fv}\right|$, and meridional, $\left|\frac{\partial v/\partial t+\mathbf{V}\cdot\nabla v}{fu}\right|$, components (bottom).

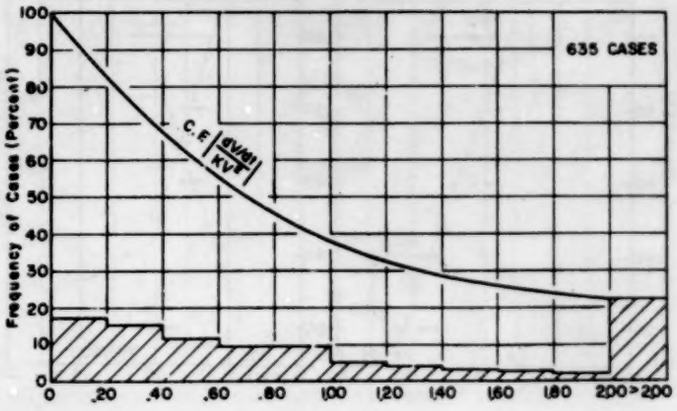

FIGURE 6.—Ratio of tangential and normal components of partial acceleration, $\left|\frac{dV/dt}{KV^2}\right|$, at 300 mb.

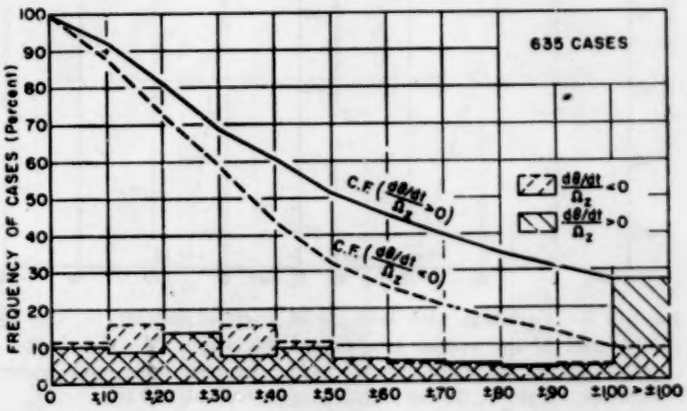

FIGURE 7.—Algebraic ratio of the angular velocity of the wind and the angular velocity of the earth about the local vertical $(d\theta/dt)/\Omega_z$ at 300 mb.

through the introduction of the geostrophic approximation, half the time an error exceeding 29 percent is introduced into the derived results.

The magnitudes of the ratios of zonal and meridional components of partial acceleration and Coriolis acceleration are given in the lower diagram of figure 5. These data suggest that the neglect of the acceleration in the zonal component of the equation of motion results in an untenable approximation, since for this component the mode of the ratio is 0.30–0.40 and the median is 0.41. In the case of the meridional component of the equation of motion, however, the ratio of partial acceleration and Coriolis acceleration has a mode of only 0–0.10 and a median value of only 0.25. In this diagram the relatively large percentage of cases where the ratio exceeds 1.00 is due mainly to the existence of "cusp" points in the trajectories. At such points the velocity component may go toward zero at a time when the component of the partial acceleration is far from zero.

The magnitude of the ratio of tangential and normal components of partial acceleration is of interest since the gradient wind approximation assumes the tangential component to be negligible in comparison with the normal component. It is seen from figure 6 that the mode of this ratio is 0–0.20 while the median is 0.67. In 38 percent of the cases the tangential component of the partial acceleration is larger than the normal component. From consideration of the median ratio of the tangential and normal components of partial acceleration and the median ratio of partial acceleration and Coriolis acceleration we estimate that through the use of the gradient wind approximation half the time an error exceeding 11 percent is introduced into the derived results.

5. FREQUENCY OF OCCURRENCE OF "ABNORMAL" FLOW

In figure 7 is indicated the ratio of the algebraic angular velocity of the air parcel or transosonde and the angular velocity of the earth about the local vertical. It is seen that in 27 percent of the cases the angular velocity of the air parcel exceeds that of the earth about the local vertical

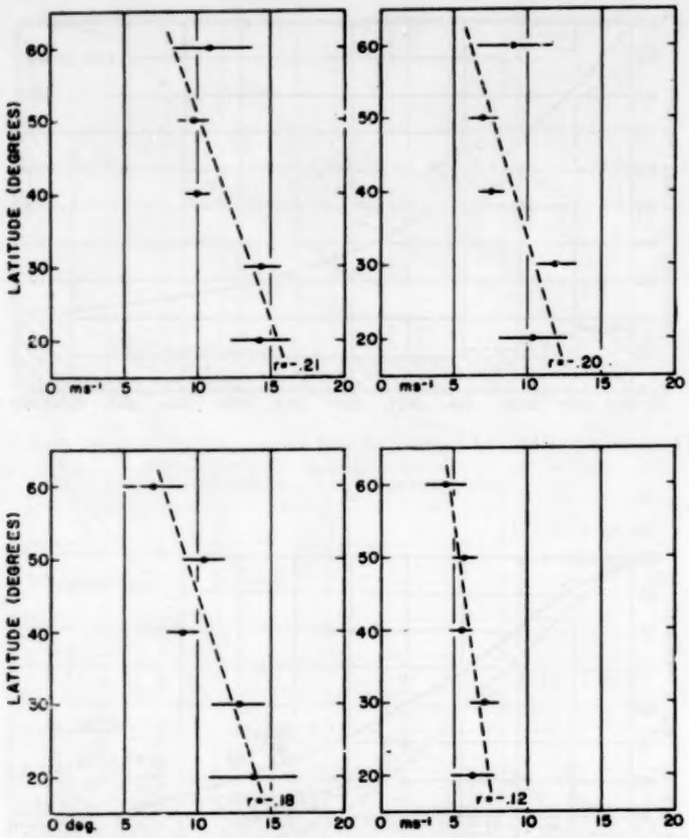

FIGURE 8.—Variation with latitude of angle of indraft, $|i|$, (lower left), and of the vector geostrophic deviation, $|\mathbf{V}-\mathbf{V}_g|$, (upper left) and its along-contour, $|V-V_g|$, (upper right) and cross-contour, $|V \sin i|$, (lower right) components at 300 mb.

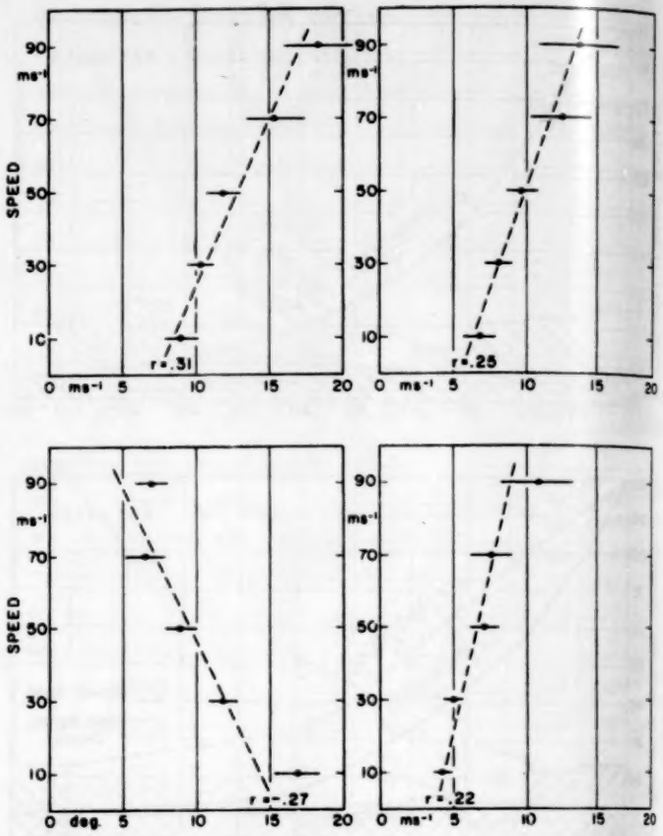

FIGURE 9.—Variation with speed of angle of indraft, $|i|$, (lower left), and of the vector geostrophic deviation, $|\mathbf{V}-\mathbf{V}_g|$, (upper left) and its along-contour, $|V-V_g|$, (upper right) and cross-contour, $|V \sin i|$, (lower right) components at 300 mb.

when the angular velocity is positive (cyclonic flow), but that this criterion is satisfied in only 9 percent of the 398 cases when the angular velocity of the air parcel is negative (anticyclonic flow). Thus in 5 percent of the total 635 cases the flow allegedly possesses anticyclonic rotation in space. Flow which satisfies this criterion is called "abnormal" or "anomalous" flow by Holmboe et al. [7] and Gustafson [8].

6. VARIATION OF AGEOSTROPHIC PARAMETERS WITH LATITUDE AND SPEED

In this section and in section 7 the data are presented in the form of group means, regression lines, and correlation coefficients (figs. 8–11). On either side of the group means, lines have been drawn extending a distance equal to two standard errors from the mean. If the data are randomly drawn from a normal population there is only a 5 percent chance that the true group mean lies outside the extent of these lines. An estimate of significance of variability at the 5 percent level can then be obtained by noting whether a straight vertical line can be drawn so as to intersect all these lines extending either side of the group mean. The regression lines and correlation coefficients serve to yield an indication of the overall trend but it is not meant to imply thereby that these trends are actually linear in nature. It is also possible to determine the correlation coefficient which would indicate significance at the 5 percent level. Based on the z transformation presented in Hoel [9], it is found that for the number of cases available here a correlation greater than ± 0.08 is significant at the 5 percent level.

With regard to the variation of the parameters with respect to latitude it must be emphasized that the results are biased since the transosondes sample chiefly cyclonic flow patterns at southerly latitudes and anticyclonic flow patterns at northerly latitudes. If transosondes were released from stations along a given meridian but at different latitudes, it is probable that different mean values would be found from those presented below.

Figure 8 gives the variation with latitude of the absolute magnitude of the angle of indraft and the vector geostrophic deviation and its along-contour and cross-contour components. All four parameters decrease in magnitude with increasing latitude, with the smallest decrease being found for $V \sin i$ ($r=-0.12$). The group means show that the variability is ragged. The magnitude of

the vector geostrophic deviation varies from a mean of 10 m. sec.$^{-1}$ at northerly latitudes to 14 m. sec.$^{-1}$ at southerly latitudes with most of the change occurring abruptly at latitude 35°. The absolute magnitude of the angle of indraft varies from a mean value of about 8 degrees at northerly latitudes to a mean value of 13 degrees at southerly latitudes, while the absolute magnitude of $V \sin i$ varies from a mean value of 4–5 m. sec.$^{-1}$ in northerly latitudes to a mean value of 7–8 m. sec.$^{-1}$ in southerly latitudes.

Figure 9 gives the variation with speed of the absolute magnitude of the angle of indraft and the vector geostrophic deviation and its along-contour and cross-contour components. While the angle of indraft shows a significant decrease in magnitude with increase in speed ($r=-0.27$) the ageostrophic parameters show significant increases in magnitude with increase in speed. It is of interest to note that the magnitude of the cross-contour flow increases with increase in speed despite the counteracting tendency of the angle of indraft. The vector geostrophic deviation varies in average magnitude from 8 m. sec.$^{-1}$ at low speeds to 18 m. sec.$^{-1}$ at high speeds. The absolute magnitude of the angle of indraft varies from 17 degrees at low speeds to 7 degrees at high speeds, while the absolute magnitude of the cross-contour flow varies from 4 m. sec.$^{-1}$ at low speeds to 11 m. sec.$^{-1}$ at high speeds.

7. VARIATION WITH LATITUDE AND SPEED OF ERRORS RESULTING FROM THE USE OF GEOSTROPHIC AND GRADIENT WIND EQUATIONS

The two diagrams in figure 10 give the variations with latitude of the ratio of partial acceleration and Coriolis acceleration and the ratio of tangential and normal components of partial acceleration. As would be expected, the ratio of partial acceleration and Coriolis acceleration varies greatly with latitude ($r=-0.32$), ranging from a mean value of 0.30 at northerly latitudes to a mean value of 0.70 at southerly latitudes. The group means indicate that the ratio is almost constant north of latitude 40°, with a rapid, nearly linear increase in the value of the ratio as one progresses southward from latitude 40°. The ratio of the tangential and normal components of the partial acceleration shows little variation with latitude ($r=-0.03$). The group means also indicate no significant variations except at latitude 60° where the large values of the normal components of partial acceleration on the crests of trajectories overbalance the tangential components.

The two diagrams in figure 11 give the variations with speed of the ratio of partial acceleration and Coriolis acceleration and the ratio of tangential and normal components of partial acceleration. As would be expected, the ratio of partial acceleration and Coriolis acceleration shows a significant decrease in magnitude with increase in speed ($r=-0.38$) with the mean value of the ratio

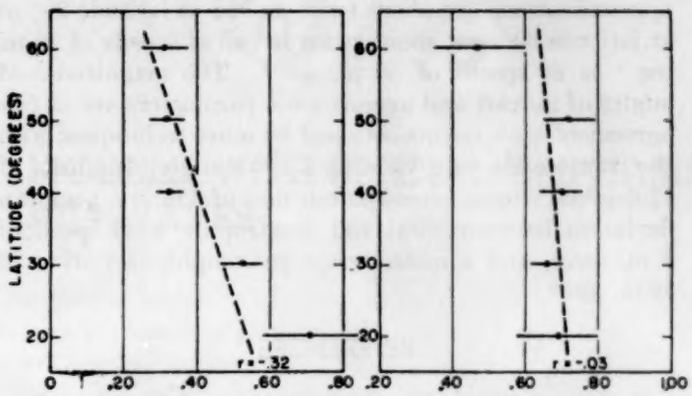

FIGURE 10.—Variation with latitude of ratio of partial and Coriolis acceleration, $\left|\frac{\partial \mathbf{V}/\partial t + \mathbf{V}\cdot\nabla\mathbf{V}}{fV}\right|$, (left) and ratio of tangential and normal components of partial acceleration, $\left|\frac{dV/dt}{KV^2}\right|$, (right) at 300 mb.

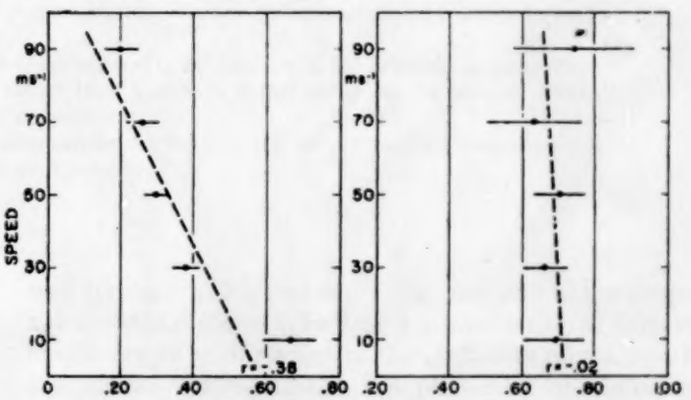

FIGURE 11.—Variation with speed of ratio of partial and Coriolis acceleration, $\left|\frac{\partial \mathbf{V}/\partial t + \mathbf{V}\cdot\nabla\mathbf{V}}{fV}\right|$, (left) and ratio of tangential and normal components of partial acceleration, $\left|\frac{dV/dt}{KV^2}\right|$, (right) at 300 mb.

varying from 0.66 at low speeds to 0.20 at high speeds. The ratio of tangential and normal components of partial acceleration shows no significant variation with speed ($r=-0.02$), the group means at all speeds resting close to 0.70.

8. CONCLUSION

Statistics based on 635 evaluations from 300-mb. constant level balloon data indicate that through the use of the geostrophic wind approximation half the time an error greater than 29 percent will be introduced into the derived results, whereas through the use of the gradient wind approximation half the time an error greater than 11 percent will be introduced into the derived results. On a percentage basis both the geostrophic and gradient wind

approximations are about twice as bad at latitude 20° as at latitude 60° and about twice as bad at speeds of 10 m. sec.$^{-1}$ as at speeds of 50 m. sec.$^{-1}$. The magnitudes of angles of indraft and ageostrophic parameters are in fair agreement with results obtained by other techniques, with the transosonde data yielding a mean angle of indraft of 11 degrees, a mean cross-contour flow of 6 m. sec.$^{-1}$, a mean deviation between wind and geostrophic wind speed of 9 m. sec.$^{-1}$, and a mean vector geostrophic deviation of 12 m. sec.$^{-1}$.

REFERENCES

1. M. Neiburger et al., "On the Computation of Wind from Pressure Data," *Journal of Meteorology*, vol. 5, No. 3, June 1948, pp. 87–92.
2. L. Machta, A Study of the Observed Deviations from the Geostrophic Wind, ScD thesis, Dept. of Meteorology, Massachusetts Institute of Technology, 1948. (Unpublished).
3. W. L. Godson, "A Study of the Deviations of Wind Speeds and Directions from Geostrophic Values," *Quarterly Journal of the Royal Meteorological Society*, vol. 76, No. 327, Jan. 1950, pp. 1–15.
4. C. L. Durst and G. H. Gilbert, "Constant-Height Balloons—Calculation of Geostrophic Departures," *Quarterly Journal of the Royal Meteorological Society*, vol. 76, No. 327, Jan. 1950, pp. 75–86.
5. M. Neiburger and J. K. Angell, "Meteorological Applications of Constant-Pressure Balloon Trajectories," *Journal of Meteorology*, vol. 13, No. 2, Apr. 1956, pp. 166–194.
6. A. D. Anderson, "A Study of the Accuracy of Winds Derived from Transosonde Data," (Memo. Rep. 498), Naval Research Laboratory, Washington, D.C., 1955, 10 pp.
7. J. Holmboe, G. E. Forsythe, and W. Gustin, *Dynamic Meteorology*, New York, John Wiley and Sons, 1945, 378 pp.
8. A. F. Gustafson, "On Anomalous Winds in the Free Atmosphere," *Bulletin of the American Meteorological Society*, vol. 34, No. 5, May 1953, pp. 196–201.
9. P. G. Hoel, *Introduction to Mathematical Statistics*, New York, John Wiley and Sons, 1947, 258 pp.

ON BAROTROPIC AND BAROCLINIC MODELS, WITH SPECIAL EMPHASIS ON ULTRA-LONG WAVES

A. WIIN-NIELSEN, Air Weather Service
Joint Numerical Weather Prediction Unit, Suitland, Md.

[Manuscript received April 1, 1959; revised May 22, 1959]

ABSTRACT

The problem of control of the ultra-long waves in numerical prediction is considered. Sections 2–4 contain a discussion of the one-level forecasts. It is shown that the vertical variation of the horizontal wind and the static stability are the main factors in determining the value of divergence at 500 mb. An independent estimate of the size of the term governing the ultra-long waves in the atmosphere agrees well with the one determined by Cressman on an empirical basis.

Section 5 points out that any two-parameter model has to contain an effect similar to the one contained in the one-parameter model controlling the ultra-long waves. A modification of a two-parameter model is made in such a way that the ultra-long waves are controlled.

Section 6 describes a perturbation analysis of the model developed in Section 5 in order to investigate the effect of the modification also on the shorter waves. It is found that a certain stabilization of the shorter waves is produced. Baroclinic instability and growth rate are investigated.

Sections 7 and 8 contain a justification of certain approximations used in the earlier sections regarding the vertical variation of static stability and the profile of vertical velocity.

1. INTRODUCTION

The Joint Numerical Weather Prediction Unit has recently improved the 500-mb. barotropic forecasts by paying special attention to the behavior of the very long atmospheric waves. The non-divergent barotropic forecasts were first empirically corrected by Wolff [18], who used the observed fact that the very long atmospheric waves do not change either position or ampltitude to any great extent from day to day. He therefore forced the waves with wave-number one, two, and three to be stationary throughout the forecast period. Shortly after, Cressman [6] used a special case of Phillips' [13] two-layer model to show that a model atmosphere consisting of two homogeneous layers, where the motion in the lower fluid is parallel to the contour of the interface, and where the motion in the upper fluid is negligible, would decrease the retrogression of the very long atmospheric waves to a considerable extent. The forecast equation used by Cressman is the same as the one used by Bolin [2] in his so-called tropopause model. Both of these authors had difficulties in the determination of the proper value for certain constants appearing in the prognostic equation, mainly because a model atmosphere consisting of two homogeneous layers is rather difficult to "translate" to the real atmosphere. Cressman decided therefore to determine the value of the coefficient by computing a number of forecasts on the same data with different values of the coefficient and then choosing the coefficient that gave the best forecast. This procedure may not lead to the proper value of the coefficient, because a minimization of forecast height errors with respect to the coefficient might tend to compensate for correlated, but physically unrelated errors, as was also mentioned by Cressman.

In view of the situation mentioned above it seems to be in order to try to formulate the barotropic, divergent model in such a way that the value of the constants can more easily be related to the real atmosphere. Sections 2 through 4 of this paper are devoted to this purpose.

An analysis of baroclinic instability and especially of the phase-speed of waves in a baroclinic atmosphere, as for instance made by Eliassen [9], shows that the phase-speed for large values of the wavelength approaches the Rossby speed for a non-divergent atmosphere. For large values of the wavelength one actually obtains two solutions for the phase-speed. One of them is not likely to be observed in the atmosphere because it corresponds to a situation where the temperature wave is out of phase with the pressure, corresponding to warm troughs and cold ridges. The other solution is the one approaching the Rossby speed.

This result shows that one will find about the same difficulties as in the non-divergent barotropic model with respect to the ultra-long waves, when one integrates a baroclinic model of the usual type over an almost hemispheric region. It is therefore a necessity to correct the baroclinic forecast equations in such a way that the

511937—59——2

retrogression of the ultra-long waves is reduced to a considerable extent. Section 5 describes a simple two-parameter model where this effect is included.

Recently Burger [3] pointed out that the vorticity equation loses its prognostic value when the wavelength is of the same order of magnitude as the radius of the earth. As long as we base our forecasts on the vorticity equation we can therefore probably not do anything better than express the quasi-stationary character of the ultra-long waves. The two models presented here do therefore not claim to have any skill in the regime of the ultra-long waves. The problem which has been attacked is to incorporate effects in barotropic and baroclinic models which control the long waves and at the same time to investigate the changes which may be caused by such effects on the shorter waves.

2. DERIVATION OF THE PROGNOSTIC EQUATION IN THE BAROTROPIC CASE

In the derivation we shall consider the vorticity equation in the form

$$\frac{\partial \zeta}{\partial t}+\mathbf{V}\cdot\nabla\eta=f_0\frac{\partial \omega}{\partial p} \tag{2.1}$$

where $\mathbf{V}$ is the horizontal wind vector, ζ is the vertical component of the relative vorticity, $\eta=\zeta+f$, f is the Coriolis parameter, and $\omega=dp/dt$ the vertical velocity in a coordinate system with pressure as the vertical coordinate.

This form of the vorticity equation, where the value of the Coriolis parameter in the divergence term is a standard value, $f=f_0$, is consistent with certain general integral constraints, as shown by the author [17], when the horizontal wind in the vorticity advection term is non-divergent. The derivation of the barotropic vorticity equation is usually based upon the equivalent-barotropic atmosphere (Charney [5]), where the horizontal wind in the complete atmosphere is assumed to vary vertically in strength, but not in direction. It is then shown that the simple barotropic vorticity equation can be applied to the vertical mean flow in the atmosphere provided the effect of surface pressure changes is neglected. The assumption

$$\mathbf{V}=A(p)\mathbf{V}^* \tag{2.2}$$

which defines the equivalent-barotropic atmosphere and where $\mathbf{V}^*$ for instance may be taken as the 500-mb. flow, will in general apply with good accuracy in a layer around the 500-mb. level, while the accuracy becomes smaller the farther we are from the 500-mb. level. We shall in the following make use of (2.2) only in a thin layer around the 500-mb. level. Equation (2.2) expresses then, according to the geostrophic thermal wind relation, that the thermal wind is parallel to the wind itself, or in other words that the isotherms at 500 mb. are parallel to the contour lines. The last requirement is probably fulfilled to the greatest extent in the mid-troposphere, while temperature advection by the horizontal wind is greater both higher up and lower down in the troposphere, according to observations.

The equivalent-barotropic atmosphere is usually treated without any reference to the thermodynamics of the atmosphere. If, however, the relation (2.2) is approximately satisfied at least around the 500-mb. level it must mean that the local temperature changes to the largest extent are compensated by vertical velocities, and that the adiabatic equation therefore takes the form

$$\frac{\partial}{\partial t}\left(\frac{\partial \phi}{\partial p}\right)+\sigma\omega=0, \quad \sigma=-\alpha\frac{\partial \ln\theta}{\partial p} \tag{2.3}$$

at the 500-mb. level. In (2.3) $\phi=gz$ is the geopotential, α the specific volume, and θ the potential temperature.

The expression (2.2) applies actually to the distribution of the horizontal wind. If the horizontal wind is assumed quasi-geostrophic, we obtain from (2.2):

$$\frac{\partial}{\partial t}\left(\frac{\partial \phi}{\partial p}\right)=\frac{dA}{dp}\frac{\partial \phi^*}{\partial t}. \tag{2.4}$$

The vertical velocity can then be obtained from (2.3) in the form:

$$\omega=-\frac{dA/dp}{\sigma}\frac{\partial \phi^*}{\partial t}. \tag{2.5}$$

We shall further in the thermodynamic equation (2.5) replace the geopotential ϕ^* by a stream function ψ^* satisfying the relation

$$\psi^*=\frac{\phi^*}{f_0}. \tag{2.6}$$

The implication of this assumption in the thermodynamic equation, and only here, has been discussed by Phillips [15]. Introducing (2.6) in (2.5) we obtain:

$$\omega=-\frac{dA/dp}{\sigma}f_0\frac{\partial \psi^*}{\partial t}. \tag{2.7}$$

In order to obtain the prognostic equation from (2.1) it is now necessary to evaluate $\partial\omega/\partial p$ from (2.7). Let us assume for simplicity that dA/dp is a constant. The main problem is then in which way the vertical stability σ varies with pressure. It will be shown (section 7) that a variation of the vertical stability expressed by the formula

$$\sigma=\sigma^*\left(\frac{p}{P}\right)^{-2}, \quad P=500 \text{ mb.} \tag{2.8}$$

describes the vertical variation of temperature in a mean atmosphere with good accuracy. In (2.8) σ^* is the static stability at 500 mb. The accuracy is especially good around 500 mb., because the vertical stability at 500 mb. is used to fit the distribution (2.8) to the atmosphere.

From (2.7) and (2.8) we obtain then, provided $A(p)$ varies linearly with pressure:

$$\left(\frac{\partial \omega}{\partial p}\right)_{500}=-\frac{2f_0}{\sigma^* P}\left(\frac{dA}{dp}\right)\frac{\partial \psi^*}{\partial t} \tag{2.9}$$

which, inserted in (2.1), leads to the prognostic equation:

$$\frac{\partial}{\partial t}(\nabla^2\psi^*-q\psi^*)+J(\psi^*,\eta^*)=0 \tag{2.10}$$

where

$$q=\frac{2f_0^2}{\sigma^* P}\cdot\left(-\frac{dA}{dp}\right). \tag{2.11}$$

3. DISCUSSION OF THE PROGNOSTIC EQUATION

The Helmholz term appearing in (2.10) is in this formulation due to two factors, the increase of the horizontal wind with height and the decrease of temperature with height in the atmosphere. Both of these factors are well known from observations, and it is therefore somewhat easier to determine the proper value of q to be used here than in Bolin's and Cressman's prognostic equations. In order to determine q we need a value for σ^* and for $(-dA/dp)$.

The value for σ^* may be determined from the expression

$$\sigma=-\alpha\frac{\partial \ln\theta}{\partial p}=\frac{R^2T}{gp^2}(\gamma_d-\gamma) \tag{3.1}$$

where R is the gas constant, γ_d the dry adiabatic lapse rate, and γ the local lapse rate.

It has been the general experience among people working with models in numerical prediction that the standard atmosphere is too unstable. Using $\gamma=0.5°$ C. per 100 m., which corresponds to about 80 percent of γ in the standard atmosphere, we obtain:

$$\sigma^*=4.2 \text{ MTS units.} \tag{3.2}$$

We have already assumed that $A(p)$ varies linearly with pressure in the derivation of (2.9). We may now obtain dA/dp by noting that $A(p^*)=1$ according to (2.2) and further assume that $A(2P)=0.2$, which means that the surface wind is about 20 percent of the 500-mb. wind, an assumption used, for instance, in the incorporation of the mountain effect in the barotropic model. This gives:

$$-dA/dp=0.8/P=16\times10^{-3} \tag{3.3}$$

and

$$q\cong1.5\times10^{-12} \tag{3.4}$$

The prognostic equation (2.10) may now be compared with Cressman's prognostic equation reproduced here without the term accounting for the mountain effect:

$$\frac{\partial}{\partial t}\left(\nabla^2\psi^*-\mu\frac{\eta^*}{\overline{\psi^*}}\psi^*\right)+J(\psi^*,\eta^*)=0 \tag{3.5}$$

In this equation the symbols have the same meaning as before. $\overline{\psi^*}$ is a representative mean value of the stream function obtained through the solution of the balance equation, while μ is the coefficient, which actually is equal to $1\Big/\frac{h}{z}\left(1-\frac{\rho'}{\rho}\right)$ where h is the height of the interface, z the height of the 500-mb. surface, and ρ' and ρ the densities of the upper and lower fluid. We are now in the position to evaluate the value of μ, which would correspond to the estimate of q given in (3.4), if we linearize the coefficient in (3.5). We obtain then:

$$\mu=\frac{g\overline{z^*}}{f_0^2}\,q\simeq8 \tag{3.6}$$

This independent estimate of μ is about equal to the highest value of μ used by Cressman in his empirical determination of the coefficient. Cressman varied μ from 0 to 8. It will be seen that μ is inversely proportional to σ^*. A value of σ^* higher than the one used here corresponding to $\gamma=0.5°$C./100 m. is probably not possible as a mean value for the atmosphere. If we therefore accept this value of σ^*, it is found that values of μ less than 8 can be obtained only with $-dA/dp$ smaller than the value used here. It is interesting to note that a value of $\mu=4$, which is the value used at the moment in the operational forecasting, would correspond to $-dA/dp=0.4/P$. This would mean that the surface wind should be about 60 percent of the 500-mb. wind, which sounds unreasonable. On the basis of this discussion one is therefore tempted to conclude that a value of μ somewhat greater than 4 ought to be used.

4. A SIMPLE WAVE ANALYSIS

It is of interest to make a simple wave analysis of the prognostic equation (2.10) in order to obtain a first idea of the influence which different values of q will have on the motion of long and short waves in the atmosphere.

Consider a stream function

$$\psi(x,y,t)=-Uy+Ae^{ik(x-ct)} \tag{4.1}$$

where the superscript * now has been dropped and where $U=$constant is the zonal component of the wind. This stream function will satisfy (2.10) provided the phase speed c satisfies the relation

$$c=\frac{U-\beta/k^2}{1+q/k^2}=\frac{c_{ND}}{1+q/k^2} \tag{4.2}$$

In the derivation of (4.2) $\beta=df/dy$ has been considered as constant and is evaluated at 45° N. $k=2\pi/L$, where L is the wavelength. If N is the number of waves around the hemisphere, i.e., $2\pi R\cos\varphi=N\cdot L$, we may also write (4.2) in the form

$$c=\frac{U-2\Omega R\cos^3\varphi/N^2}{1+qR^2\cos\varphi/N^2} \tag{4.3}$$

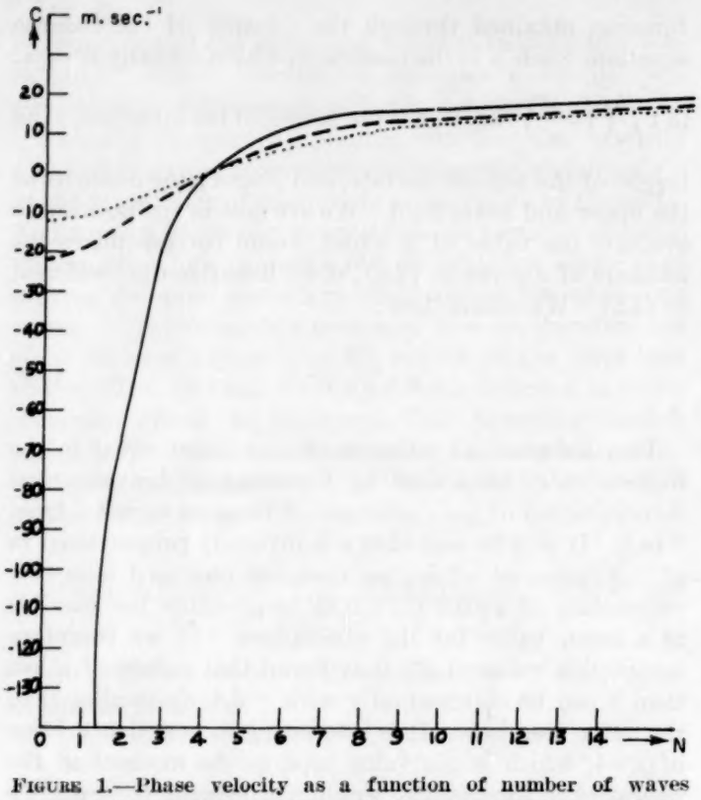

FIGURE 1.—Phase velocity as a function of number of waves around the hemisphere. The solid line corresponds to $q=0$, the dashed line to $q=(3/4)10^{-12}$ and the dotted line to $q=(3/2)10^{-12}$.

The values of c shown in figure 1 in m. sec.$^{-1}$ are computed for $U=20$ m. sec.$^{-1}$, $\varphi=45°$ N., and for $q=0$, $(3/4)\times10^{-12}$, and $(3/2)\times10^{-12}$, which would correspond to approximately $\mu=0$, 4, and 8. It is seen that $q=(3/2)\times10^{-12}$, the value estimated in this study, reduces the retrogression further than the operational value. For wave number 1 the phase-velocity changes from about -19 m. sec.$^{-1}$ to about -11 m. sec.$^{-1}$, while on the other hand c is changed from 12 m. sec.$^{-1}$ to 10 m. sec.$^{-1}$ for $N=8$, corresponding to a wavelength of about 3500 km. It is therefore likely that a change of q from the present value, $(3/4)\times10^{-12}$, to the value determined here, $(3/2)\times10^{-12}$, would not change the forecast appreciably, except for the ultra-long waves, which in fact are better forecasted by the greater value of q, according to Cressman.

5. THE BAROCLINIC CASE

The incorporation of a control of the ultra-long waves in a baroclinic model is complicated by the fact that we want the corrected model to keep essentially the same properties it had for the shorter waves. A pronounced difference between a barotropic and a baroclinic model is that the baroclinic model contains a mechanism for instability by which waves may grow in amplitude. Once we have decided in which way we want to incorporate the control of the long waves we have therefore to investigate whether the phase-speed and the instability criteria for the modified model are left essentially unchanged, or if they are changed, we have to investigate whether the change is in a direction which is supported by observations or experience.

One of the results in the first sections of this paper is that the behavior of the ultra-long waves is sensitive to even very small divergences. We may therefore expect that if we introduce a mean divergence different from zero in a baroclinic model we will be able to control the ultra-long waves. The main problem is to relate the mean divergence to the parameters which carry the history of the flow. It means, for a two-parameter model of the usual type, to a height and a thickness. In the following simple two-parameter model we shall try to introduce such a net divergence in the vertical direction by relating the vertical mean divergence to the flow parameters in a way similar to the one used in the barotropic case treated earlier in this paper.

The prognostic equations we are going to use will be the vorticity equation in the form:

$$\frac{\partial\zeta}{\partial t}+\mathbf{V}\cdot\nabla(\zeta+f)=f_0\frac{\partial\omega}{\partial p} \tag{5.1}$$

and the adiabatic equation

$$\frac{\partial}{\partial t}\left(\frac{\partial\psi}{\partial p}\right)+\mathbf{V}\cdot\nabla\left(\frac{\partial\psi}{\partial p}\right)+\frac{\sigma}{f_0}\omega=0 \tag{5.2}$$

where f_0 is a standard value of the Coriolis parameter.

We shall in the following denote the 200, 400, 600, 800, and 1000-mb. surfaces with subscripts 0, 1, 2, 3, and 4. Applying equation (5.1) to the 400 and 800-mb. surfaces and approximating $\partial\omega/\partial p$ by finite differences we obtain with $P=40$ cb.:

$$\frac{\partial\zeta_1}{\partial t}+\mathbf{V}_1\cdot\nabla(\zeta_1+f)=\frac{f_0}{P}(\omega_2-\omega_0) \tag{5.3}$$

and

$$\frac{\partial\zeta_3}{\partial t}+\mathbf{V}_3\cdot\nabla(\zeta_3+f)=\frac{f_0}{P}(\omega_4-\omega_2). \tag{5.4}$$

We shall in the following apply the approximate boundary condition $\omega_4=0$, thereby disregarding mountain effects in the model. The practice before has been to set $\omega_0=0$. This means that we assume that the vertical velocity has a zero point somewhere between the two zero points at the surface of the earth and at the top of the atmosphere. Although it is true that such a zero point exists in most cases the result is that putting this zero point invariably at 200 mb. reduces the vertical mean divergence in the layer between 200 and 1000 mb. to zero, and we cannot any longer control the long waves. We shall therefore not put $\omega_0=0$, but try to work with the layer between 1000 mb. and 200 mb. as an "open" system.

With $\omega_4=0$ it is now convenient to add and subtract the equations (5.3) and (5.4). At the same time we shall

assume that for any quantity α we have

$$\alpha_2=\frac{1}{2}(\alpha_1+\alpha_3) \tag{5.5}$$

and we shall further introduce the notation:

$$\alpha'=\frac{1}{2}(\alpha_1-\alpha_3). \tag{5.6}$$

Using this procedure we obtain:

$$\frac{\partial\zeta_2}{\partial t}+\mathbf{V}_2\cdot\nabla(\zeta_2+f)+\mathbf{V}'\cdot\nabla\zeta'=-\frac{f_0}{2P}\omega_0 \tag{5.7}$$

$$\frac{\partial\zeta'}{\partial t}+\mathbf{V}_2\cdot\nabla\zeta'+\mathbf{V}'\cdot\nabla(\zeta_2+f)=\frac{f_0}{P}\omega_2-\frac{f_0}{2P}\omega_0. \tag{5.8}$$

By applying the adiabatic equation at 600 mb. the value for ω_2 may now be obtained in the usual way:

$$\frac{f_0}{P}\omega_2=\frac{2f_0^2}{\sigma_2P^2}\left(\frac{\partial\psi'}{\partial t}+\mathbf{V}^*\cdot\nabla\psi'\right)=q\left(\frac{\partial\psi'}{\partial t}+\mathbf{V}^*\cdot\nabla\psi'\right) \tag{5.9}$$

with

$$q=\frac{2f_0^2}{\sigma_2P^2}\simeq\text{constant}. \tag{5.10}$$

The value of $\omega_0/2P$ may be related to the parameters characterizing the flow in the following way. Let us apply the continuity equation at 400 and 800 mb. and obtain

$$\nabla\cdot\mathbf{V}_1=-(\partial\omega/\partial p)_1=-\frac{\omega_2-\omega_0}{P} \tag{5.11}$$

$$\nabla\cdot\mathbf{V}_3=-(\partial\omega/\partial p)_3=\frac{\omega_2}{P}. \tag{5.12}$$

Adding these two equations we obtain:

$$\nabla\cdot\mathbf{V}_2=\frac{\omega_0}{2P}. \tag{5.13}$$

We have on the other hand:

$$\overline{\nabla\cdot\mathbf{V}}=\frac{1}{2P}\int_{P/_2}^{5P/_2}\nabla\cdot\mathbf{V}\,dp=\frac{\omega_0}{2P} \tag{5.14}$$

where $\overline{\nabla\cdot\mathbf{V}}$ is the vertically averaged divergence in the layer between 200 and 1000 mb. According to (5.13) and (5.14) $\nabla\cdot\mathbf{V}_2$ represents within the approximations of the model the vertically averaged divergence. Due to the relation (5.13) we are in the position to express $\omega_0/2P$ by a procedure similar to the one used in the barotropic case.

In the incorporation of the mean divergence in the two-parameter model we should have in mind that we are first of all trying to control the behavior of the ultra-long waves. In the first approximation we are probably therefore allowed to express $\overline{\nabla\cdot\mathbf{V}}$ in the same way as in the barotropic case i.e.,

$$-\frac{f_0}{2P}\omega_0=-f_0\nabla\cdot\mathbf{V}_2=r\frac{\partial\psi_2}{\partial t} \tag{5.15}$$

with

$$r=\frac{f_0^2}{\sigma_2^2}\left(\frac{d\sigma}{dp}\right)_2\frac{dA}{dp}. \tag{5.16}$$

With $f_0=10^{-4}$ sec.$^{-1}$, $\sigma_2=3$ MTS units, $dA/dp=-\frac{0.8}{P}$, and $(d\sigma/dp)_2$ computed from a formula corresponding to (2.8) we arrive at a value of

$$r=2.22\times10^{-12}. \tag{5.17}$$

The assumption (5.15) means that we assume the ultra-long waves to have a small tilt vertically around level 2; i.e. 600 mb. It is realized that this assumption needs further investigation. In a paper by Eliasen [10] it is shown that the tilt of the long waves on the seasonal mean charts is not insignificant in the lower part of the troposphere. On the other hand, a similar Fourier analysis of the long waves at the levels 800, 700, 500, 300, and 200 mb. on a few individual days has in no case shown tilts nearly as great as those found on the normal charts. The assumption (5.15) may therefore in many cases be considered as a good first approximation.

The expression (5.15) could be introduced directly in (5.7) and (5.8). However, diagnostic computations of the vertical profile of the vertical velocity described in section 8, show that $\omega_0\ll\omega_2$. For simplicity we shall therefore neglect the second term on the right side of (5.8) in comparison with the first. This means only that we are neglecting the mean divergence in the troposphere in comparison with the divergence at 400 or 800 mb., which represent the upper and lower parts of the troposphere.

Granted that these approximations can be made we arrive at the following modified forecast equations

$$\frac{\partial\zeta_2}{\partial t}+\mathbf{V}_2\cdot\nabla(\zeta_2+f)+\mathbf{V}'\cdot\nabla\zeta'=r\frac{\partial\psi_2}{\partial t} \tag{5.18}$$

$$\frac{\partial\zeta'}{\partial t}+\mathbf{V}_2\cdot\nabla\zeta'+\mathbf{V}'\cdot\nabla(\zeta_2+f)=q\left(\frac{\partial\psi'}{\partial t}+\mathbf{V}_2\cdot\nabla\psi'\right). \tag{5.19}$$

The only change which in fact has been made is that the term $r\frac{\partial\psi_2}{\partial t}$ has been added to the first prognostic equation, when we compare with the equations for a model where the mean divergence is zero.

It is the purpose of the following section to show that this small modification will control the ultra-long waves in the atmosphere and further to illustrate the changes which we may expect in the short waves using (5.18) and (5.19) as prognostic equations.

6. A PERTURBATION ANALYSIS OF THE BAROCLINIC CASE

Although the final proof of the applicability of a set of prognostic equations always is the successful forecasts

made from them it is of interest to make a simple analysis of the model in order to test it as far as the mathematical technique allows us to do it. The only test which can be made by a relatively simple mathematical technique is a linear perturbation investigation. The two-parameter models where the mean divergence vanishes have been investigated in this way by, for instance, Eliassen [9], Thompson [16], and Phillips [14]. It is therefore of considerable interest to make a comparative study of the model described here and the corresponding model with vanishing mean divergence.

The two parameters that characterize the model are the stream functions ψ_2 and ψ'. Let these be described by the relations

$$\psi_2(x,y,t)=-U_2y+\hat{\psi}_2e^{ik(x-ct)} \tag{6.1}$$

and

$$\psi'(x,y,t)=-U'y+\hat{\psi}'e^{ik(x-ct)} \tag{6.2}$$

where U_2 and U' are constants, $\hat{\psi}_2$ and $\hat{\psi}'$ are the amplitudes, $k=2\pi/L$ is the wave number, and c is the phase-speed (wave velocity).

Inserting (6.1) and (6.2) into (5.18) and (5.19) one finds that ψ_2 and ψ' are solutions to the prognostic equations provided

$$c=\frac{2+r^*}{2(1+r^*)}U_2-\frac{2+r^*+q^*}{2(1+r^*)(1+q^*)}\beta^*\pm\frac{\sqrt{D}}{2(1+r^*)(1+q^*)}. \tag{6.3}$$

For any quantity α the superscript * means

$$\alpha^*=\frac{\alpha}{k^2} \tag{6.4}$$

Further

$$D=[(1+q^*)\,r^*\,U_2+(q^*-r^*)\,\beta^*]^2 -4\,(1+r^*)(q^{*2}-1)U'^2. \tag{6.5}$$

It should be mentioned that the corresponding formula for the usual two-parameter model with vanishing mean divergence simply may be obtained by putting $r^*\equiv 0$. This simple relation makes a comparison between the two models fairly easy.

As we are here especially interested in the ultra-long waves we shall first investigate what happens when $k\to 0$ ($L\to\infty$). Considering the three terms in (6.3) we find directly that

$$\left.\begin{aligned}&\lim_{k\to 0}\frac{2+r^*}{2(1+r^*)}U_2=\frac{1}{2}U_2\\&\lim_{k\to 0}\frac{2+r^*+q^*}{2(1+r^*)(1+q^*)}\beta^*=\frac{r+q}{2rq}\beta\\&\lim_{k\to 0}\frac{\sqrt{D}}{2(1+r^*)(1+q^*)}=\frac{1}{2}U_2+\frac{q-r}{2rq}\beta.\end{aligned}\right\} \tag{6.6}$$

We find therefore that

$$\lim_{k\to 0}c=\begin{cases}U_2-\dfrac{\beta}{q}, & \text{if the plus sign is chosen}\\[2ex] -\dfrac{\beta}{r}, & \text{if the minus sign is chosen}\end{cases} \tag{6.7}$$

The result (6.7) shows that both of these solutions remain finite for $k\to 0$. The interesting solution is the one corresponding to the minus sign. With the numerical values chosen here we find for the latter solution

$$c_{k=0}=-\beta/r=-7.2\ \text{m.sec.}^{-1} \tag{6.8}$$

as compared to $c_{k=0}=-\infty$ for $r=0$ corresponding to a vanishing mean divergence. We may therefore conclude that the model controls the ultra-long waves in the sense that the retrogression is greatly reduced.

Next, we shall investigate in which way the baroclinic instability is being changed by the introduction of a mean divergence. Unstable solutions are found in cases where

$$D<0 \tag{6.9}$$

From the expression (6.5) for D it is seen that only *stable* solutions are possible, when

$$q^*<1$$

With

$$q=\frac{2f_0^2}{\sigma_2P^2}\simeq 4\times 10^{-12}$$

we find that $q^*<1$, if $L<3.1\times 10^3$ km. Consequently all waves with a wavelength smaller than 3100 km. are stable. This result is the same as for the model with vanishing mean divergence.

Unstable solutions are possible if L is greater than this critical wavelength. The division between the unstable and stable region may be found by equating D to zero. It is seen immediately that a certain difference now appears between the models with and without mean divergence. In the case of no mean divergence the division between the stable and unstable region is given by a single relation between the models with and without mean divergence. However, when we have a mean divergence the zonal wind U_2 also enters into the relation. By inspection of (6.5) it is seen that the greater the velocity U_2 is, the greater U' has to be in order to create instability. This relation is illustrated in figure 2, where the critical vertical wind shear $(dU/dz)_c$ expressed now in the unit m. sec.$^{-1}$ km.$^{-1}$ is plotted as a function of wavelength in units of thousands of km. It is seen that the curve for $U_2=20$ m. sec.$^{-1}$ lies higher than the one corresponding to $U_2=10$ m. sec.$^{-1}$. The curve corresponding to no zonal velocity, $U_2=0$ m. sec.$^{-1}$, is also drawn as representing an extreme case. The dashed curve in figure 2 represents $(dU/dz)_c$ as a function of wavelength for the model with vanishing mean divergence. This curve is obtained from (6.5) by putting $r=0$.

Considering first the ultra-long waves we find that they are closer to an unstable situation in the model with mean divergence. However, disregarding the case where $U_2=0$ as an extreme case, we find that vertical wind shears as observed in the atmosphere would never make these waves unstable. We may therefore conclude that we have obtained a considerably reduced retrogression of ultra-long waves without introducing any instability in this part of the spectrum.

Turning our attention toward the smaller wavelength in the spectrum we find that the introduction of a mean divergence in the model changes the instability to some extent. We find for instance with the value of the static stability chosen here that the wavelength of maximum instability is around 4000 km. in both models. However, in the model without mean divergence a vertical shear of only 1.6 m. sec.$^{-1}$ km.$^{-1}$ is necessary to produce instability. The corresponding figures are about 3.1 and 5.8 m. sec.$^{-1}$ km.$^{-1}$ for U_2 equal to 10 m. sec.$^{-1}$ and 20 m. sec.$^{-1}$, respectively. Briefly, we may therefore conclude that the way in which we have introduced the mean divergence into the model tends to stabilize the shorter waves somewhat.

It is a general impression that a two-parameter model without mean divergence will develop pressure systems too much in cases when they actually are deepening. From the result of the instability analysis made here it is seen that a model with mean divergence will counteract this tendency. Actual computations will of course have to prove this tentative conclusion.

It has been pointed out by other investigators (Eady [8], Charney [4]) that according to linear baroclinic instability theory the westerlies should constantly be in a state of instability. The result that the present model seems to decrease the instability makes it interesting to investigate whether this also is the case for this model. Although our instability criterion is derived for flow patterns without horizontal shear we shall nevertheless try to compare the results with the mean state of the real atmosphere. The wavelength of maximum instability seems to be around 4000 km. We shall therefore investigate the problem mentioned above by setting $L=4000$ km. and then computing the critical vertical wind shear as a function of latitude using values of U_2; i.e., U at 600 mb., taken from a mean cross-section of the atmosphere. The critical wind shear may then be compared with the actual wind shear in the mean cross-section. For this purpose the mean cross-section prepared by Hess [11] has been used. The result of the computation is shown in figures 3a and 3b for winter and summer, respectively. A marked difference compared to earlier results is that the mean atmosphere is stable at almost all latitudes. The only exception worth mentioning seems to be north of 60° N. in summer, when the mean atmosphere seems to be a little unstable.

Another measure of the degree of instability which is present in the model is the time it takes to double the

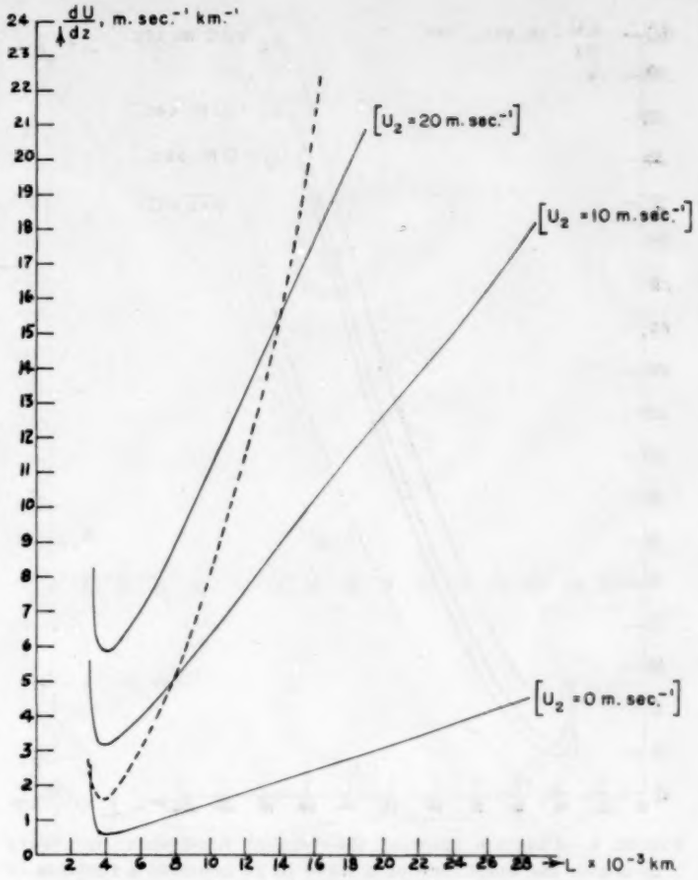

FIGURE 2.—Diagram giving the division between stable and unstable regions for different values of the zonal velocity, U_2. The dashed line is the corresponding curve for a model with vanishing mean divergence. The horizontal axis gives wavelength in thousands of km., the vertical axis vertical wind shear in the unit m. sec.$^{-1}$ km.$^{-1}$.

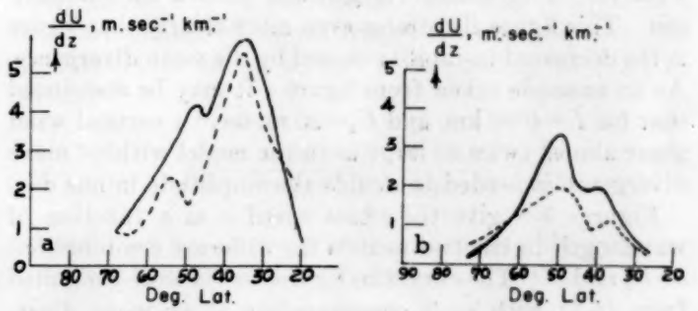

FIGURE 3.—The dashed curves give the averaged vertical wind shear in the layer between 800 and 400 mb. in the unit m. sec.$^{-1}$ km.$^{-1}$ as a function of latitude obtained from Hess' [11] cross-section. The solid curves give the critical wind shear corresponding to the zonal wind as taken from the cross-section at 600 mb. (a) Winter, (b) Summer.

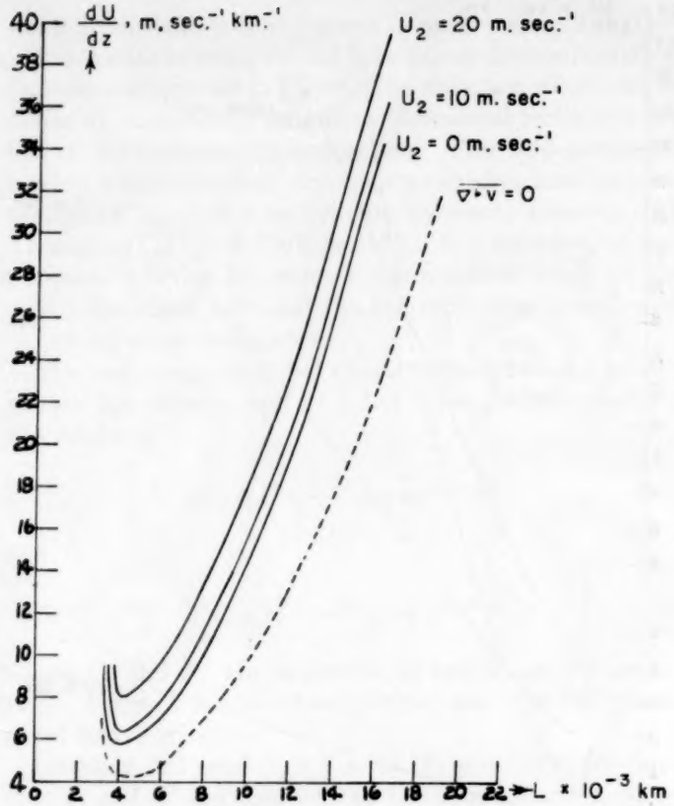

FIGURE 4.—Diagram showing the vertical wind shear necessary to double the amplitude of a wave in 24 hours as a function of wavelength for different values of the zonal velocity U_2. The dashed curve gives the same for the model with vanishing mean divergence.

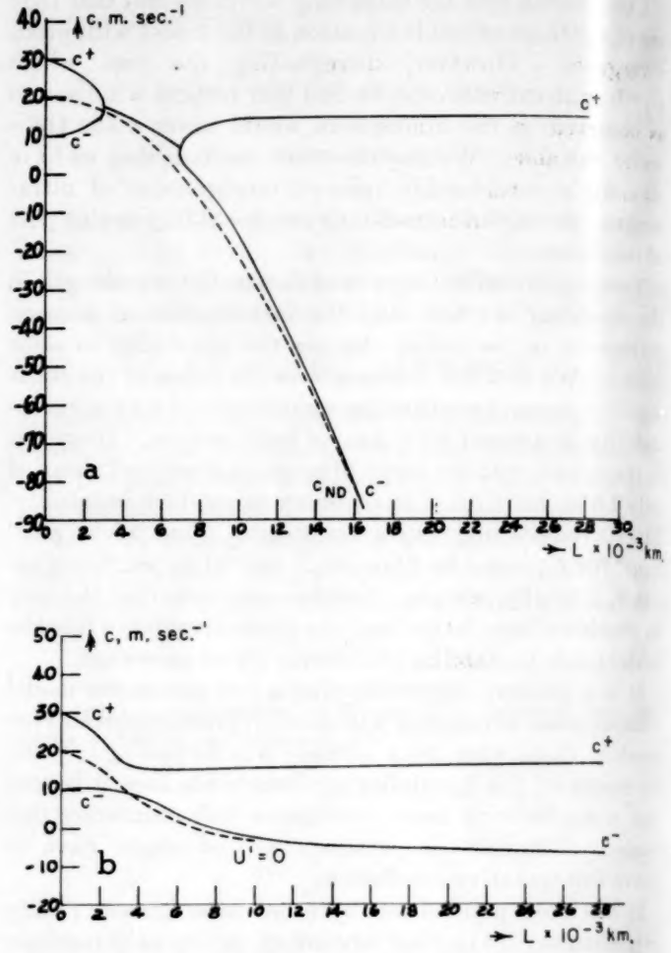

FIGURE 5.—(a) Phase-velocity as function of wavelength for the model without mean divergence, (b) the corresponding figure for a model with mean divergence. The dashed line in (a) is the Rossby speed, while the dashed curve in (b) corresponds to $U'=0$ (no vertical wind shear). Parameters: $U_2=20$ m. sec.$^{-1}$, $dU/dz=4$ m. sec.$^{-1}$ km.$^{-1}$.

amplitude of a certain perturbation. This time will of course also depend on the wind speed U_2 in the model with mean divergence. Figure 4 contains curves giving the vertical wind shear necessary to double the amplitude in 24 hours as a function of wavelength for different values of U_2 in the model with mean divergence. The curve corresponding to the same condition for the model with vanishing mean divergence is plotted for comparison. This figure illustrates even more clearly than figure 2, the decreased instability caused by the mean divergence. As an example taken from figure 4 it may be mentioned that for $L=4000$ km. and $U_2=20$ m. sec.$^{-1}$ a vertical wind shear almost twice as large as in the model without mean divergence is needed to double the amplitude in one day.

Figures 5–8 give the phase speed c as a function of wavelength in the two models for different combinations of U_2 and U'. The curves in figures 5a–8a were computed from (6.3) with $r=0$, corresponding to no mean divergence, and in the figures 5b–8b with $r\neq 0$. The main feature in these figures is of course the great difference between the curves c^- (corresponding to the negative sign in front of the square root), assuring us that no excessive retrogression takes place in the modified model. Figure 5 illustrates a case where the modified model is stable for all wavelengths, while the model without mean divergence actually is unstable in a band from about 3100 km. to about 7000 km. Note also in figure 6 that the modified model is unstable in a shorter interval than the non-modified. This is, however, not invariably so. When the zonal speed U_2 is small and dU/dz is large the modified model will be unstable in a broader band of wavelength. This fact is illustrated in figures 7a and 7b, corresponding to $U_2=10$ m. sec.$^{-1}$ and $dU/dz=8$ m. sec.$^{-1}$ km.$^{-1}$. Figures 8a and 8b finally illustrate a case where $U_2=10$ m. sec.$^{-1}$ and $dU/dz=4$ m. sec.$^{-1}$ km.$^{-1}$. In these diagrams the band of unstable waves is about the same.

Figures 5a–8a contain for comparison the speed of waves in a non-divergent, barotropic atmosphere, the Rossby speed, while figures 5b–8b contain the wave speed corresponding to $dU/dz=0$. For large values of the wavelength the speed for dU/dz 0 and $dU/dz=0$ are

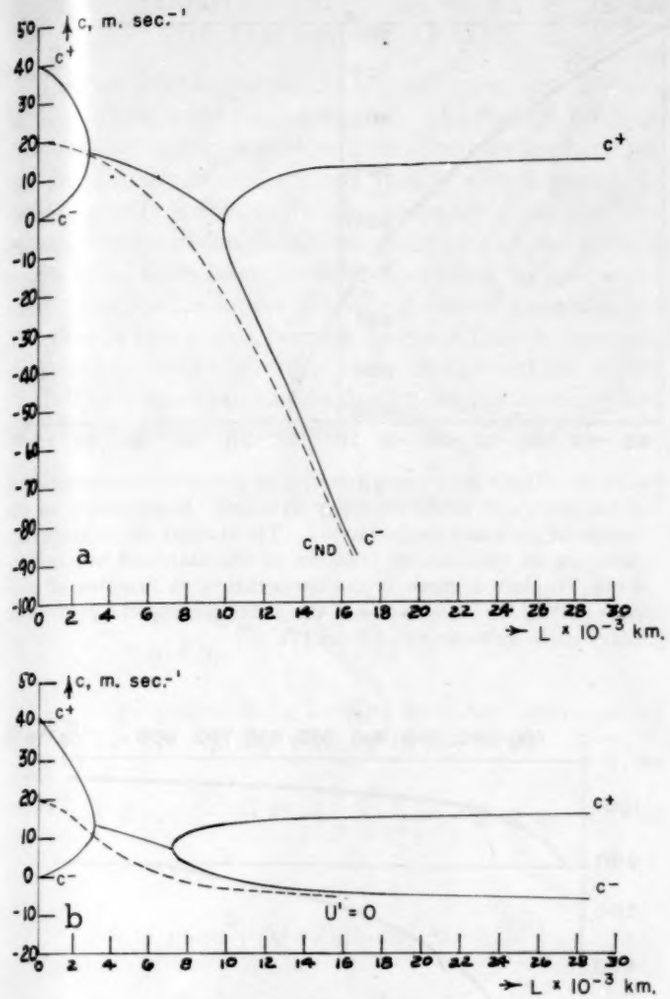

FIGURE 6.—Same as figure 5, but with parameters: U_2=20 m. sec.$^{-1}$, dU/dz=8 m. sec.$^{-1}$ km.$^{-1}$.

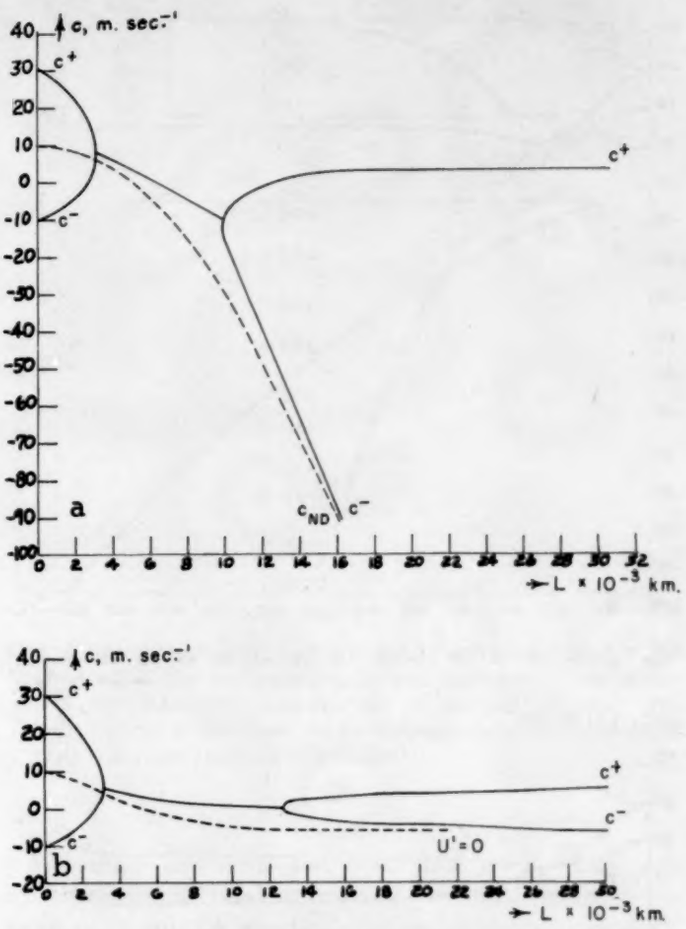

FIGURE 7.—Same as figure 5, but with parameters: U_2=10 m. sec.$^{-1}$, dU/dz=8 m. sec.$^{-1}$ km.$^{-1}$.

about the same, while the speed of the waves in a baroclinic atmosphere is somewhat larger than in an atmosphere with no vertical wind shear.

7. ON THE VERTICAL VARIATION OF STATIC STABILITY

The evaluation of divergence in sections 2 and 5 depends to a large extent on the vertical variation of static stability. We have in the earlier sections used a variation described by (2.8), where the static stability varies inversely to the square of pressure.

The tropospheric part of a mean atmosphere is usually characterized by a certain lapse-rate, $\gamma=-\partial T/\partial z$. The most straightforward way to compute the static stability $\sigma=-\alpha\partial\ln\theta/\partial p$ as it appears in models for numerical integration would therefore be to assume a certain value for γ and then compute the variation of σ. It is, however, of great convenience in many problems to have σ as a rather simple function of pressure. In this section we shall show that a formula of the form (2.8) will describe the vertical variation of temperature in the atmosphere to a good approximation. Let us write (2.8) in the form:

$$\sigma=\frac{a}{p^2} \tag{7.1}$$

where a is a constant determined in such a way that σ at some pressure level, for instance 600 mb., is equal to a standard value determined from a mean atmosphere. Let us next try to find $T=T(p)$ corresponding to (7.1) by writing

$$\sigma=-\alpha\frac{\partial\ln\theta}{\partial p}=\frac{R}{p}\left(\frac{R}{c_p}\frac{T}{p}-\frac{dT}{dp}\right) \tag{7.2}$$

we find that the temperature has to satisfy the following differential equation of the Euler type

$$p\frac{dT}{dp}-\frac{R}{c_p}T+\frac{a}{R}=0. \tag{7.3}$$

The solution to (7.3) is

$$T=T(p)=\frac{a}{R^2}c_p+Cp^{\frac{R}{c_p}}. \tag{7.4}$$

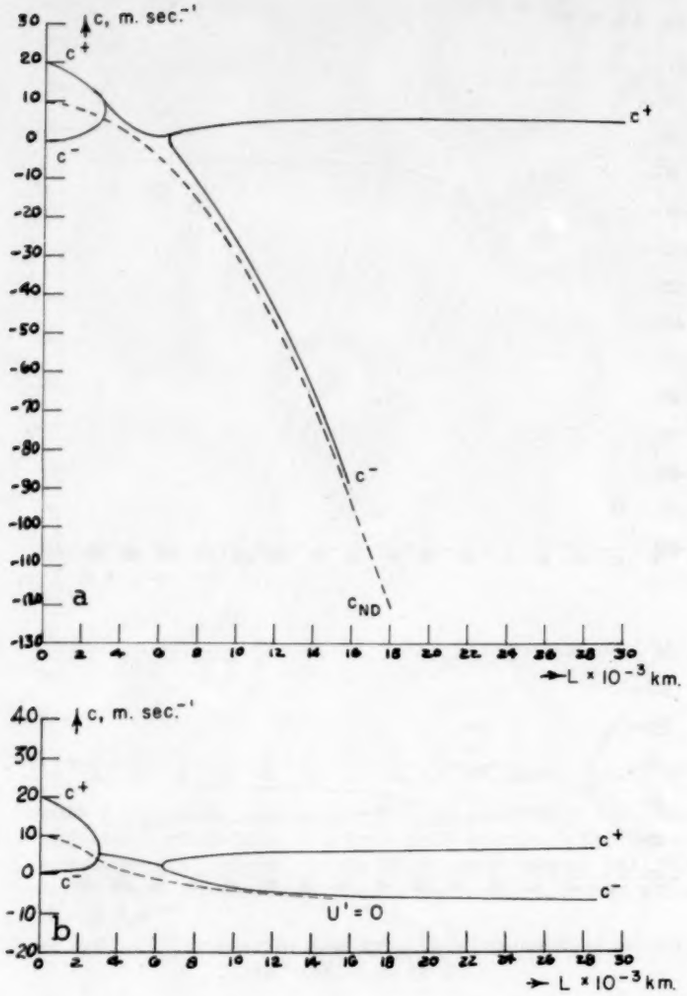

FIGURE 8.—Same as figure 5, but with parameters: $U_2=10$ m. sec.$^{-1}$, $dU/dz=4$ m. sec.$^{-1}$ km.$^{-1}$.

The arbitrary constant C can be determined by fixing the temperature at a certain pressure, say, 600 mb. We obtain then

$$T=T(p)=\frac{a}{R^2}c_p+\left(T_2-\frac{a}{R^2}c_p\right)\left(\frac{p}{p_2}\right)^{\frac{R}{c_p}}. \qquad (7.5)$$

The temperature distribution given by (7.5) is plotted in figure 9 as the full curve. The dashed curve gives the temperature distribution in the standard atmosphere, while the dotted curve is taken from Defant and Taba [7] corresponding to the air mass between the polar-front jet and the subtropical jet. It is seen that the three curves follow each other quite closely, and we may therefore conclude that the assumption (2.8) represents mean conditions in the troposphere in the westerlies quite well.

For use in the next section we shall need the temperature distribution in the stratosphere. For simplicity we shall assume that the stratosphere is isothermal with a temperature corresponding to the one obtained from (7.5)

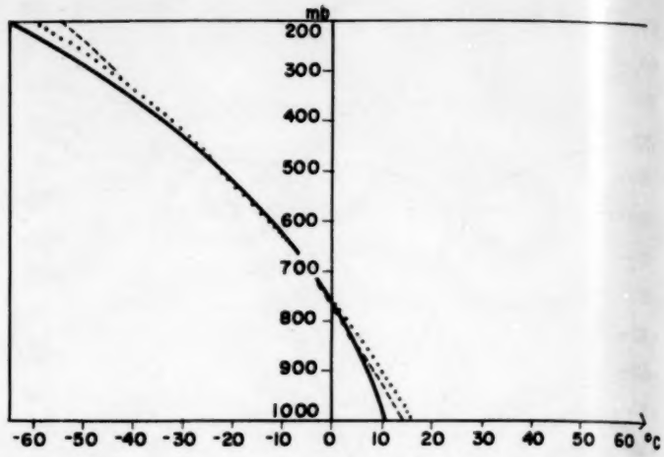

FIGURE 9.—Temperature as a function of pressure corresponding to a variation of static stability inversely proportional to the square of pressure (solid curve). The dashed curve gives temperature as function of pressure in the standard atmosphere, while the dotted curve is the temperature as function of pressure in the air mass between the polar jet and the subtropical jet as given by Defant and Taba [7].

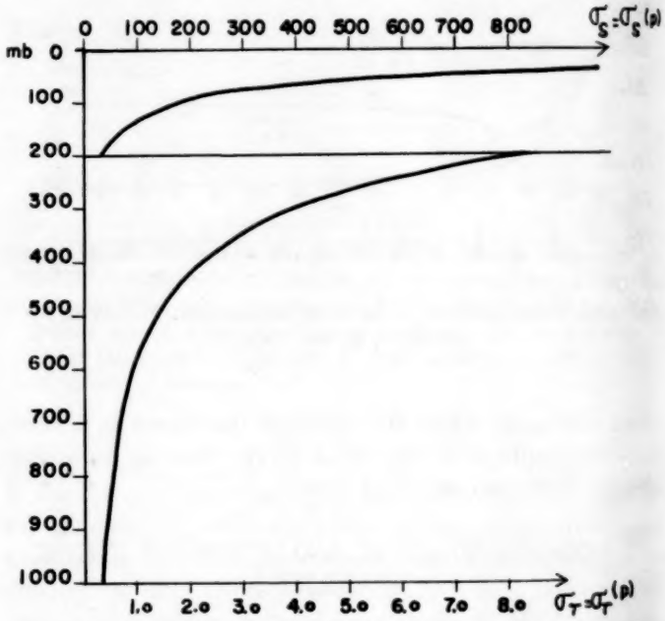

FIGURE 10.—Static stability as a function of pressure in troposphere and stratosphere, when the stability is inversely proportional to the square of pressure.

for $p=p_0=200$ mb. The stability will then vary in the following way:

$$\sigma_S=\frac{R^2T_S}{c_p}\frac{1}{p^2}=\frac{b}{p^2}. \qquad (7.6)$$

The stability profile as determined from (7.1) and (7.6) is shown in figure 10. It is seen that the static stability varies greatly in troposphere and stratosphere and further that the tropopause is characterized by a jump in stability.

8. SOME EXAMPLES OF VERTICAL PROFILES OF THE VERTICAL VELOCITY

In section 5 we neglected the vertical velocity at 200 mb. in comparison with that at 600 mb. As the 200-mb. surface usually in the westerlies is in the stratosphere one can from many considerations justify this neglect. In order actually to measure the ratio between the two quantities certain diagnostic computations of the vertical profile of ω have been performed. These computations were made with a model slightly different from the one described in this paper, because special attention was paid to the influence of the stratosphere on the vertical profile of ω. The ω-equation was obtained from the vorticity and adiabatic equations in the forms

$$\frac{\partial \zeta}{\partial t}+\mathbf{V}\cdot\nabla(\zeta+f)+\omega\frac{\partial \zeta}{\partial p}=(\zeta+f)\frac{\partial \omega}{\partial p} \tag{8.1}$$

and

$$\frac{\partial}{\partial t}\left(\frac{\partial \psi}{\partial p}\right)+\mathbf{V}\cdot\nabla\left(\frac{\partial \psi}{\partial p}\right)+\frac{\sigma}{f}\omega=0 \tag{8.2}$$

by the usual procedure. In this way we arrive at an equation for the vertical velocity in the form

$$(\nabla^2\psi+f)\frac{\partial^2\omega}{\partial p^2}+\sigma\nabla^2\omega+\frac{k}{p}\frac{\partial\nabla^2\psi}{\partial p}\omega=F(x,y,p) \tag{8.3}$$

with

$$F(x,y,p)=\frac{\partial}{\partial p}(\mathbf{V}\cdot\nabla\eta)-\nabla^2\left(\mathbf{V}\cdot\nabla\frac{\partial \psi}{\partial p}\right). \tag{8.4}$$

In the troposphere we assume that

$$\mathbf{V}=\mathbf{V}_2+A(p)\mathbf{V}', \quad \sigma=\frac{a}{p^2} \tag{8.5}$$

and in the stratosphere that

$$\mathbf{V}=B(p)\mathbf{V}_0, \quad \sigma=\frac{b}{p^2}. \tag{8.6}$$

The functions $A(p)$ and $B(p)$ were in fact determined in such a way that they are consistent with the assumption that $\nabla\sigma=0$ (see Berkofsky [1]) and further such that the wind is continuous at $p=p_0=200$ mb. (see fig. 11). When the approximations (8.5) and (8.6) are introduced in (8.3) we arrive at two equations, one for the troposphere and one for the stratosphere.

As we are here interested in the vertical variation of ω, we shall replace $\nabla^2\omega$ by $-\beta\omega$, where β is an inverse measure of horizontal scale. By doing this we restrict ourselves to a consideration of essentially one scale. β was here chosen as corresponding to the wavelength of maximum instability ($L=4000$ km.). With this restriction the two equations obtained from (8.3) reduce to ordinary differential equations in ω, which then should be solved using appropriate boundary conditions.

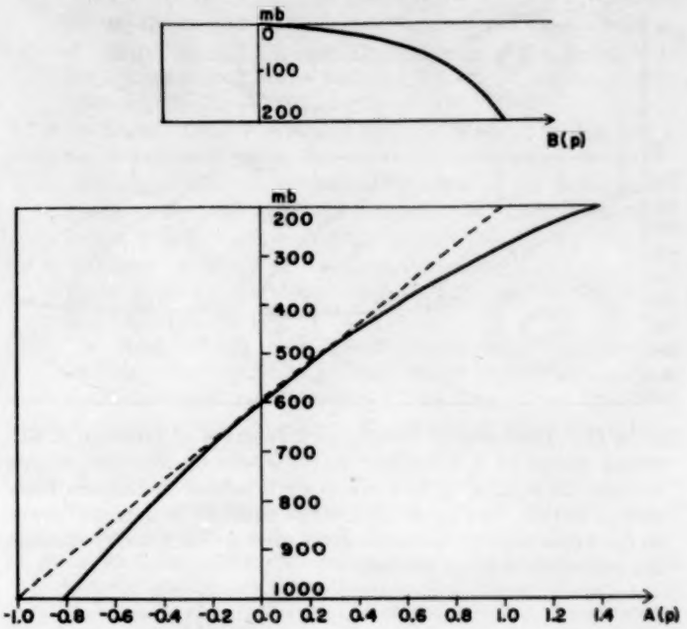

FIGURE 11.—The functions $A(p)$ and $B(p)$ characterizing the variation of the horizontal wind with pressure in the model used for diagnostic computations of vertical velocity. The dashed curve in the lower figure corresponds to the case where $A(p)$ is a linear function of pressure.

We shall use $\omega=0$ for $p=0$ and $p=p_4=1000$ mb. Furthermore, we need an internal boundary condition for $p=p_0=200$ mb., where the solution to the stratospheric equation should be matched together with the solution to the tropospheric equation. The level $p=p_0=200$ mb. represents in the present considerations the tropopause as well as the level of maximum wind. These two levels need not in all cases be the same in reality, but synoptic investigations (Defant and Taba [7]) show that they are close to each other, usually with the level of maximum wind a little lower than the tropopause. We way, therefore, at the level $p=p_0$ apply a boundary condition natural for a discontinuity surface for stability. Such boundary conditions have been treated by Lowell [12]. The vertical velocity should be continuous at the tropopause and further should $(\partial\omega/\partial p)_S\simeq(\partial\omega/\partial p)_T$ which means that the first derivative in the p-direction should be continuous. These two conditions have therefore been applied at $p=p_0$.

The solution to the two equations obtained from (8.3), with the boundary conditions mentioned above, is quite laborious. For the general case it has not been possible to find analytical solutions. A numerical integration of the two equations has therefore been performed. The method used in the numerical solutions has been the Runge-Kutta method, which is most convenient in cases of internal boundary conditions. Examples of solutions are presented in figures 12 and 13. In these cases the stream functions at 600 mb. and for the thermal flow

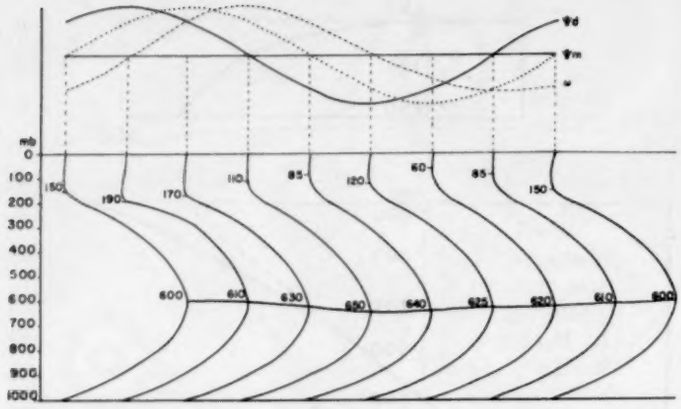

FIGURE 12.—The vertical velocity as a function of pressure in different points of a baroclinic wave, where the thermal stream function is lagging ⅛ of a wavelength behind the stream function at 600 mb. (see upper part of the figure). The dashed curve in the upper part of the figure gives the vertical velocity through the baroclinic wave at 600 mb.

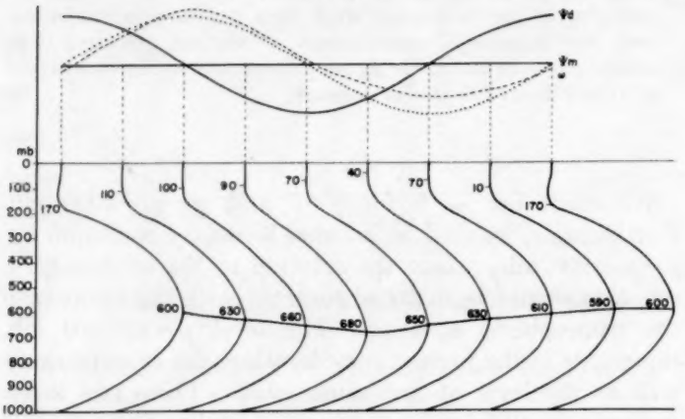

FIGURE 13.—Same as figure 12, but with phase-difference of ¼ of a wavelength between the thermal stream function and the stream function at 600 mb.

between 800 and 400 mb. were specified as simple sinusoidal waves having a certain phase difference. Figure 12 corresponds to the case where the thermal field is lagging ⅛ of the wavelength behind the field at 600 mb., while figure 13 has a phase difference of ¼ of a wavelength. All constants were computed for eight different points. The computation gave then the eight vertical profiles represented in the figures, which in the upper part contain a schematic picture of the temperature and pressure wave and also the horizontal profile through the baroclinic wave of the vertical velocity at 600 mb. On each of the profiles is given the level of maximum vertical velocity and the levels where ω has a zero point different from those at the boundaries. It should further be mentioned that each profile is normalized in such a way that the maximum value is unity.

Of importance for the discussion in the preceding sections are the following features:

(a) A zero point for the vertical velocity appears somewhat higher than the level of maximum horizontal wind. The pressures of the zero points vary systematically through the wave, and we may state that the values of ω obtained above the zero point are extremely small.

(b) ω_0 at 200 mb. is not exactly zero, but it is true that $\omega_0 \ll \omega_2$ where ω_2 is at 600 mb. This characteristic justifies the approximation made in section 5.

(c) The non-divergent level varies systematically through the baroclinic wave with the result that this level does not coincide with a pressure level.

(d) It is a limitation in the present calculation that the tropopause level has been assumed at a constant pressure (200 mb.). In reality we may therefore expect a larger variation of the level of nondivergence.

9. SUMMARY AND CONCLUSIONS

Sections 2–4 contain a derivation and discussion of the prognostic equation for the 500-mb. flow where attention is focused on the term which controls the ultra-long waves. It is shown that the numerical value of the coefficient is related to the vertical variation of the horizontal wind and the corresponding variation of the static stability. The numerical value determined in this way agrees well with the one obtained empirically by Cressman [6] and Bolin [2].

Section 5 generalizes the results obtained in sections 2–4 to a simple two-parameter model. It is shown that the simplest way to control the ultra-long waves in a baroclinic model is to introduce a mean divergence in the troposphere. The mean divergence may in the first approximation be estimated barotropically corresponding to the well-known fact that the mean motion in the atmosphere is almost barotropic.

The influence of an existing mean divergence in the atmospheric layer under consideration on the baroclinic instability is investigated in section 6. The main result is that the mean divergence stabilizes the shorter waves to some extent, beside the effect of decreasing the retrogression of the ultra-long waves considerably. An application of the stability criteria derived in this section to a mean cross-section for the atmosphere shows that the mean atmosphere is baroclinically stable at almost all latitudes.

A justification of certain approximate relations used in the earlier sections is given in sections 7 and 8 of which the former is concerned with the vertical variation of the static stability, while the latter gives certain diagnostic results of computations of vertical profiles of the vertical velocity.

Any model designed for numerical prediction of tropospheric flow pattern must contain an effect which at least expresses the quasi-stationary behavior of the ultra-long waves. According to results obtained by Burger [3] we

cannot expect to express more than this as long as we use the vorticity equation as the prognostic equation. One possible way of controlling the ultra-long waves is demonstrated in this paper, where we have made use of the observed barotropic character of these waves. Certain modifications of the behavior of shorter waves is also obtained by this procedure. It is quite likely that a more sophisticated introduction of the mean divergence, which seems to be the important quantity, into a tropospheric model may change the behavior of the Rossby type of waves still more.

ACKNOWLEDGMENTS

The author would like to thank Dr. G. P. Cressman and Dr. F. G. Shuman for a number of interesting discussions on the subject treated in this paper.

REFERENCES

1. L. Berkofsky, "A Three-Parameter Baroclinic Numerical-Prediction Model," *Journal of Meteorology*, vol. 13, No. 1, Feb. 1956, pp. 102–111.
2. B. Bolin, "An Improved Barotropic Model and Some Aspects of Using the Balance Equation for Three-Dimensional Flow," *Tellus*, vol. 8, No. 1, Feb. 1956, pp. 61–75.
3. A. P. Burger, "Scale Consideration of Planetary Motions of the Atmosphere," *Tellus*, vol. 10, No. 2, May 1958, pp. 195–205.
4. J. G. Charney, "The Dynamics of Long Waves in a Baroclinic Westerly Current," *Journal of Meteorology*, vol. 4, No. 5, Oct. 1947, pp. 135–162.
5. J. G. Charney, "On a Physical Basis for Numerical Prediction of Large-Scale Motions in the Atmosphere," *Journal of Meteorology*, vol. 6, No. 6, Dec. 1949, pp. 371–385.
6. G. P. Cressman, "Barotropic Divergence and Very Long Atmospheric Waves," *Monthly Weather Review*, vol. 86, No. 8, Aug. 1958, pp. 293–297.
7. F. Defant and H. Taba, "The Break Down of Zonal Circulation During the Period January 8 to 13, 1956, the Characteristics of Temperature Field and Tropopause and its Relation to the Atmospheric Field of Motion," *Tellus*, vol. 10, No. 4, Nov. 1958, pp. 430–450.
8. E. T. Eady, "Long Waves and Cyclone Waves," *Tellus*, vol. 1, No. 3, Aug. 1949, pp. 33–52.
9. A. Eliassen, "Simplified Dynamic Models of the Atmosphere, Designed for the Purpose of Numerical Weather Prediction," *Tellus*, vol. 4, No. 3, Aug. 1952, pp. 145–156.
10. E. Eliasen, "A Study of the Long Atmospheric Waves on the Basis of Zonal Harmonic Analysis," *Tellus*, vol. 10, No. 2, May 1958, pp. 206–216.
11. S. L. Hess, "Some New Mean Meridional Cross Sections Through the Atmosphere," *Journal of Meteorology*, vol. 5, No. 6, Dec. 1948, pp. 293–300.
12. S. C. Lowell, "The Boundary Conditions at the Tropopause," *Tellus*, vol. 3, No. 2, May 1951, pp. 78–81.
13. N. A. Phillips, "A Simple Three-Dimensional Model for the Study of Large-Scale Extratropical Flow Patterns," *Journal of Meteorology*, vol. 8, No. 6, Dec. 1951, pp. 381–394.
14. N. A. Phillips, "Energy Transformations and Meridional Circulations Associated with Simple Baroclinic Waves in a Two-Level, Quasi-Geostrophic Model," *Tellus*, vol. 6, No. 3, Aug. 1954, pp. 273–286.
15. N. A. Phillips, "Geostrophic Errors in Predicting the Appalachian Storm of November 1950," *Geophysica*, vol. 6, No. 3–4, 1958, pp. 389–405.
16. P. D. Thompson, "On the Theory of Large-Scale Disturbances in a Two-Dimensional Baroclinic Equivalent of the Atmosphere," *Quarterly Journal of the Royal Meteorological Society*, vol. 79, No. 339, Jan. 1953, pp. 51–69.
17. A. Wiin-Nielsen, "On Certain Integral Constraints for the Time-Integration of Baroclinic Models," *Tellus*, vol. 11, No. 1, Feb. 1959, pp. 45–59.
18. P. M. Wolff, "The Error in Numerical Forecasts Due to Retrogression of Ultra-Long Waves," *Monthly Weather Review*, vol. 86, No. 7, July 1958, pp. 245–250.

511937—59——4

CORRESPONDENCE

Comments on "The Hurricane Season of 1958"

EUGENE W. HOOVER

District Forecast Office, U.S. Weather Bureau, Washington, D.C.

May 19 1959

In a recent article [1] the Staff, Weather Bureau Office, Miami, Fla., examined the interaction between hurricanes Helene and Ilsa, 1958, and suggested that their relative motion had been counterclockwise. Reexamination of the data shows that the relative motion was clockwise and that some changes should be made in table 1 and figure 7 of the article to take into account the following items:

1. The motion of Ilsa relative to the midpoint must be exactly equal in magnitude but opposite in direction to the motion of Helene relative to the midpoint. This follows because by definition the midpoint remains the same distance from each of the storms. Thus, in table 1 in the columns headed "Ilsa—Midpoint" and "Helene—Midpoint," the two courses at each time should differ by 180° and the two speeds should be equal.

2. The speed of the midpoint cannot exceed the arithmetic mean of the speeds of Helene and Ilsa. Thus, in table 1, under the column headed "midpoint," the speed of 9.6 knots at 0000 GMT on the 27th is not consistent with Ilsa's motion of 335°, 8 knots and Helene's motion of 305°, 10 knots. The midpoint, whose motion is the vector mean of the motions of Helene and Ilsa, should have a speed less than 9 knots.

3. The relative motions of Helene and Ilsa should not be considered with reference to a west-east line, as in figure 7 of the article, but with reference to the line connecting their centers at the beginning of the period, i.e., a line oriented approximately northwest-southeast. The correction of figure 7 by properly reorienting the dashed lines shows that the centers of the two storms had a clockwise, converging relative motion during the last 36-hour period covered by table 1.

It is not suggested here that the concept of interaction between vortices, which calls for counterclockwise relative motion, is not valid, but in this particular case, during the 36-hour period, other factors were exerting a greater influence to produce a net clockwise relative movement of the hurricanes.

REFERENCE

1. Staff, Weather Bureau Office, Miami, Fla., "The Hurricane Season of 1958," *Monthly Weather Review*, vol. 86, No. 12, December 1958, pp. 477–485.

NOTE ON FREQUENCY OF HIGH WINDS OVER THE UNITED STATES

H. E. LANDSBERG AND B. RATNER

Office of Climatology, U.S. Weather Bureau, Washington, D.C.

[Manuscript received April 28, 1959; revised May 20, 1959]

Problems of jet aircraft operations and radioactive fallout have created much interest in high-speed upper-air currents. Also, ever since Rossby's [4] classical paper there has been a lively interest in the dynamics of the jet stream and associated models of atmospheric circulation.

Some earlier climatological assessment of the mean position and strength of the jet stream is contained in the monograph on the jet stream by Riehl et al. [3]. In recent years more reliable observations of high-speed winds have become available. Since 1957 the National Weather Records Center has kept special records on punch cards of all very high wind speeds at United States stations.

For purposes of quick description we set an admittedly arbitrary limit of 100 miles per hour and had a machine compilation made of the frequency of observations equal to or above this value. This collection covers 36 stations with the best upper-wind-observing equipment (either GMD–1 or GMD–1A). It is unlikely that many observations there were missed because of limiting angles.

Although only the data for 1957 and 1958 were available for summarization, the results are sufficiently interesting to warrant a preliminary note. The data are presented in the form of three charts. Lines of equal frequency of occurrence indicate the distribution of high-speed winds in January, July, and for all observations in the two years.

Figure 1 shows the midwinter conditions. The axis of highest frequencies coincides well with the corresponding average position of the jet stream given by Namias and

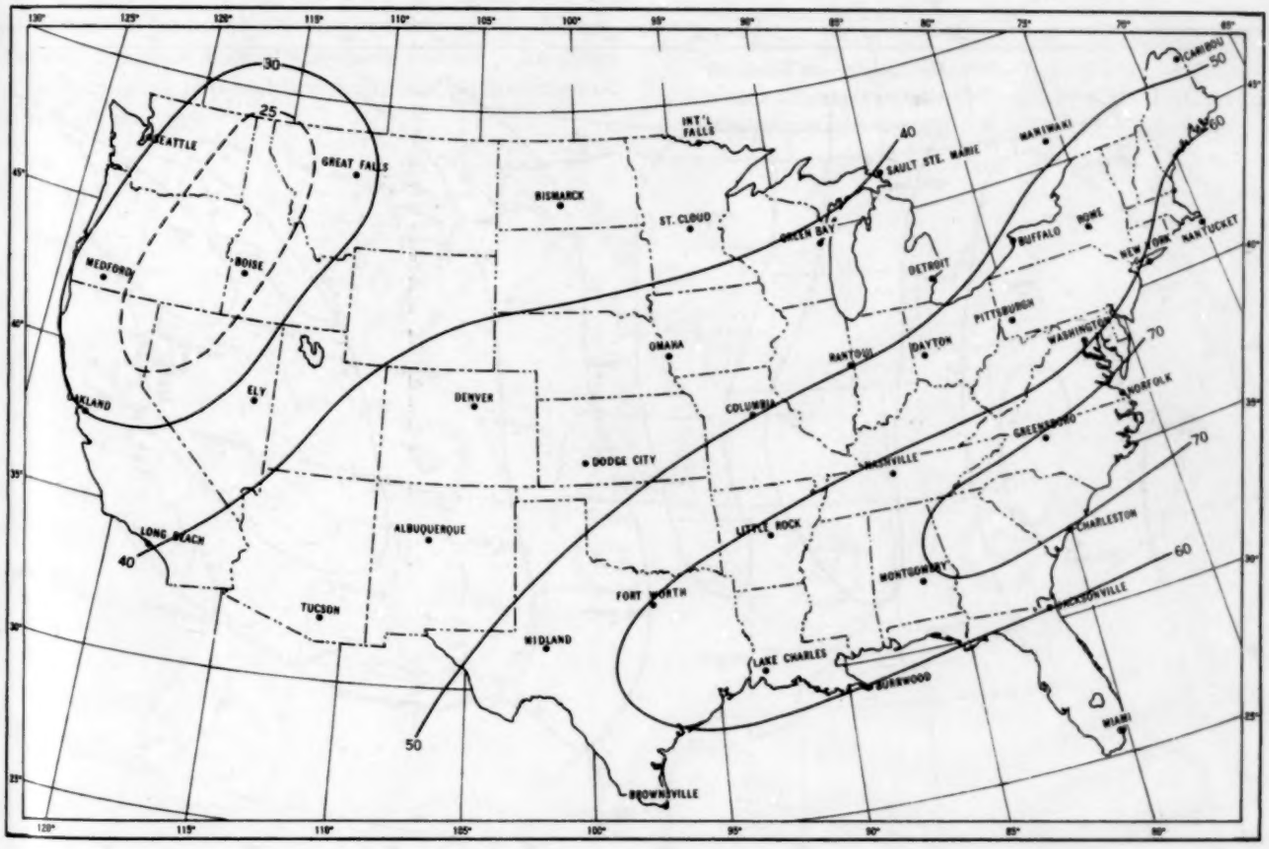

FIGURE 1.—Percentage of soundings with winds ≧ 100 m.p.h. January 1957–58.

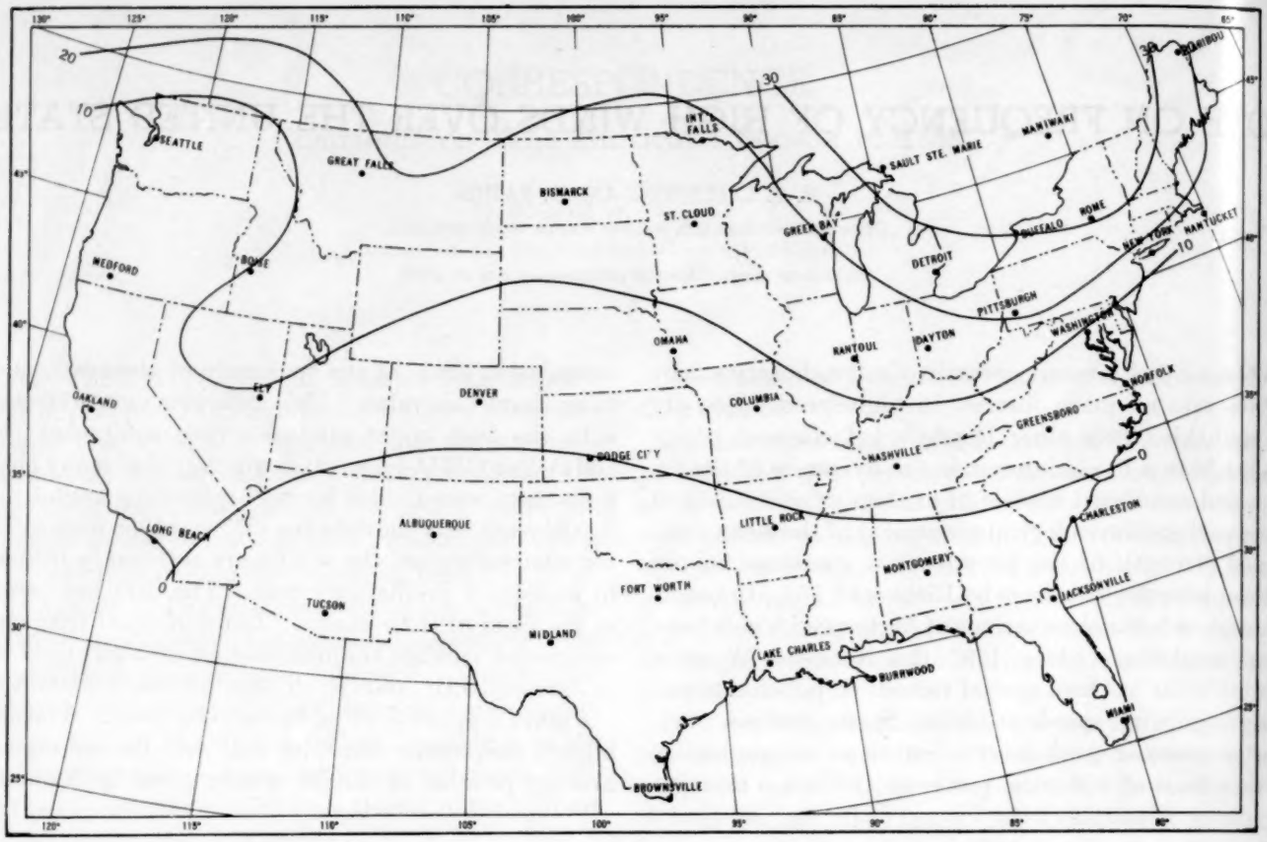

FIGURE 2.—Percentage of soundings with winds ≧ 100 m.p.h. July 1957–58.

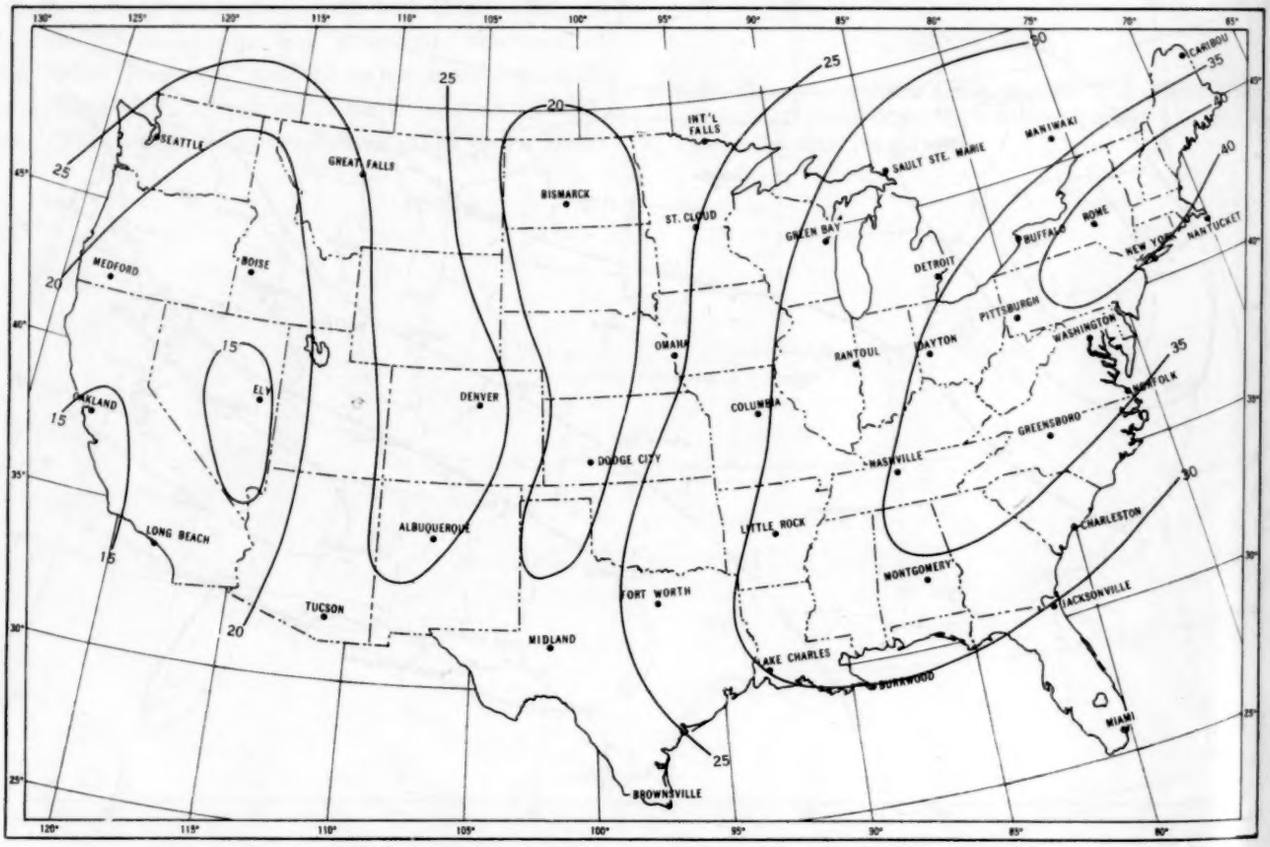

FIGURE 3.—Percentage of soundings with winds ≧ 100 m.p.h. All months 1957–58.

Clapp [2]. It is concentrated just north of the Gulf of Mexico inland and extends eastward to Cape Hatteras. At that point on the Atlantic coast not less than 77 percent of the ascents showed winds ≧100 m.p.h. in the two Januarys.

During July, shown in figure 2, the maximum of high wind frequencies occurs just north of the Great Lakes and extends eastward to the St. Lawrence Valley. A little over 30 percent of the observations in this area show high winds aloft. The core seems to be a little farther east than in the corresponding average jet stream position of Namias and Clapp [2]. This difference may well be caused by the very short record in our series, while their data were based on calculations from mean upper-air charts. Notable in figure 2 is the almost complete absence of winds above 100 m.p.h. south of 35° N. latitude.

The mean annual pattern shown in figure 3, although a mixture of all seasons, has the virtue of having the highest number of observations. These average about 730 per station in the chosen network. The meridional pattern is quite pronounced. There is no zonal high-speed band, at least for the frequencies of winds ≧100 m.p.h. These high speeds are most common over the northeastern area where they reach over 40 percent of all observations. This maximum is located at about 42° N. latitude.

Interesting also is the narrow zone of increased high-speed wind frequency just east of the Rocky Mountains, followed immediately to the east by a minimum over the Great Plains. Also notable is the low frequency of high-speed winds over the central California coast. An effect of the High Sierras is possible but can not be documented by the present network.

The distribution east of the Rocky Mountains can be explained by the presence of a dynamic trough in the lee of the mountains. Boffi [1] discussed this in connection with his analysis of the stream field produced by the Andes. The marked asymmetry of west and east coasts has already been commented upon by Riehl et al. [3]. The northeast maximum in the annual pattern as well as the winter maximum centered over the Carolinas and Georgia would seem to require injection of additional energy into the basic dynamic system envisaged by Rossby [4]. Previous writers have belittled the idea of thermal contrasts being associated with the development of wind patterns. Perhaps in conjunction with conversion of latent heat into kinetic energy the thermal contrasts are likely to contribute both to the frequency and the specific latitudinal distribution of the high speed jet streams.

REFERENCES

1. J. A. Boffi, "Effect of the Andes Mountains on the General Circulation over the Southern Part of South America," *Bulletin of the American Meteorological Society*, vol. 30, No. 7, Sept. 1949, pp. 242–247.
2. J. Namias and P. F. Clapp, "Confluence Theory of the High Tropospheric Jet Stream," *Journal of Meteorology*, vol. 6, No. 5, Oct. 1949, pp. 330–336.
3. H. Riehl, M. A. Alaka, C. L. Jordan, and R. J. Renard, "The Jet Stream", *Meteorological Monographs*, vol. 2, No. 7, American Meteorological Society, Boston, 1954, 100 pp.
4. C.-G. Rossby, "On the Distribution of Angular Velocity in Gaseous Envelopes under the Influence of Large-Scale Horizontal Mixing Processes," *Bulletin of the American Meteorological Society*, vol. 28, No. 2, Feb. 1947, pp. 53–68.

A GRAPHICAL METHOD FOR COMPUTING HORIZONTAL TRAJECTORIES IN THE ATMOSPHERE*

HUGO V. GOODYEAR

Hydrologic Services Division, U.S. Weather Bureau, Washington, D.C.

[Manuscript received November 19, 1958; revised April 30, 1959]

ABSTRACT

Graphical solutions of the horizontal equations of motion are developed for computation of dynamic trajectories. Expedient techniques for using these solutions are discussed. An approximation for the frictional effect is suggested, and graphical application is outlined.

1. INTRODUCTION

The purpose of this paper is (1) to study the quantitative relationships between the changes of the pressure field encountered by a parcel and the changes in its velocity, and (2) to apply the relationships to the construction of horizontal trajectories.

Trajectories of air parcels have been computed by various investigators using the actual winds, geostrophic winds, gradient winds, constant-absolute-vorticity considerations, and combinations of the above. One of the first contributions to a dynamic approach was that of Machta [1]. Recently additional work on "dynamic" computation of trajectories has been published by Takahashi et al. [2], Franceschini and Freeman [3], Wobus [4], the Air Weather Service [5], and Hubert [6]. The methods to be presented in this paper give exactly the same results obtained by Wobus' method, and by the Air Weather Service method for the frictionless case. Franceschini and Freeman's method differs slightly. Hubert's method also differs, his approach being based entirely on hourly forecasts of geopotential or stream function fields by numerical methods. The handling of the frictional or damping terms herein differs considerably from that of Wobus. The other investigators have applied the methods only in the higher troposphere and the stratosphere, while in this paper the methods are applied near the ground.

2. THEORY

The problem is to find the trajectory of a parcel of air in the frictionless atmosphere when its initial velocity is known (or can be closely approximated) and the contour or pressure field is known or can be approximated during a later interval of time. The simplified equations of motion in the atmosphere without friction are

$$\frac{du}{dt}=fv-fv_g=fv' \tag{1}$$

and

$$\frac{dv}{dt}=-fu+fu_g=-fu' \tag{2}$$

where u and v are the east-west and north-south components of the wind, f is the Coriolis parameter, the subscript g denotes the geostrophic wind, and u' and v' denote the geostrophic deviations; i.e., $u'\equiv u-u_g$ and $v'\equiv v-v_g$.

Haurwitz [7] shows these equations have the simple geometric interpretation that the wind is accelerated along a line at right angles to the geostrophic deviation vector $\mathbf{V}'$ and in a right-hand or clockwise sense, as illustrated in figure 1. Note that $\frac{d\mathbf{V}}{dt}$ must always be directed to the right of $\mathbf{V}'$ in the Northern Hemisphere.

For computing the change in the wind during a certain interval of time, one may use the average geostrophic wind on the parcel during that interval, thus assuming that it is constant in magnitude and direction. Then, it follows from equations (1) and (2) that

$$\frac{du'}{dt}=fv' \tag{3}$$

$$\frac{dv'}{dt}=-fu' \tag{4}$$

during the interval. Now, from figure 1

$$u'=V'\cos\theta' \tag{5}$$

$$v'=V'\sin\theta' \tag{6}$$

where $V'=|\mathbf{V}'|=\sqrt{u'^2+v'^2}$. Use of (5) and (6) to transform equations (3) and (4) into a pair for V' and θ' gives

$$\frac{dV'}{dt}=0 \tag{7}$$

*This paper was written as part of the work under P.L. 71, 81st Congress under funds transferred from the Corps of Engineers.

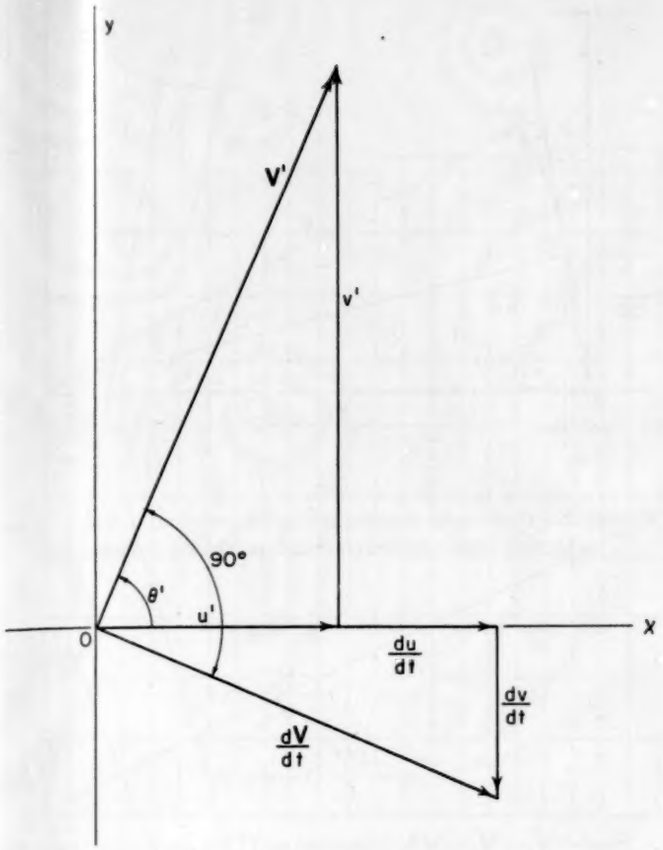

FIGURE 1.—Geometric relationship between the acceleration vector $d\mathbf{V}/dt$ and the geostrophic deviation vector $\mathbf{V}'$.

and

$$\frac{d\theta'}{dt}=-f \tag{8}$$

These equations mean that the *ageostrophic wind vector is constant in magnitude and rotates anticyclonically with a period of one-half a pendulum day.*

Thus, during the time interval in which the geostrophic wind is considered a constant (equal to its average), the change in the wind vector can be represented by the rotation of the ageostrophic wind vector, keeping constant length, clockwise at a rate equal to the Coriolis parameter.

Now, letting $\mathbf{V}_i$=initial wind, and $\mathbf{V}_f$=final wind after time interval τ

$$\mathbf{V}_f=\mathbf{V}_i+f\tau\mathbf{V}'\times\mathbf{k} \tag{9}$$

where the $\mathbf{k}$ is the vertical unit vector.

3. GRAPHICAL SOLUTION

THE ACCELERATION TERM

Since the vector $\mathbf{V}'$ is constant in magnitude, and since $\frac{d\theta'}{dt}=-f$, we may devise a simple graphical solution to evaluate the acceleration term.

In figure 2, $\mathbf{V}_i$, $\mathbf{V}_g$, and $\mathbf{V}_i'$ represent the initial wind, the geostrophic wind, and the initial geostrophic deviation.

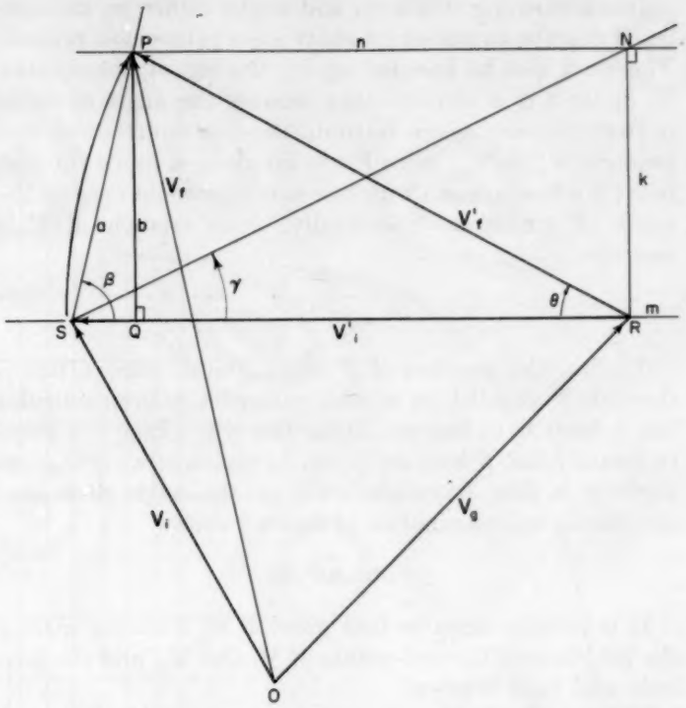

FIGURE 2.—Geometric relationships among the initial wind $\mathbf{V}_i$, the geostrophic wind $\mathbf{V}_g$, the initial geostrophic deviation $\mathbf{V}_i'$, the final geostrophic deviation $\mathbf{V}_f'$, and the final wind $\mathbf{V}_f$.

Then $\mathbf{V}'$ rotates anticyclonically at the rate f. At the end of a time increment τ, a simple rotation with an angle $\theta=f\tau$ gives the final geostrophic deviation $\mathbf{V}_f'$. Then a vector from O to the end point P of $\mathbf{V}_f'$ gives the final wind $\mathbf{V}_f$.

In the application of the relations shown in figure 2 to find the trajectory of a parcel of air during the next hour, the following steps are taken:

(1) Beginning at point O lay off on the weather map a distance OS in nautical miles equal to the observed wind $\mathbf{V}_i$ in knots.

(2) Measure the average geostrophic wind $\mathbf{V}_g$ along the path OS.

(3) Lay off OR in nautical miles equal to $\mathbf{V}_g$ in knots.

(4) With pivot of compass on terminal point R strike an arc SP of angular magnitude $f\tau$ clockwise from terminal point S.

(5) The distance OP in nautical miles equals the final velocity $\mathbf{V}_f$ in knots at the end of one hour.

(6) The trajectory during this first hour is along a vector which is the mean between $\mathbf{V}_i$ and $\mathbf{V}_f$. A simple means of obtaining this average will be treated later.

The striking of the arc in step (4) explains use of the term "arc-strike" as a name for the method.

NOMOGRAM TO AID IN DRAWING TRAJECTORY

Trajectories could be computed as described above by aid of compasses and a straight-edge, but since this in-

volves measuring distances and angles either on the analyzed chart or on a working chart it is a rather slow process. The work can be speeded up by the use of nomograms. In figure 2 it is obvious that because the angle of strike is fixed for any given latitude and time increment and because $|\mathbf{V}_i'|=|\mathbf{V}_f'|$ point P will lie along a line a through point S whose angle β with line m is dependent *only* on the angle of strike, θ. Specifically, since triangle RSP is isosceles

$$\beta=\frac{180°-\theta}{2}. \tag{10}$$

To find the position of P along line a, draw a line n through P parallel to m and construct a perpendicular line k from R to line n. Draw line SN. Line SN helps to locate point P because it can be demonstrated that its angle γ is also dependent *only* on the angle of strike; specifically an examination of figure 2 shows

$$\gamma=\arctan(\sin\theta) \tag{11}$$

It is possible then to find point P by knowing merely the positions of the end-points of $\mathbf{V}_i$ and $\mathbf{V}_g$, and the latitude and time interval.

The next item to consider is the average velocity during the time interval involved in drawing the trajectory. The velocity with which the parcel is carried forward should be an integrated average $\mathbf{V}_a$ from the initial velocity $\mathbf{V}_i$ to the final velocity $\mathbf{V}_f$.

If $\mathbf{V}_f$ is not too different from $\mathbf{V}_i$,

$$\mathbf{V}_a\approx\frac{1}{2}(\mathbf{V}_i+\mathbf{V}_f) \tag{12}$$

If $\mathbf{V}$ and $\mathbf{V}_i$ are very different, this approximation becomes less accurate and then it is necessary to approach this from a more rigorous standpoint. Wobus [4] does this averaging by means of a nomogram called a Trajectory Computer. Experience dictates that the shorter the time interval used the more accurate the trajectory will be defined—this is particularly so where the contour or pressure fields are changing rather rapidly in time or space. We must look for a system to construct our nomograms rapidly for any time interval and latitude desired.

In figure 3 is reconstructed the portion of figure 2 necessary to aid in finding the average velocity $\mathbf{V}_a$. S and R, which are the terminal points of $\mathbf{V}_i$ and $\mathbf{V}_g$, define $\mathbf{V}'$ at time $t=0$. At some later time t, $\mathbf{V}'$ has rotated through angle θ and point P is then the terminal point of $\mathbf{V}$.

It may be seen from figure 3 (see also equations (5) and (6), noting $\theta=\pi-\theta'$) that

$$u^*=V_i'-V_i\cos\theta \tag{13}$$

$$v^*=V_i'\sin\theta \tag{14}$$

where u^* and v^* are components of the velocity vector $\mathbf{V}^*$ from S to P.

From equation (8) and the relation $\theta=\pi-\theta'$, it follows that $\theta=ft$; thus equations (13) and (14) can be integrated

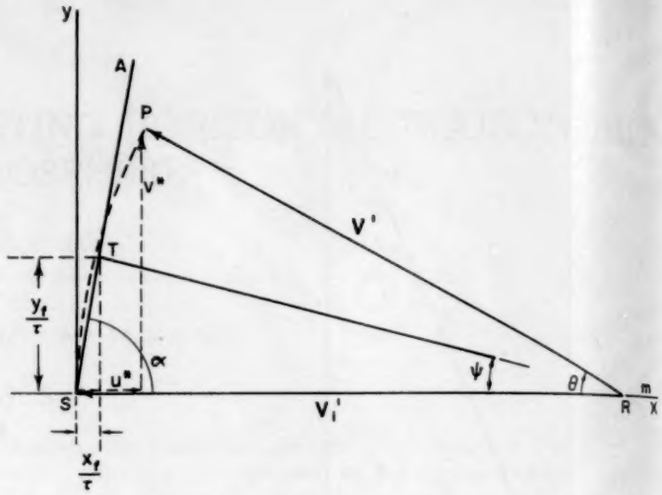

FIGURE 3.—Geometric determination of terminal point T of trajectory from vector relationships shown in figure 2.

for the time interval 0 to τ, giving

$$x_f=V_i'\tau-\frac{V_i'}{f}\sin\theta \tag{15}$$

$$y_f=\frac{V_i'}{f}(1-\cos\theta) \tag{16}$$

Since $\mathbf{V}_f-\mathbf{V}_i=\mathbf{V}^*$, equations (15) and (16) give the coordinates of the parcel relative to point S after a time interval τ. If SA is the line through S and the point (x_f, y_f), making the angle α with line m, then from figure 3 and (15) and (16):

$$\tan\alpha=\frac{y_f}{x_f}=\frac{1-\cos\theta}{\theta-\sin\theta} \tag{17}$$

Now since the average velocity $\mathbf{V}_a$ for the particular arc-strike, θ, has the components x_f/τ and y_f/τ, it follows from (17) that the end point of the vector $\mathbf{V}_a$ lies along a line which makes angle α with line m, and α is dependent *only* on the angle of strike; specifically, from (17):

$$\alpha=\arctan\left(\frac{1-\cos\theta}{\theta-\sin\theta}\right) \tag{18}$$

Similarly, by integration of equations (5) and (6), it can be shown that x_f/τ and y_f/τ lie on a line through point R that makes angle $\theta/2$ with line m. Thus in figure 3, $\psi=\theta/2$.

With equations (10), (11), and (18) it is possible to construct quickly a nomogram to compute trajectories at any latitude and for any time period. Example: to construct a computing nomogram for the 30°N. latitude and for intervals of 2 hours. The angle of strike $\theta=ft=4\Omega\sin\phi=30°$ where $\Omega\approx\frac{360°}{24\text{ hr.}}$, the angular speed of the earth's rotation. From equation (10), $\beta=\frac{180°-\theta}{2}=\frac{180°-30°}{2}=75°$. From equation (11), $\gamma=\arctan\sin 30°=26.6°$.

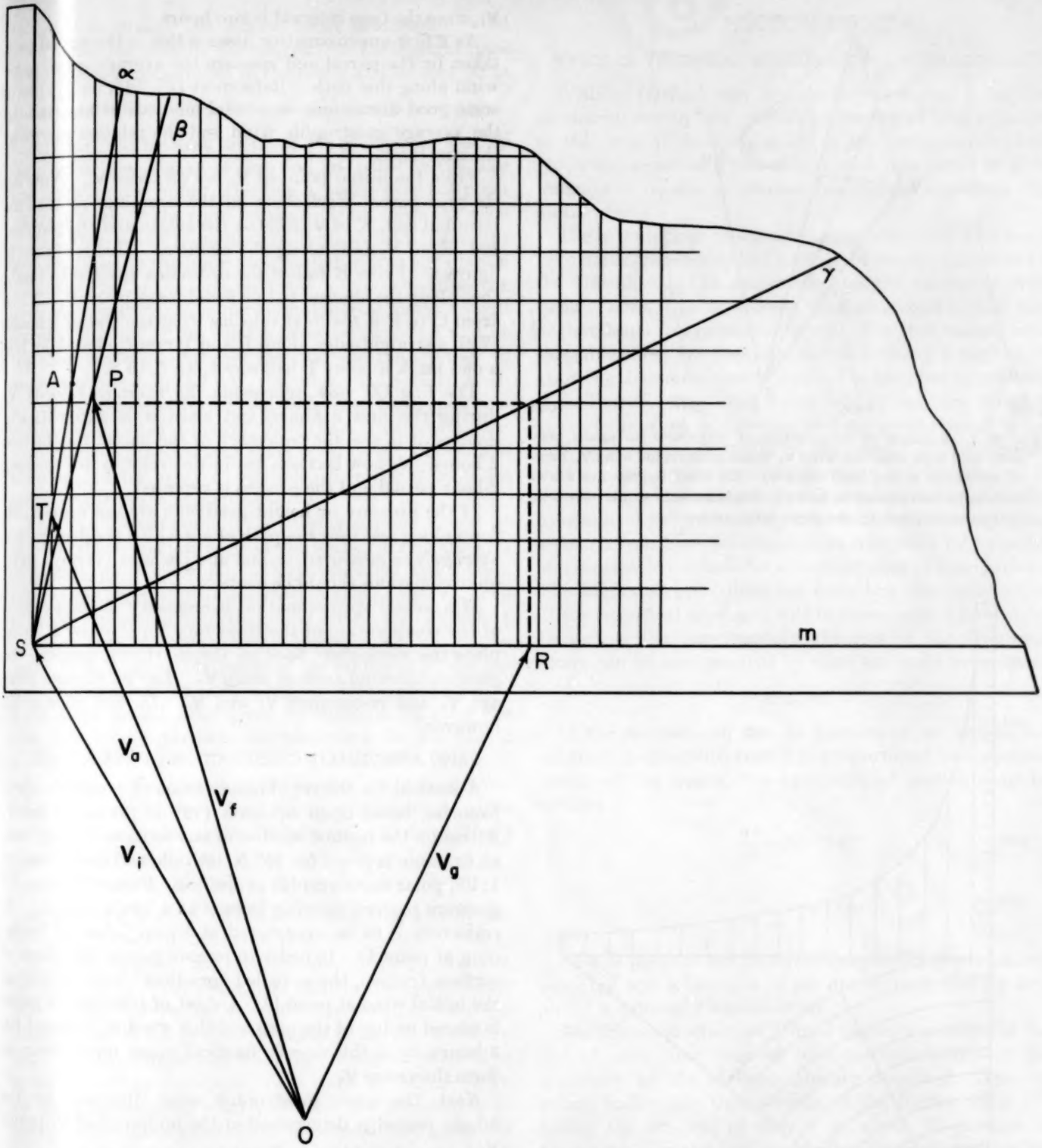

FIGURE 4.—Nomographic determination of terminal point T of trajectory. The lines emanating from point S at angles α, β, and γ are fixed for constant latitude and time interval.

From equation (18), $\alpha=\arctan\dfrac{1-\cos\theta}{\theta-\sin\theta}$

$$=\arctan\frac{1-\cos 30^\circ}{\frac{\pi}{6}-\sin 30^\circ}=80^\circ.$$

On a piece of graph paper of suitable size draw three lines with angles of 75°, 26.6°, and 80° all emanating from the origin S as in figure 4. For convenience the trajectory is best drawn on transparent paper. Lay this over the map and mark reference points so that the same relative position of paper and chart may be easily found. Mark the point where the trajectory is to be started. (The initial wind here should be known or closely approximated.) From this point lay off a line twice the vector

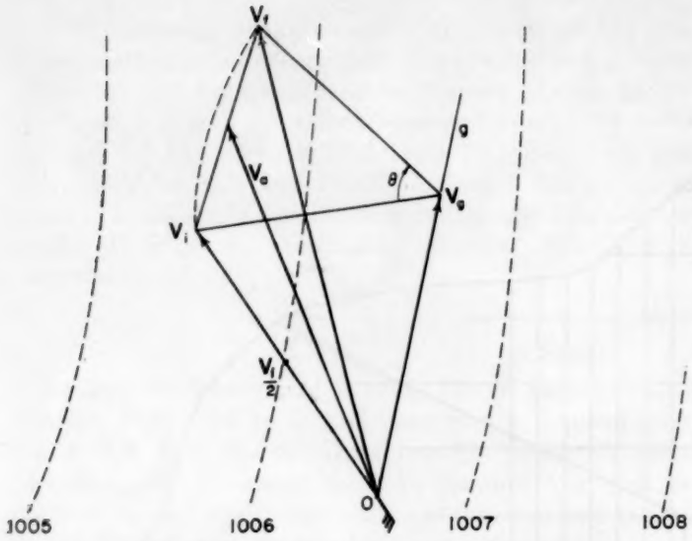

FIGURE 5.—Example of construction of trajectory for model pressure field with observed wind V_i, mean geostrophic wind V_g, angle of arc-strike θ, and final wind V_f. All wind vectors are drawn to lengths corresponding to 3-hr. displacements so that the 3-hr. trajectory is given by the mean wind vector V_a.

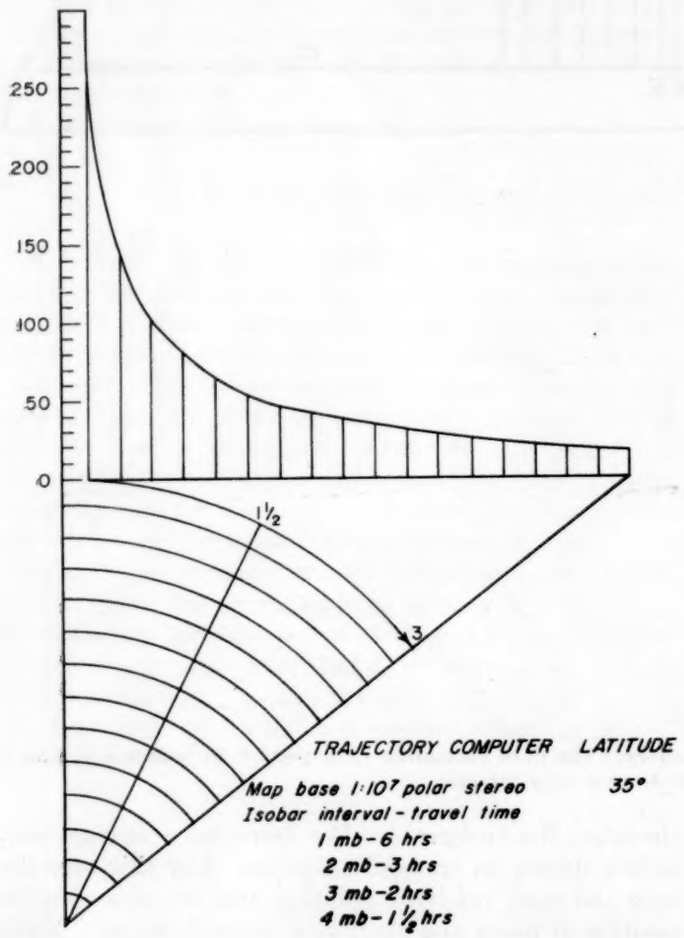

FIGURE 6.—Overlay for rapidly constructing trajectories at latitude 35° for a polar stereographic map base of scale 1:10⁷.

V_i, since the time interval is two hours.

As a first approximation assume this is the actual path taken by the parcel and measure the average geostrophic wind along this path. References [3], [4], and [5] have some good discussions on several methods of ascertaining the average geostrophic wind and the relative merits of these methods.

From the initial point of V_i lay off twice V_g. Now lay the transparent work-sheet on the computer so that the terminal end, S, of V_i falls on the origin and the terminal end, R, of V_g falls along the abscissa. This is shown in figure 4. From R follow the ordinates upward to line γ, then along the abscissa to line β and mark point P. A line from O to P is the final velocity V_f at the end of 2 hours. With a straight-edge along R and P mark point A on line α and mark a point T halfway from A to S.

The line OT now represents the average velocity V_a during the first 2 hours, and since it is automatically doubled it is also the trajectory of the parcel for the first 2 hours. V_f now becomes the initial velocity for the next 2-hour period and the process is repeated.

If the pressure or height gradients are not nearly uniform along and near the path along which the geostrophic average was measured, second and perhaps (rarely) third approximations should be made.

If a second approximation is necessary in the example of the computation of the trajectory for the first 2 hours, place the work-sheet back on the chart and measure the geostrophic wind average along V_a. Lay off the new average V_g and re-compute V_f and V_a. *Do not change* V_i, however.

RAPID APPROXIMATE CONSTRUCTION OF TRAJECTORIES*

A method for the rapid construction of frictionless trajectories, based upon equation (12) is presented below. Although the method applies to any latitude or map base, an example is given for 35° N. latitude and a map base of 1:10⁷, polar stereographic projection. Figure 5 is a model pressure pattern showing isobars at a 1-mb. interval. A trajectory is to be constructed at 3-hour intervals beginning at point O. In order to remove partly the effects of surface friction, the so-called "gradient" wind is used as the initial wind at point O. A sheet of transparent paper is placed on top of the map and this wind is projected for 3 hours, or in this case 90 nautical miles, downstream to form the vector V_i.

Next, the mean geostrophic wind direction for the 3-hour period is determined at the midpoint of V_i (point $\frac{V_i}{2}$). This same direction is laid off from O to form the line g. The 3-hour mean geostrophic wind speed is measured using a transparent overlay illustrated in figure 6. The upper part of the overlay gives the distance moved by a parcel moving with the mean geostrophic wind. The scale on the left is in nautical miles. The straight and curved lines are spaced at intervals of 20 nautical miles.

*The method was developed by Mr. K. Peterson.

In order to obtain the 3-hour mean geostrophic wind speed, place the scale on the map so that the straight lines on the overlay are parallel to the line g and so that point $\frac{\mathbf{V}_i}{2}$ lies on the base line. The point $\frac{\mathbf{V}_i}{2}$ should be approximately mid-way between the point where an isobar touches the edge of the overlay at zero and the point on the base line 2 mb. to the right. Holding a pencil over the point which is 2 mb. to the right on the baseline, move the scale so that this point is coincident with point O and the straight lines on the scale are parallel to line g. Place a dot at the edge of the scale on line g. This determines the ector $\mathbf{V}_g$, the distance a parcel starting at point O will travel in 3 hours if the wind is geostrophic. If a 6, 2, or 1½-hour travel distance is desired, use the overlay to measure across 1, 3, or 4 mb., respectively. Such an overlay can be prepared for any latitude, map base, map projection, and isobar interval with the aid of a standard geostrophic wind scale and a distance scale. If overlays are prepared for every 5° latitude, the error at latitudes between overlays is negligible.

Place the bottom point of the overlay at point $\mathbf{V}_g$ and let point $\mathbf{V}_i$ touch the left edge of the scale. Using the arcs as a guide, go to the right (anticyclonically) and place a point at the right edge of the scale, locating point $\mathbf{V}_f$. The vector $\mathbf{V}_f$ represents the actual wind after 3 hours. Bisect the chord from $\mathbf{V}_i$ to $\mathbf{V}_f$ to obtain the point $\mathbf{V}_a$. (It can be shown that $\mathbf{V}_a$ should be between the midpoint of the arc and the chord, but the error is negligible). The vector $\mathbf{V}_a$ is the mean actual wind given by equation (12) for the time period; it represents the trajectory for the first 3 hours.

The angle at the bottom of the overlay is obtained from the relation $\theta = f\tau$; here $f\tau = 30°(\sin\phi)\tau$ where ϕ is the latitude and τ is the arc-strike interval. At $\phi = 35°$ and with a 3-hour arc-strike,

$$\theta = 30°(0.574)(3) = 51.8°$$

The above equation can be used to obtain arc-strike angles for any latitude and arc-strike interval.

In order to obtain the next 3-hour trajectory, transfer the transparent paper to the next map, in this case, 3 hours later. Take the vector $\mathbf{V}_f$ and translate it so that the initial point O is coincident with the point $\mathbf{V}_a$. This new vector is used as the actual wind for the next 3 hours. The remainder of the technique is the same as before—draw the mean geostrophic wind direction, use the overlay to determine the mean geostrophic movement, and strike the arc to obtain the new 3-hour final wind and mean wind. This procedure can be repeated indefinitely, but since the trajectories are frictionless, and since their accuracy is dependent on the accuracy with which the geostrophic wind field, both present and future, can be delineated, they must be used with care when projected for much more than 12 hours. While the large-scale features might be forecast with sufficient accuracy, the fine-grain structure might not, and any result dependent on the latter will suffer.

4. FRICTION EFFECT

EFFECT OF FRICTIONAL ACCELERATION ON TRAJECTORIES

Without friction, once a trajectory is started it may be carried on step by step, chain fashion, for as long a period as the contour field is known or can be approximated. However, experience has shown that this tends to give unrealistic results as inertial oscillations dominate the motion.

The introduction of some damping effect will give more reasonable trajectories but will not, of course, eliminate all the difficulties. The major effect of the viscous or frictional forces is to slow down the parcel speeds, and this neglect leads to systematic errors. For this reason, considerable effort has been directed to devising a method of applying frictional corrections. The simplest hypothesis regarding the frictional forces is that they are directed against the wind in direction and are proportional to the first or some higher power of the speed. It is suggested that a closer approximation to reality can be obtained if a correction is made using such a relationship with the constants of proportionality determined statistically from a comparison between trajectories computed by dynamic and kinematic methods for a large number of observations. The suggested procedures are described here; evaluation of the empirical constants will be reported at a later date. Doubtless, the more modern theories of the frictional forces can be incorporated by more elaborate procedures.

THEORY

If the acceleration due to friction of an unspecified nature is defined such that it is proportional to a constant power of the speed, the equations of motion may be written.

$$\frac{du}{dt} = fv' - ku^n$$

$$\frac{dv}{dt} = -fu' - kv^n$$

These equations can be solved graphically if n is known. probably n is a function of the speed itself, but for simplicity a value of 2 was assumed.

The frictional effect, as defined above, was added at the end of each time interval to the computations of the trajectory by the methods already described. This involves finding the time-average of the friction term kV^2 during the interval of time τ in which V_i changes to V_F, where V_F is the final speed after the friction effect has been added.

$$V_F = V_f - \int_0^\tau kV^2 dt = V_f - \bar{F}\tau \tag{19}$$

where $\bar{F}$ is average frictional acceleration, V_F is speed at time τ. The average acceleration a during the interval τ is

$$\bar{a} = \frac{V_F - V_i}{\tau} \tag{20}$$

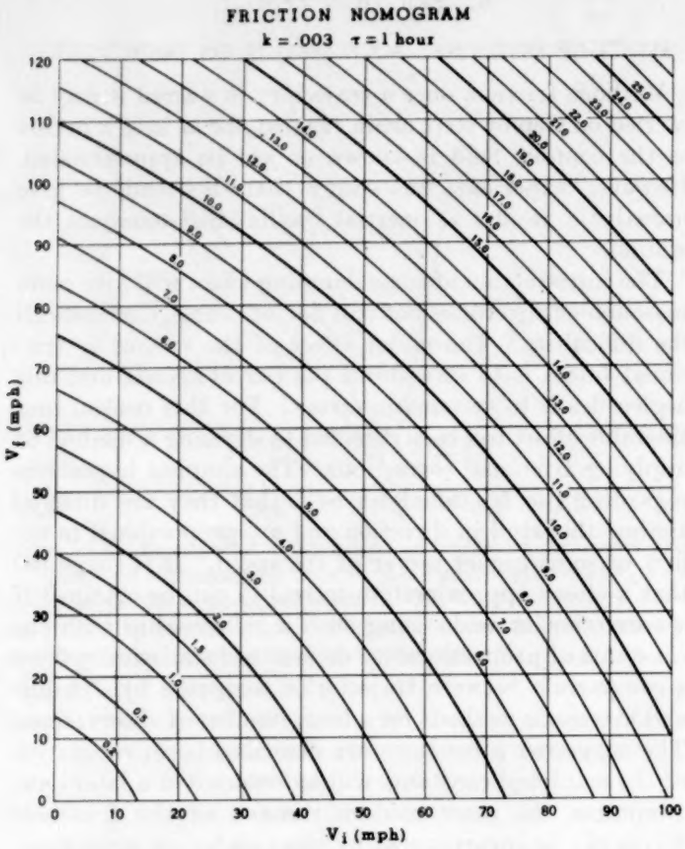

FIGURE 7.—Friction nomogram based on equation (22) with $k=0.003$, $\tau=1$ hr.

Putting $V=V_i+\bar{a}\,t$ and using equation (20) to eliminate $\bar{a}$, we can evaluate the integral in the middle member of (19). This gives

$$\int_0^\tau kV^2dt=k\tau\left[V_iV_F+\frac{(V_i-V_F)^2}{3}\right] \tag{21}$$

Putting (21) into (19) gives

$$V_F=V_f-k\tau\left[V_iV_F+\frac{(V_i-V_F)^2}{3}\right] \tag{22}$$

GRAPHICAL SOLUTION OF EQUATIONS

Equation (22) can be solved graphically. See figure 7.

In equation (22) $k\tau$ occurs outside the brackets in the last term. This suggests that once a system of isolines of friction deceleration values is calculated this same chart can be used for other values of k and τ by the simple expedient of multiplying the values of the isolines by an appropriate factor. This expedites the testing of different values of k in different situations, either actual or models. To use the friction nomogram, figure 7, enter the abscissa with the value of the initial wind speed V_i and the ordinate with the value of the final wind speed V_f obtained by the arc-strike technique. At the point thus obtained interpolate between curved isolines. This interpolated value is subtracted from V_f to yield V_F, the final speed after reduction due to friction.

APPLICATION TO TRAJECTORIES

As previously mentioned, the friction effect is added stepwise at the end of each trajectory computation. This can be considered only an approximation. Nevertheless, if the method proposed is to be useful, it must be able to predict certain singularities in the field of motion. For example, any wind, initially not in balance, in a straight uniform pressure gradient field will eventually approach a value such that the accelerations on any parcel of air total zero. At this point there is a balance among the forces due to the Coriolis effect, the pressure gradient, and friction.

Furthermore, if the wind is initially considerably out of balance the time required for the wind to adjust to within 5 percent of the theoretical balance velocity is of the order of 10 hours under the conditions assumed. As an actual example, consider a wind with initial components $u=20$ kt. and $v=35$ kt.; the geostrophic wind is a constant at $v_g=40$ kt. and $u_g=0$. For $k=0.003$ mi.$^{-1}$ and at 30° N. latitude, the wind will be in balance when $v=34$ kt. and $u=15$ kt. It takes 26 hours, computed by the methods suggested here, for the wind to adjust to within ± 5 percent of the balance values.

Experiments were made around a hurricane using different values of k. A value of 0.020 gave trajectories that were quite unreasonable in that they headed more directly across the isobars than is observed. With a value of 0.0003 the winds acquired speeds that were much higher than observed and overshot the isobars leading to considerable motion toward higher pressure. A value of 0.003 gave trajectory winds more nearly like those observed.

RESULT OF FRICTIONAL ACCELERATION

The fact that adding friction always accelerates the air parcel toward a certain balance value leads to an interesting corollary. This is that if several winds of different values (both in speed and direction) are all subjected to the same geostrophic field and this field is changing with time the different winds will approach the same value because of frictional acceleration. This is not necessarily the value where balance requirements are satisfied since the geostrophic wind itself may be changing.

The results of a test of this corollary are shown graphically in figure 8. The four initial winds, A, B, C, and D, are shown at the bottom left of the figure. After 6 hours in a geostrophic wind field which appears as at upper center, their values became as at the lower center, and after the next 6 hours with geostrophic wind as at upper right the final values are as at lower right. Note that at the end of each of the two 6-hour intervals the differences among the several winds are progressively reduced.

Trajectories in several hurricanes were computed by this method, using actual data for pressure fields. The results are encouraging. The use of $k=0.003$ mi.$^{-1}$ yielded trajectories that in most respects are similar to trajectories drawn from actual wind data where available. These

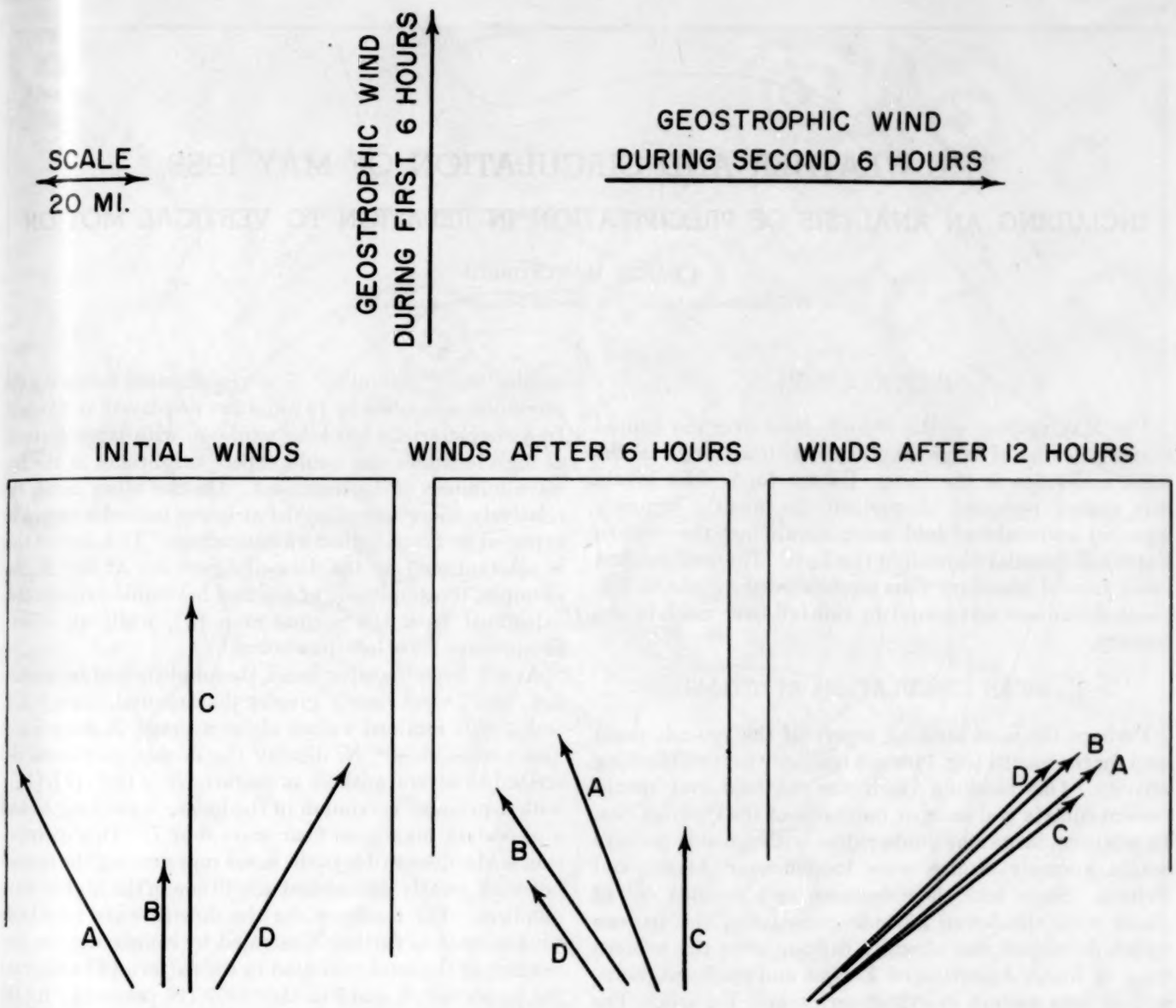

FIGURE 8.—Illustration of tendency of different initial winds subjected to the same changing pressure field to approach the same value because of frictional acceleration.

trajectories together with evaluations of k itself will be discussed at greater length in a subsequent article.

ACKNOWLEDGMENTS

The author wishes to express his gratitude to Dr. Charles S. Gilman, at whose suggestion this study was made. His many helpful criticisms were of invaluable aid. Thanks are also due to Messrs. Kendall R. Peterson, Sydney Molansky, Robert W. Schoner, Calvin W. Cochrane, Earnest A. Rodney, and Vance A. Myers for their thought-provoking discussions.

REFERENCES

1. L. Machta, **The Effect of Varying Pressure Gradient on Air Trajectories, MS Thesis, New York Univ., 1946 (Unpublished).**
2. K. Takahashi et al., "Analysis of Extraordinarily Heavy Rains at the End of Bai-u," *Journal of Meteorological Society of Japan*, Ser. 2, vol. 32, No. 9/10, Sept./Oct. 1954, pp. 281–289.
3. G. A. Franceschini and J. C. Freeman, "Computation of Horizontal Trajectories in the Atmosphere." Texas A and M Research Foundation, *Scientific Report* No. 1 on Contract AF 19 (604)–1302, Jan. 1955, 18 pp.
4. H. B. Wobus, "Wind and Pressure Gradient Computation with Application to Trajectory Computations," *Proceedings of the Workshop on Stratospheric Analysis and Forecasting*, District of Columbia Branch, American Meteorological Society, 1957, pp. 129–143.
5. U.S. Air Force, Air Weather Service, "Constant-Pressure Trajectories," AWSM 105–47, (AFR 190–16), Sept. 1956, 86 pp. (see pp. 29–38).
6. W. E. Hubert, "Hurricane Trajectory Forecasts From a Non-Divergent, Non-Geostrophic, Barotropic Model," *Monthly Weather Review*, vol. 85, No. 3, March 1957, pp. 83–87.
7. B. Haurwitz, *Dynamic Meteorology*, McGraw-Hill Book Co., Inc., New York and London, 1st ed., 1941, 365 pp. (see pp. 155–156).

THE WEATHER AND CIRCULATION OF MAY 1959

INCLUDING AN ANALYSIS OF PRECIPITATION IN RELATION TO VERTICAL MOTION

CHARLES M. WOFFINDEN

Extended Forecast Section, U.S. Weather Bureau, Washington, D.C.

1. INTRODUCTION

The May pattern at the 700-mb. level over the United States was one of large amplitude with a trough in the West and ridge in the East. Except for a short break, this system persisted throughout the month, bringing repeated outbreaks of cold maritime air into the western states and unusual warmth in the East. The well-marked mean frontal boundary thus established gave rise to frequent storminess and abundant rainfall over much of the country.

2. MEAN CIRCULATION AT 700-MB.

Perhaps the most striking aspect of the 700-mb. mean map for the month (fig. 1) was a tendency toward blocking activity. One blocking High was centered over northeastern Siberia and another northeast of the Caspian Sea. In addition, large amplitude ridges with sizeable positive height anomaly centers were located over Alaska and Britain. Since both these features were roughly out of phase with the lower latitude circulation, the pattern which developed was strongly difluent over the western coast of North America and Europe and confluent downstream over eastern North America and Eurasia. The Pacific westerlies to the south of the block were relatively flat with a tendency toward a weak trough off Japan and another in the central Pacific. This latter feature, though weak in the mean and variable during the month, was in a position to support the trough in the western United States and its disappearance about mid-month led to the only major (though transitory) change from the dominant weather pattern for the month.

The pattern depicted in figure 1 differed in several significant aspects from that of April [1]. The change chart (fig. 2) indicates a marked increase in blocking activity with large rise centers over northern Asia and the eastern Atlantic. Also, the deepening in the western United States together with the ridging in the East were sufficient to reverse the circulation regime over the country.

Since blocking played a major role during the period, its effect was studied by preparing harmonic analyses for the meridional component of the 700-mb. flow around each latitude circle. The graphs of amplitude versus wave number at 60° N. and 40° N. were computed following the procedure described in [4] and are displayed as figure 3. In a characteristic blocking situation with large features at high latitudes one would expect amplitudes in the low wave numbers to be dominant. On the other hand, the relatively short wave lengths at lower latitudes would be expected to favor higher wave numbers. To a degree this is substantiated by the data of figure 3. At 60° N., for example, the amplitude of the 2nd harmonic exceeds that calculated from the normal map [8], while all others, except wave 5, are less than normal.

At 40° N. on the other hand, the amplitude of harmonics 5, 6, and 7 were clearly greater than normal, though 1, 2, and 3 still retained values about average in magnitude. The curves at 40° N. display the double maximum described by several authors as characteristic (c.f., [9], [10]) with a primary maximum in the longer wave lengths and a secondary maximum near wave 6 or 7. This distribution is also discernible in the curve representing the normal but with greatly diminished amplitude in the higher wave numbers. The tendency for the shorter wave lengths to predominate is further illustrated by comparing the percentage of the total variation in the pattern [4] accounted for by wave 5, 6, and 7 in May 1959 (26 percent) with the corresponding percentage for the normal (4 percent). Thus the waves within this band were unusually energetic this month, and even wave 7 was sufficiently strong and persistent to account for a surprising 12 percent of the total variation in the pattern.

The zonal index underwent a double oscillation during the month (fig. 4). The first was minor in nature, but the second was more pronounced and amounted to a major index cycle for this season of the year. It began when the zonal index briefly reached 10 m.p.s. for the 5-day period ending May 11, dropped to a low value of 4.4 m.p.s. for the period ending the 27th, and then recovered rapidly, again exceeding 10 m.p.s. by June 6.

3. MEAN TEMPERATURE IN THE UNITED STATES

The change in circulation over the United States from April to May brought about a corresponding reversal in the temperature pattern. The observed temperature distribution in May (fig. 5) was one of sharp contrasts with

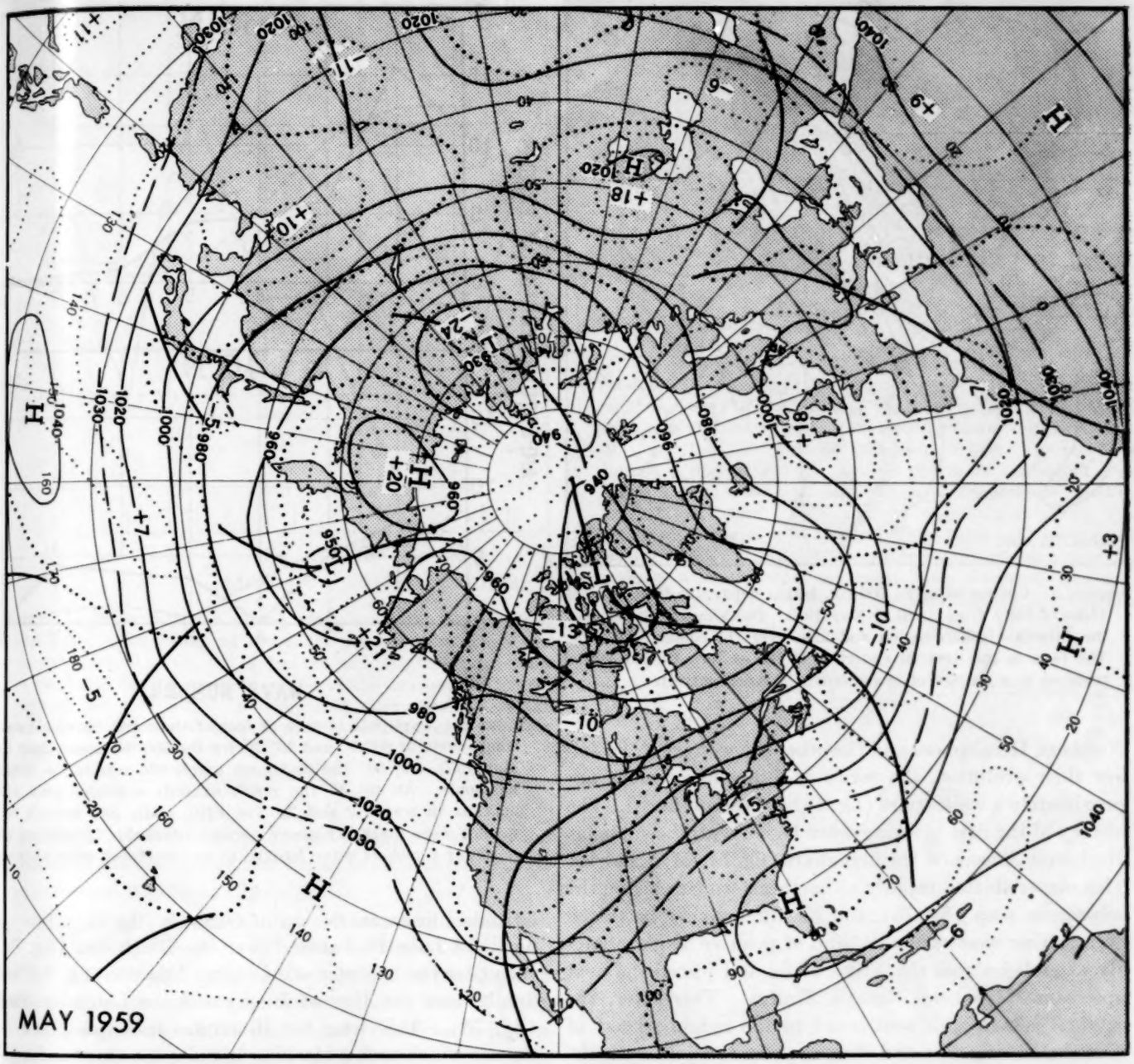

FIGURE 1.—Mean 700-mb. height contours (solid) and departures from normal (dotted) (both in tens of feet) for May 1959. Over the United States the pattern of trough in the West and ridge in the East represented a reversal from the preceding month. Blocking was active, as indicated by the extensive areas of positive anomaly over polar and subpolar regions.

cold maritime air masses predominating in the mean trough in the West and warm tropical air in the eastern ridge. In the West this resulted in a regime which was cooler in May than in April by two classes over a broad area covering most of the western Plateau (fig. 6). At Fresno, Calif., the temperature dropped 4 classes from much above normal in April to much below in May. Maximum warming, on the other hand, occurred in the eastern Texas-Louisiana area, with a finger of two-class changes extending northward to the Lakes.

At Ely, Nev., the average monthly temperature of 47.4° F. was the coldest of record for May. On the other hand, Muskegon, Mich., experienced the warmest May since records began with an average 60.5° for the month.

4. EVOLUTION OF BLOCKING

The tendency for blocking to be frequent in May has been discussed by several authors [5, 7], and this month was no exception. Two remarkable surges occurred, one of which influenced primarily the eastern sector of the

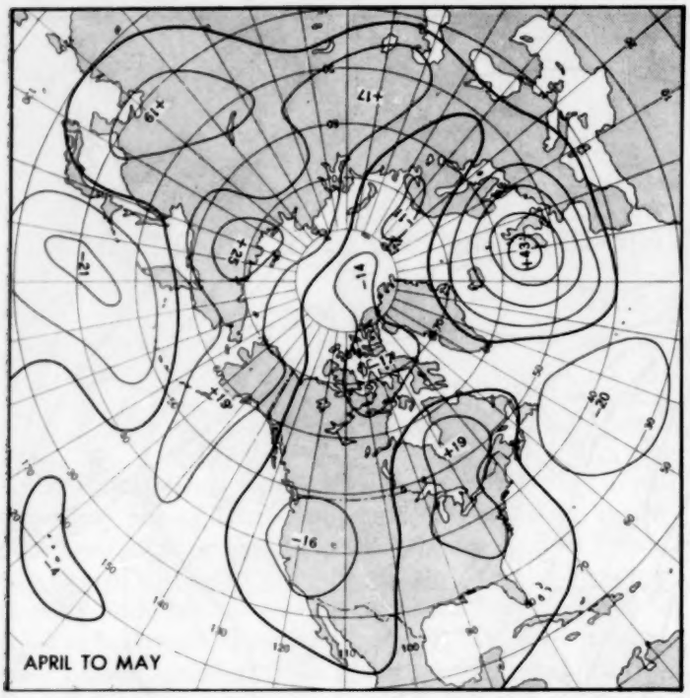

FIGURE 2.—Change of mean 700-mb. height departure from normal (tens of feet) from April to May 1959. Blocking increased over the Siberia-Alaskan region and also over the eastern Atlantic. The falls in the western and rises in the eastern United States resulted in a change of phase from the April pattern.

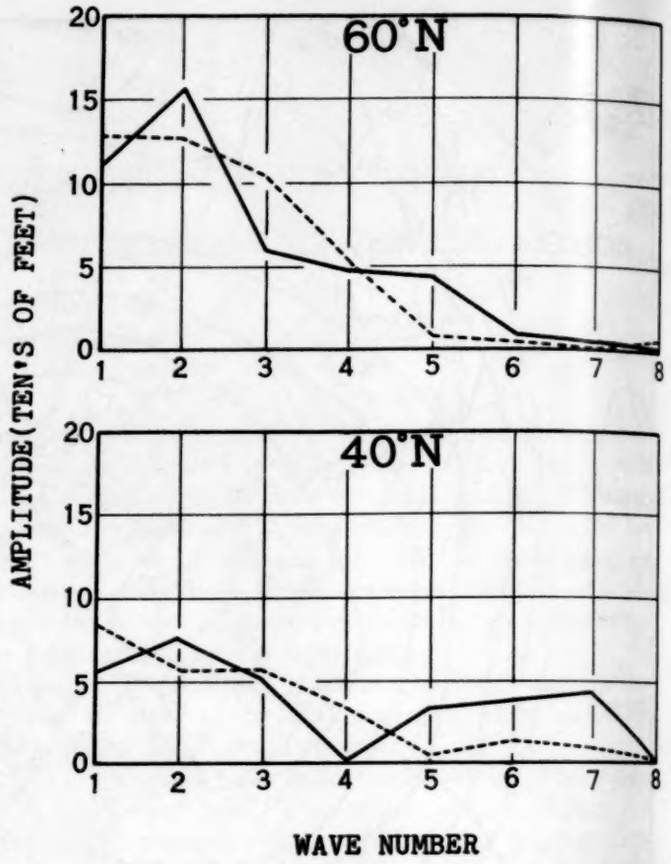

FIGURE 3.—Amplitude in tens of feet of the zonal harmonic wave components at 60° N. and 40° N. for the 700-mb. mean chart for May 1959. At 60° the maximum amplitude was in the second harmonic. At 40° N. the graph exhibits a double peak with maxima in waves 2 and 7. The fifth, sixth, and seventh harmonics were markedly above normal (dashed), illustrating the tendency for short wave lengths to be associated with blocking.

Northern Hemisphere and the other the western. To follow their evolution, the series of 5-day mean maps approximately a week apart (fig. 7) has been prepared. The history of the first blocking wave began with the subpolar High over Alaska on the first chart (fig. 7a) of this series. This center shifted rapidly to northeastern Siberia on the subsequent map (fig. 7b), and its influence can be traced even farther westward as a band of positive height anomaly extended across the Arctic basin and joined the next upstream ridge near Novaya Zemlya. Thereafter, the original center sank southward to the neighborhood of Kamchatka (fig. 7c) and then appeared to join with the subtropical ridge in the western Pacific (fig. 7d).

However, the blocking surge, as distinguished from this center, can be traced on to the west as heights subsequently rose over 600 ft. in the Scandinavian region from the second to the third chart of the series, resulting in a marked retrogression of the Russian blocking ridge to that region. The North Atlantic was next affected, and a closed anticyclone appeared just north of Britain (fig. 7d). By the end of the month, this surge seemed to come to an abrupt end as heights fell rapidly at northerly latitudes from Europe to North America.

So far this phenomenon has been treated in terms of ridges, but one could equally well direct attention to the remarkable sequence of Lows cut off or depressed to lower latitudes: first over the sea of Okhotsk (fig. 7a), then just north of Lake Baikal and over the Black Sea (fig. 7b), then near the Adriatic and Central Atlantic (fig. 7c), and finally over the Bay of Biscay and the Labrador Shelf (fig. 7d). This long list illustrates the widespread influence which such a blocking impulse can exert and highlights its possible importance as a tool in longer period forecasting. From its position over Alaska at the beginning to that north of Scotland near the end of the period it traversed approximately 205° of longitude in 19 days or about 11° of longitude per day, an unusually rapid pace.

For the western sector of the hemisphere, however, the more important blocking complex was that centered off the Labrador coast as the month opened (fig. 7a). In successive weeks this surge, spreading upstream:

1. Amplified the United States ridge and cut off the Low near Newfoundland (fig. 7b).

2. Amplified the ridge in western Canada and cut off the Low near James Bay (fig. 7c).

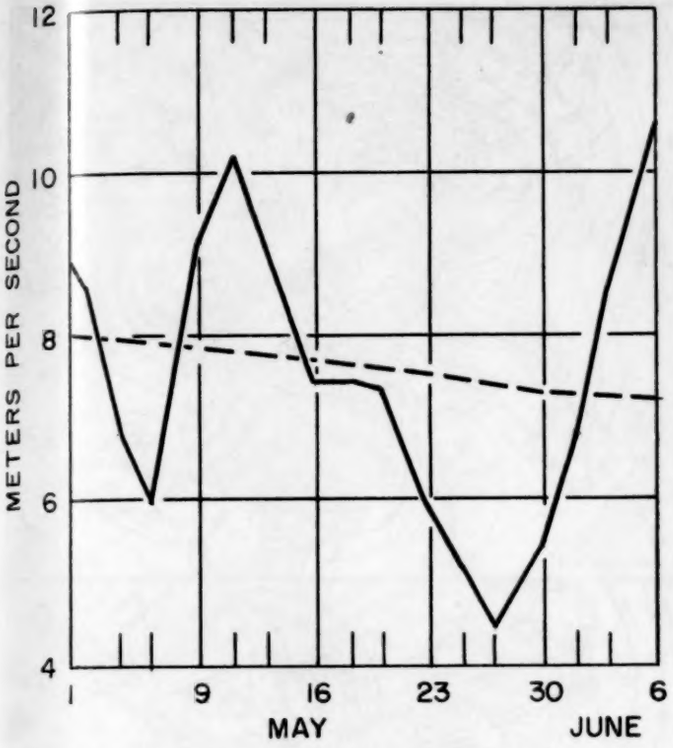

FIGURE 4.—Time variation during May and early June 1959 of the 5-day mean values of the zonal westerlies in meters per second (plotted on the last day of the period). The zonal index is computed for the western sector of the hemisphere for the latitude belt 35°—55° N. A pronounced index cycle followed an earlier minor variation, with the zonal index reaching a minimum during the last week of May.

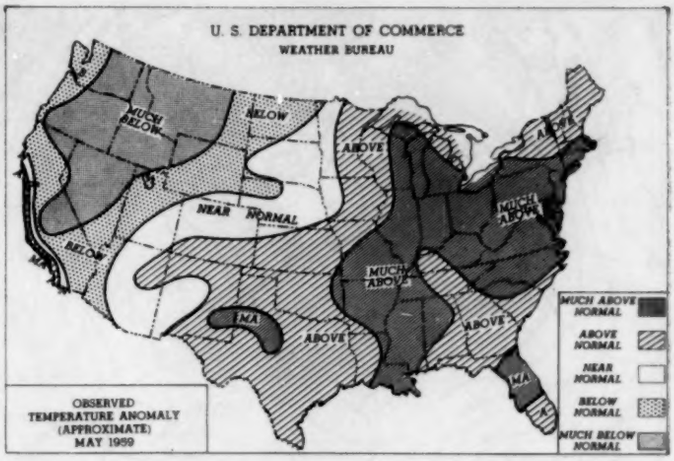

FIGURE 5.—Observed temperature anomaly for May 1959 expressed in five classes defined so that near, below, and above normal each comprises one-fourth of the monthly mean temperatures for May over the 30-year period 1921 through 1950. The remaining fourth is divided equally between the much above and much below categories. A strong east-west temperature gradient existed, with very cold conditions prevailing over the West (with the exception of coastal California) and very warm weather over roughly the eastern two-thirds of the country. A marked frontal system separated these extremes, and wave activity resulted in widespread precipitation and severe storms.

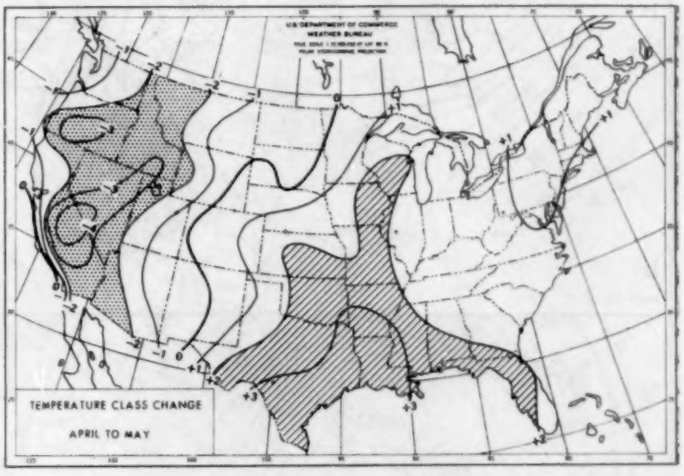

FIGURE 6.—The number of classes the anomaly of temperature changed from April to May 1959. Marked cooling took place over a broad area of the West, with warming over most of the remainder of the United States except for the northeastern States.

3. Amplified the eastern Pacific ridge, cut off the depression in the Southwest, and began to depress the cyclone in the eastern Aleutians (fig. 7d).

4. Amplified the pattern over northeastern Siberia and cut off the deep system in the eastern Aleutians (fig. 7e).

This singular evolution paralleled the first such system in many respects and can be described as typical of many blocking sequences. It was intimately connected with the index cycle previously described, the low point of the latter being reached as the blocking reached maximum coverage and development in the western sector of the hemisphere. Also, subsequent continued retrogression of blocking into Asia in early June allowed the zonal index to again climb to above 10 m.p.s. and complete the cycle. The average speed of retrogression of blocking in this case was about 6° of longitude per day, which is considerably slower than the first case described.

5. WEEKLY WEATHER AND CIRCULATION OVER THE UNITED STATES

The wave train over the United States was progressive for the first portion of the month. The trough initially along the west coast (fig. 7a) marched steadily eastward and by the fourth map of the series (fig. 7d) was well out in the Atlantic. It has been mentioned that blocking served to amplify first the ridge in advance of this trough (fig. 7b) (thus advecting warm moist air into the Mississippi Valley) and subsequently the Canadian ridge in its rear (fig. 7c) (thus bringing down unusually cold air).

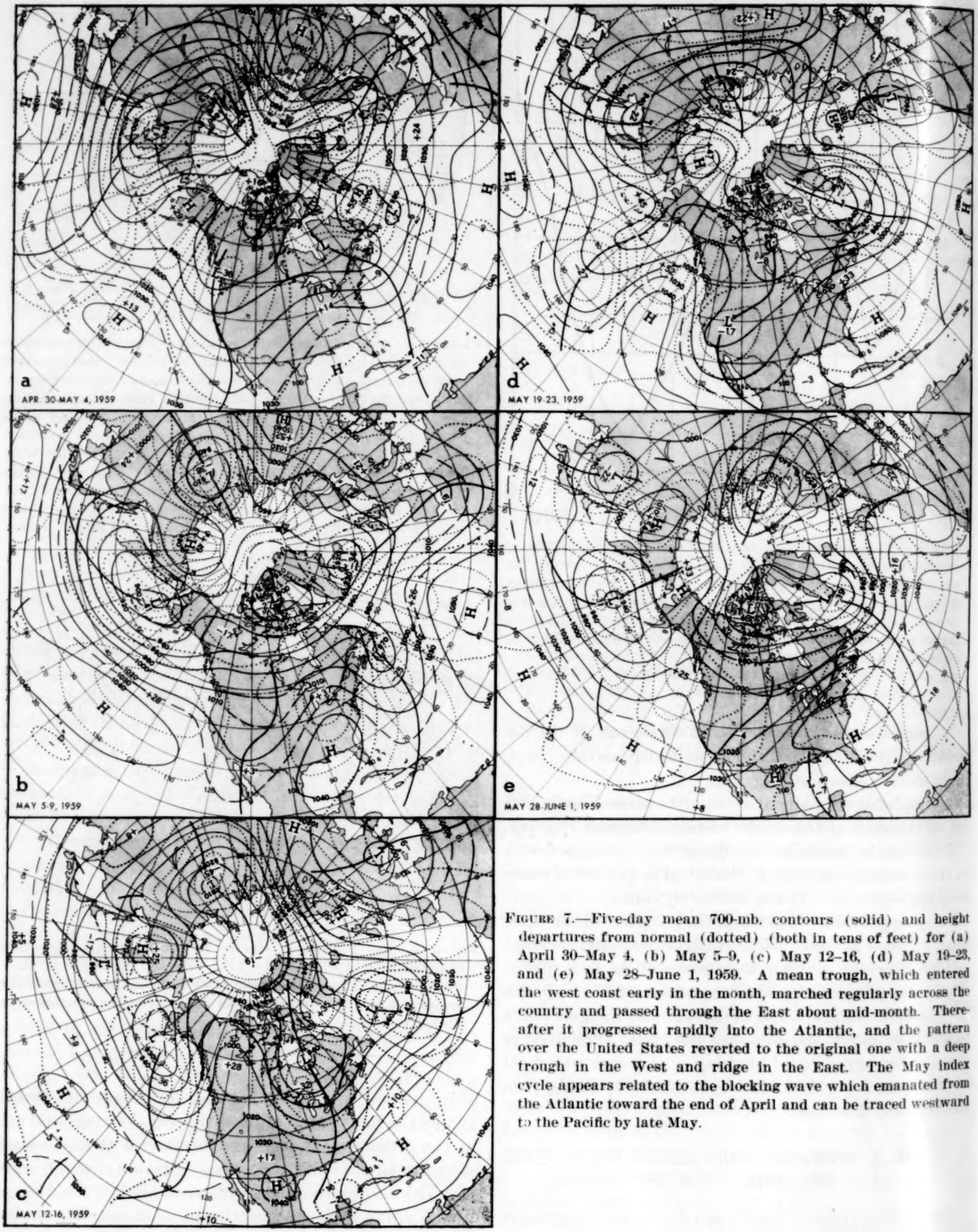

FIGURE 7.—Five-day mean 700-mb. contours (solid) and height departures from normal (dotted) (both in tens of feet) for (a) April 30–May 4, (b) May 5–9, (c) May 12–16, (d) May 19–23, and (e) May 28–June 1, 1959. A mean trough, which entered the west coast early in the month, marched regularly across the country and passed through the East about mid-month. Thereafter it progressed rapidly into the Atlantic, and the pattern over the United States reverted to the original one with a deep trough in the West and ridge in the East. The May index cycle appears related to the blocking wave which emanated from the Atlantic toward the end of April and can be traced westward to the Pacific by late May.

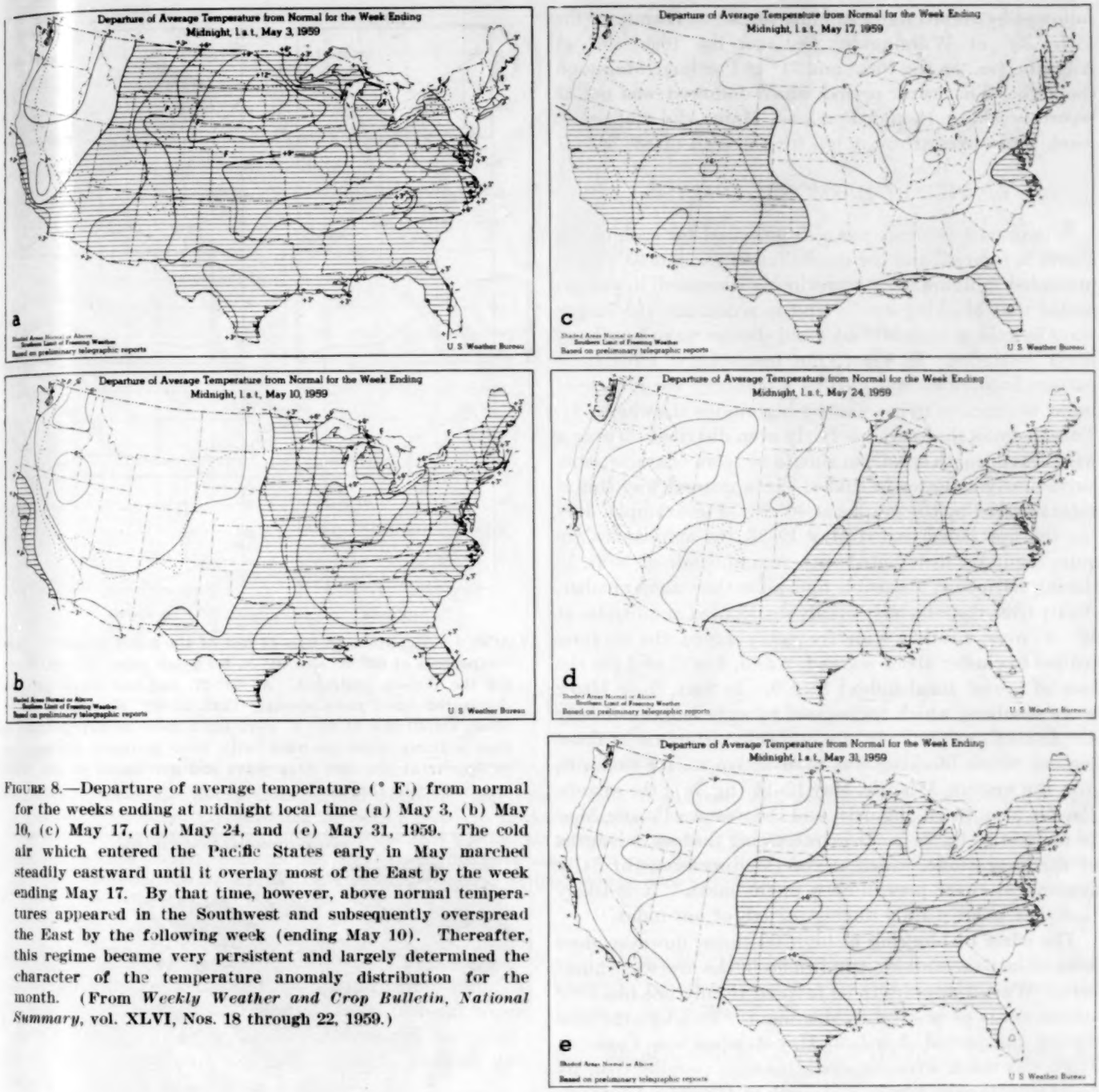
Departure of Average Temperature from Normal for the Week Ending
Midnight, l.s.t., May 3, 1959
a
U.S. Weather Bureau
Departure of Average Temperature from Normal for the Week Ending
Midnight, l.s.t., May 17, 1959
c
U.S. Weather Bureau
Departure of Average Temperature from Normal for the Week Ending
Midnight, l.s.t., May 10, 1959
b
U.S. Weather Bureau
Departure of Average Temperature from Normal for the Week Ending
Midnight, l.s.t., May 24, 1959
d
U.S. Weather Bureau
Departure of Average Temperature from Normal for the Week Ending
Midnight, l.s.t., May 31, 1959
e
U.S. Weather Bureau

FIGURE 8.—Departure of average temperature (° F.) from normal for the weeks ending at midnight local time (a) May 3, (b) May 10, (c) May 17, (d) May 24, and (e) May 31, 1959. The cold air which entered the Pacific States early in May marched steadily eastward until it overlay most of the East by the week ending May 17. By that time, however, above normal temperatures appeared in the Southwest and subsequently overspread the East by the following week (ending May 10). Thereafter, this regime became very persistent and largely determined the character of the temperature anomaly distribution for the month. (From *Weekly Weather and Crop Bulletin, National Summary*, vol. XLVI, Nos. 18 through 22, 1959.)

Along the boundary between these contrasting air masses severe frontal weather developed with thunderstorms, hail, high winds, and a number of tornadoes. As a result precipitation was heavy over much of the area between the Rockies and the Alleghenies, and was locally excessive over the Mississippi and Ohio Valleys. The eastward progress of this frontal boundary can be traced with the aid of figure 8 which shows the cold air reaching the East during the week ending May 17 (fig. 8c). This brought the only cold snap of the month to that region. Thereafter the basic circulation pattern of the month (fig. 1) became reestablished as a deep trough entered the West (fig. 7d) and the ridge over the Rockies sheared from its previous connection with the blocking ridge over northwestern Canada (fig. 7c) and amplified as it moved rapidly to the east coast (fig. 7d). It is noteworthy that the East experienced a complete reversal from very warm the second week (fig. 8b), to very cold the next (fig. 8c), and back to the original regime the fourth week (fig. 8d).

Numerous records of daily maximum and minimum temperatures were set, including maxima during the early period of 99° F. at Huron, S. Dak., on the 1st; 95° at Louisville, Ky., on the 4th; 95° at Augusta, Ga., on the 3d; and 82° at Portland, Maine, on the 11th. These were

followed by record daily minima of 24° at Huron on the 15th; 38° at Wilmington, Del., on the 16th; 46° at Augusta, Ga., on the 16th; and 31° at Portland, Maine, on the 18th. The warm period which followed was not as record-breaking, though Portland, Maine, did manage to reach a new record maximum for the 28th of 88° F.

6. WEEKLY HARMONIC ANALYSIS

A harmonic analysis was also prepared for each of the charts in figure 7, and the results for 60° N. and 40° N. are presented in figure 9. As previously discussed, it was expected that blocking would tend to accentuate the longer wave lengths at high latitudes and shorter wave lengths at lower latitudes. However, the hemispheric circulation pattern is often complicated by a tendency for low zonal index in one area to be offset by high index elsewhere [2]. This suggests that perhaps fairly even distribution over a wide wave length spectrum should be more characteristic, particularly at lower latitudes. In a general way this is substantiated by the graphs at 40° N. For example, during the low index period May 19–23, the amplitudes are quite regularly distributed with an amplitude of 50 ft. in the 9th harmonic, a sizeable figure for that wave number. Apart from the relatively evenly distributed amplitudes at 40° N. over a rather wide frequency range, the maxima tended to cluster about waves 1, 2 or 3, 6 or 7, and (in the case of lowest zonal index) 8 or 9. In fact, these latter wave numbers, which correspond to wave lengths of only 45° and 40°, respectively, are quite characteristic of those regions where blocking was most active as, for example, over the western Atlantic, May 12–16 (fig. 7c); the eastern Pacific, May 19–23 (fig. 7d), and the western Pacific, May 28 to June 1 (fig. 7e). It is interesting that wave lengths of this magnitude, which are of the dimensions of daily systems, at times prevail even in the mean. It is likely that they occur mainly during periods of low index.

The effect of blocking at high latitudes, however, does seem to be to accentuate amplitudes in the low wave numbers. Wave 1 appears to be favored if only one blocking system exists or is strongly dominant. This was the case during the period April 30–May 4 when the Eurasian High was much stronger along the 60th parallel than its counterparts over Alaska and south of Greenland. However, the latter two did make substantial contributions to the amplitude of waves 2 and 3 which were also unusually large during this period.

On the other hand, when dual blocking Highs exist across the pole from each other, and this is often the case during periods of lowest index, wave 2 is principally affected. The graph at the 60° parallel for May 19–23 (fig. 9) may be cited as an example.

7. PRECIPITATION

A large portion of the United States enjoyed adequate rainfall during May (fig. 10). Heaviest amounts fell over

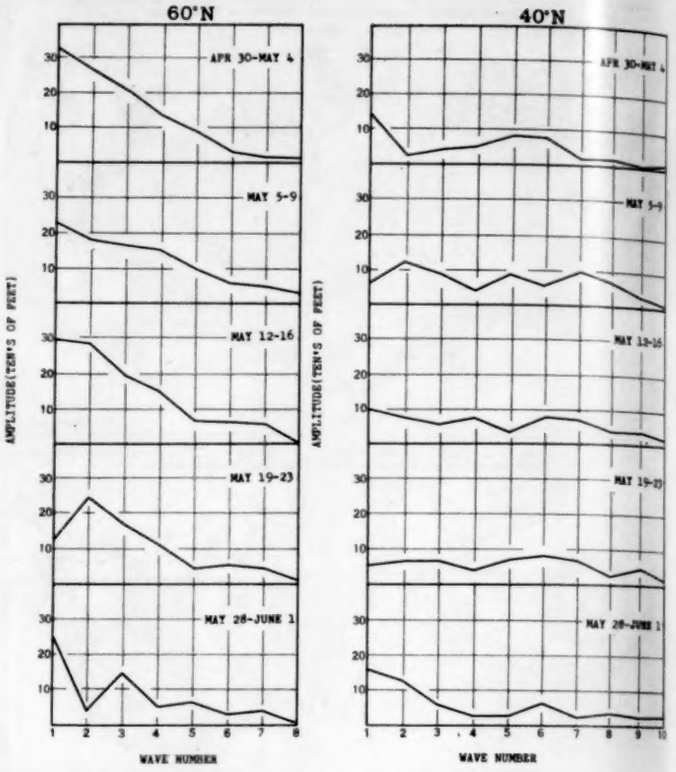

FIGURE 9.—Amplitude in tens of feet of the zonal harmonic wave components at 60° N. and 40° N. for 5-day mean 700-mb. charts for the periods indicated. At 60° N. the low wave numbers dominated much more strongly than at 40° N. On the other hand, amplitudes at 40° N. were much more evenly distributed over a fairly wide spectrum, with some tendency for maxima to appear at the very long wave end and again in the wave number band 5 through 7.

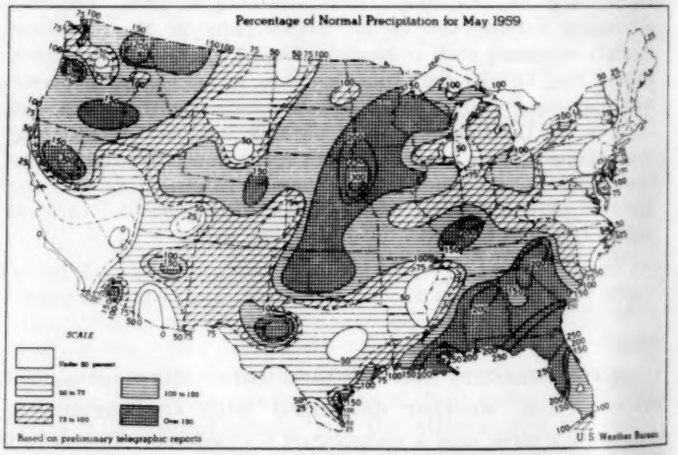

FIGURE 10.—Percentage of normal precipitation for May 1959. Precipitation was heavy over much of the Nation. Note the continued dryness in the Southwest and near the border of Montana and Wyoming with the Dakotas. (From *Weekly Weather and Crop Bulletin, National Summary*, vol. XLVI, No. 23, 1959.)

the Central Plains in advance of the mean trough position for the month (fig. 1), in the Northwest, and also in the Southeast. The heavy precipitation in the Southeast oc-

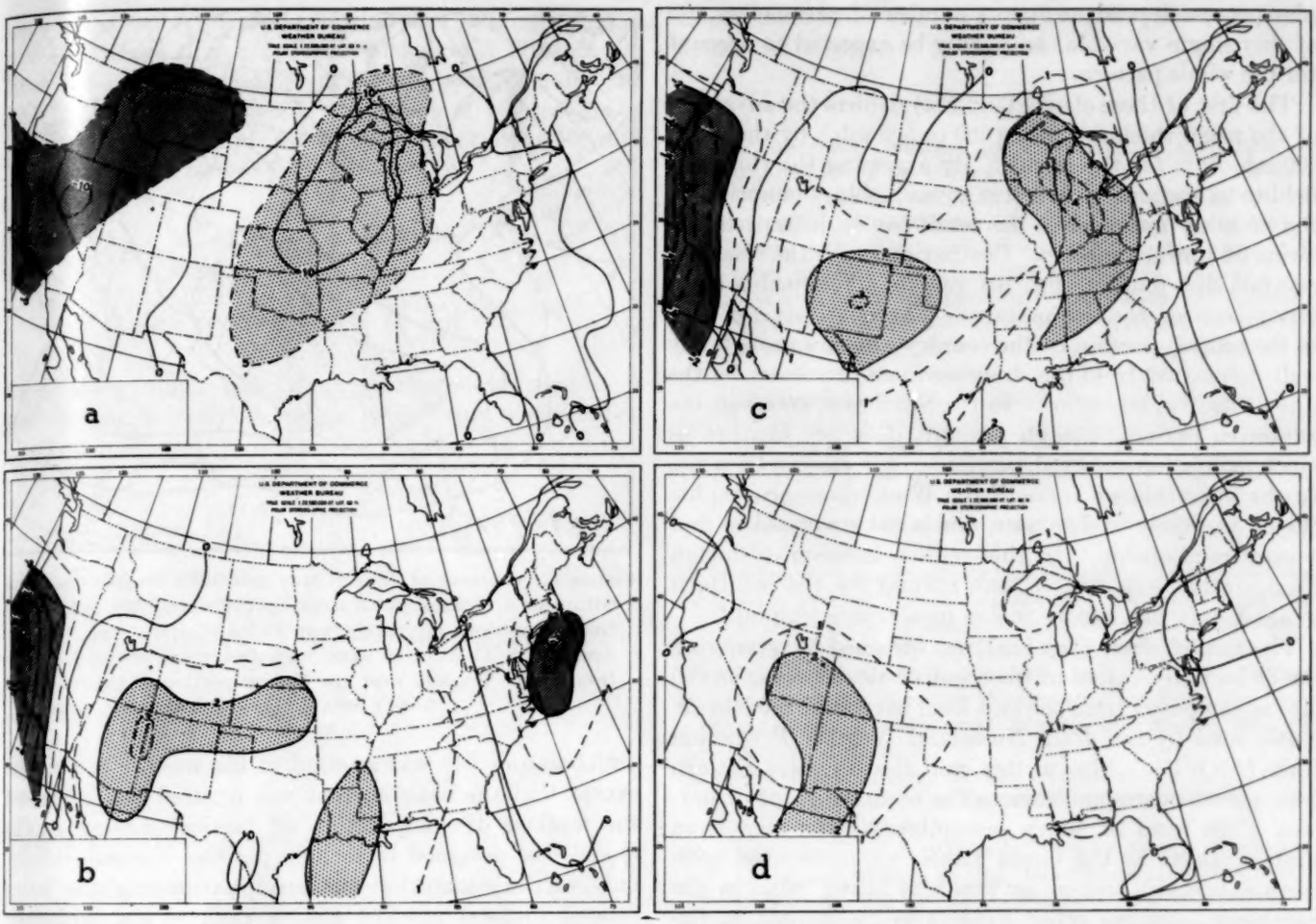

FIGURE 11.—Estimate of 30-day mean vertical motion for May 1959 in units of mm./sec., with positive values representing upward motion, obtained by: (a) advecting the mean 850–500-mb. thickness with the mean 500-mb. flow, (b) averaging 60 twice-daily values at 600 mb. computed from initial data by the JNWP baroclinic model, (c) applying the JNWP baroclinic model to the observed mean monthly 500-mb. contours and 850–500-mb. thickness data, (d) applying an equivalent barotropic model to the mean 500-mb. contours for the month. Only positive values of vertical motion were included.

curred during the latter half month, partly in connection with frequent locally heavy showers and thunderstorms, and also with a large contribution from tropical storm Arlene, particularly along the coastal section of Louisiana. Total rainfall at Rome, Ga., for example, reached 9.54 inches to set a new record since 1856.

The continued dry weather in the Southwest aggravated the existing drought situation in that area. Tucson, Ariz., experienced its first rainless May since 1949. The 0.32 in. recorded from January 1 to May 31 made this the driest comparable period since records began in 1868. Also, Oakland and Sacramento, Calif., with only traces, reported this month to be among the driest of record. Since January 1 El Paso, Texas, experienced only 0.73 in. (43 percent of normal) while Wichita Falls, Texas, reported this May to be the 10th consecutive month with subnormal precipitation.

New England and the Central Atlantic States were also relatively dry under the influence of anticyclonic flow and offshore winds. Hartford, Conn., and Scranton, Pa., for example, reported the driest May of record with monthly totals of only 0.73 and 0.77 in. respectively.

8. SPECIFICATION OF PRECIPITATION BY VERTICAL MOTION

The advent of the electronic computing machine has made possible routine computation of vertical motion in the middle troposphere. Several authors have recently discussed the relationship between this parameter and observed rainfall. Sanders [6], for example, investigated the occurrence of cloudiness and precipitation at certain cities in the United States and discussed their relationship to concurrent values of the dynamical, orographic, and frictional contributions to the vertical motion.

In the following experiment, several estimates of vertical motion were computed (fig. 11) and compared to the observed rainfall anomaly pattern (fig. 10). Since production of precipitation is a discontinuous and com-

plex process dependent upon a number of parameters, use of this single variable can hardly be expected to account for the whole pattern.

The first of these charts (fig. 11a) depicts the advection of the mean thickness field (850 to 500 mb.) by the mean 500-mb. flow for the month. By assuming the thickness field to be stationary, which is a reasonable assumption on the monthly mean basis, the result can be interpreted in terms of upward motion. Comparison with the observed rainfall distribution (fig. 10) reveals a reasonable similarity between the two patterns. The relatively wet area in the central portion of the country appears to be fairly well delineated from the drier northeastern states by the line of neutral advection. In the Southeast, however, the advective pattern, though positive, does not support as much rainfall as occurred, particularly in eastern Georgia. In the mountainous areas of the West where orographic effects are likely to dominate, one is not surprised to find a poor relationship. In this region, however, although precipitation was greater than normal for the month, it totalled only one to two inches in absolute amount.*

The second chart (fig. 11b) was obtained by averaging the twice daily values of observed vertical motion at 600 mb. as computed from the two-level baroclinic model currently used by the Joint Numerical Weather Prediction Unit (JNWP). Also in this case, the resultant pattern bore a close correspondence to the observed rainfall pattern. The band of heavy precipitation extending from western Texas to the Great Lakes was associated with average upward motion as were the heavy rains in the Southeast. On the other hand, average descent in the Northeast and extreme Southwest was apparently quite effective in keeping those regions dry. As in the previous case, the correspondence was poor over the Northwest.

Figure 11c shows the vertical velocity obtained by using the monthly mean height at 500 mb. and thickness from 850 to 500 mb. as input data to the JNWP baroclinic model and running for one iteration. Thus this chart is closely akin to the previous one and the two would be the same if relationships between circulation and vertical motion were linear. The two charts are indeed quite similar, and most of the comments of the preceding paragraph apply in this instance also. The area of largest discrepancy over the United States lay over the States bordering Lake Michigan, where values computed in this manner were larger by 2 or 3 mm./sec. It is of interest that in both cases mean troughs were associated with rising motion in advance and sinking motion behind the trough line.

Figure 11d has been included to test the extent to which a simple model can capture the overall aspects of the monthly precipitation field, given the flow pattern. In this case the barotropic model described by Namias and

*For total precipitation in inches see *Weekly Weather and Crop Bulletin*, vol. XLVI, No. 22, June 1, 1959.

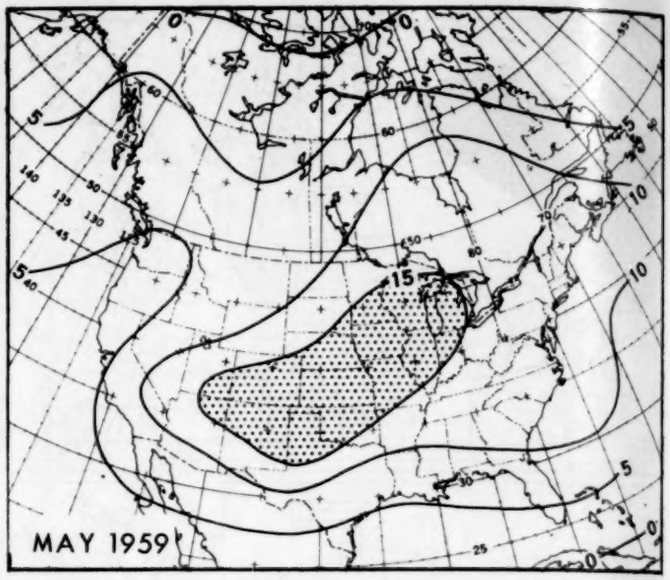

FIGURE 12.—Number of days in May 1959 with fronts of any type within unit squares (with sides approximately 500 miles). All frontal positions are taken from *Daily Weather Map*, 1300 EST. Areas with 15 days or more with fronts are stippled. Active fronts were frequent over the central portion of the country.

collaborators [3] was applied to the mean 500-mb. flow except that the basic current was omitted (see appendix for method of computation of vertical motion). The model was designed to include positive vertical velocity only, on the assumption that precipitation might be better related to total upward motion than to the arithmetic average. Figure 11d was the result after one time step. Though the pattern was ill defined because the values were small, it bore a distinct resemblance to figure 11b, with cells of maximum positive vertical motion in the Southwest, the central Gulf States, and western Great Lakes Region. Each of these cells covered a region of considerable precipitation, though the area of very heavy rainfall along the Nebraska-Iowa border was not well indicated. Since the chart series, figure 11, constitutes but a single case, little in the way of conclusions can be drawn. However, they do suggest that continued research aimed at relating mean precipitation to a vertical motion parameter might be fruitful.

In general the charts (fig. 11) define an axis of maximum ascending motion extending roughly from western Texas to the Great Lakes. It is interesting that this agrees remarkably well with the position of the most frequent frontal activity during the month (fig. 12).

APPENDIX

The vertical motion w was estimated from the following equations derived by P. F. Clapp (personal communication).

The equivalent barotropic atmosphere is characterized by invariant wind direction with height so that if $\mathbf{V}_1$ is

the wind at one level, then the wind at a different level is $\mathbf{V}_2=A\mathbf{V}_1$, where A is a function of height. Thus, if the subscript 1 is taken to refer to 500 mb. and the subscript 2 to 750 mb. and we assume conditions at 500 mb. to be nondivergent, the simplified vorticity equation at 500 and 750 mb. can then be written:

$$\frac{\partial \zeta_1}{\partial t}+\mathbf{V}_1\cdot\nabla\zeta_1+\mathbf{V}_1\cdot\nabla f=0 \tag{1}$$

$$\frac{\partial \zeta_2}{\partial t}+\mathbf{V}_2\cdot\nabla\zeta_2+\mathbf{V}_2\cdot\nabla f-f\left(\frac{\partial \omega}{\partial p}\right)_2=0 \tag{2}$$

where the symbols have their usual meaning and ω_2 is the vertical velocity in terms of pressure coordinates. Combining (1) and (2) and noting that $\zeta_2=A\zeta_1$, we obtain

$$\left(\frac{\partial \omega}{\partial p}\right)_2=\frac{1}{f}A(A-1)\mathbf{V}_1\cdot\nabla\zeta_1=\frac{K}{f}\mathbf{V}_1\cdot\nabla\zeta_1 \tag{3}$$

where K is a constant.

If we approximate $\left(\frac{\partial \omega}{\partial p}\right)_2$ by $\frac{\omega_3-\omega_1}{p_1}$ and assume that ω at 1000 mb. (denoted by ω_3) is zero, then

$$\omega_1=-\frac{p_1}{f}K\mathbf{V}_1\cdot\nabla\zeta_1 \tag{4}$$

From the hydrostatic equation

$$\omega_1=\left(\frac{dp}{dt}\right)_1=-\rho_1 g w_1 \tag{5}$$

Thus w_1 can be estimated from (4) and (5) subject to the shortcomings of the equivalent barotropic model and the assumptions made above. In figure 11d it has been scaled in units of millimeters per second.

REFERENCES

1. J. F. Andrews, "Weather and Circulation of April 1959—Including the Role Played by an Index Cycle," *Monthly Weather Review*, vol. 87, No. 4, April 1959, pp. 153–161.
2. W. H. Klein, "The Weather and Circulation of April 1954—A Month with a Confluent Jet Stream," *Monthly Weather Review*, vol. 82, No. 4, April 1954, pp. 104–109.
3. J. Namias, and collaborators, "Application of Numerical Methods to Extended Forecasting Practices in the U.S. Weather Bureau," *Monthly Weather Review*, vol. 86, No. 12, December 1958, pp. 467–476.
4. H. A. Panofsky and G. W. Brier, *Some Applications of Statistics to Meteorology*, The Pennsylvania State University, 1958, 224 pp. (Chap. VI).
5. D. F. Rex, "Blocking Action in the Middle Troposphere and Its Effect upon Regional Climate," Parts I and II, *Tellus*, vol. 2, Nos. 3 and 4, August and November 1950, pp. 196–211 and 275–301.
6. F. Sanders, "Cloudiness and Precipitation in Relation to Large-Scale Vertical Motion and Moisture," *Scientific Report* No. 4, Department of Meteorology, Massachusetts Institute of Technology, Cambridge, Mass, March 1958, 90 pp.
7. E. J. Sumner, "A Study of Blocking in the Atlantic—European Sector of the Northern Hemisphere," *Quarterly Journal of the Royal Meteorological Society*, vol. 80, No. 345, July 1954, pp. 402–416.
8. U.S. Weather Bureau, "Normal Weather Charts for the Northern Hemisphere," *Technical Paper* No. 21, Washington, D.C., October 1952, 74 pp.
9. R. M. White and D. S. Cooley, "Kinetic-Energy Spectrum of Meridional Motion in the Mid-Troposphere," *Journal of Meteorology*, vol. 13, No. 1, February 1956, pp. 67–69.
10. C. M. Woffinden, "The Weather and Circulation of August 1958—A Month with an Unusual Temperature Reversal," *Monthly Weather Review*, vol. 86, No. 8, August 1958, pp. 312–318.

Publication of Weather Notes

Many years ago the *Monthly Weather Review* published detailed eyewitness accounts of exceptional storms. These accounts both enrich the meteorologist's knowledge of storms and provide him with particular details that cannot be found elsewhere. Because such information bears directly upon questions the meteorologist must attempt to answer about weather phenomena (for example, the identification of storms as tornadoes), and because the information has potential value in both the research and service programs of the Weather Bureau, publication of eyewitness accounts and brief analyses of exceptional storms and other meteorological phenomena was resumed in the April 1955 issue. They appear from time to time under the heading "Weather Notes."

Contributions to these "Notes" are invited from readers of the *Review*. There is no limitation placed on length of description but it is expected that most will be short accounts. Any weather peculiarities, whether storms or other phenomena, are acceptable subject matter. Material should be addressed to Editor, Monthly Weather Review, U.S. Weather Bureau, Washington 25, D.C.

U.S. GOVERNMENT PRINTING OFFICE: 1959